Optimal Sizing of Solar and Battery Assets in Decentralized Micro-Grids with Demand-Side Management

MASSACHUSETTS INSTITUTE OF TECHNOLOGY
MAR 02 2017
LIBRARIES
ARCHIVES

by
Varun Mehra

Submitted to the Department of Electrical Engineering and Computer Science and Institute for Data, Systems, and Society
in partial fulfillment of the requirements for the degrees of
Master of Science in Electrical Engineering and Computer Science
and
Master of Science in Technology and Policy
at the
MASSACHUSETTS INSTITUTE OF TECHNOLOGY
February 2017

© Massachusetts Institute of Technology 2017. All rights reserved.

Author ..... Signature redacted .....
Department of Electrical Engineering and Computer Science and
Institute for Data, Systems, and Society
January 30, 2017

Certified by.. Signature redacted .....
Professor Rajeev Ram
Department of Electrical Engineering and Computer Science
Thesis Supervisor

Accepted by ..... Signature redacted .....
W. A. Coolidge Professor Munther Dahleh
Director, Institute for Data, Systems, and Society

Accepted by .... Signature redacted .....
Professor Leslie A. Kolodziejski
Chair, Department of Electrical Engineering and Computer Science
Committee on Graduate Students

Optimal Sizing of Solar and Battery Assets in Decentralized Micro-Grids with Demand-Side Management

by

Varun Mehra

Submitted to the Department of Electrical Engineering and Computer Science and
Institute for Data, Systems, and Society
on January 30, 2017, in partial fulfillment of the
requirements for the degrees of
Master of Science in Electrical Engineering and Computer Science
and
Master of Science in Technology and Policy

Abstract

Solar-based community micro-grids and individual home systems have been recognized as key enablers of electricity provision to the over one billion people living without energy access to-date. Despite significant cost reductions in solar panels, these options can still be cost-prohibitive mainly due over-sizing of generation assets corresponding with a lack of ability to actively manage electricity demand. The main contribution shared is the methodology and optimization approach of least-cost combinations of generation asset sizes, in solar panels and batteries, subject to meeting reliability constraints; these results are based on a techno-economic modeling approach constructed for assessing decentralized micro-grids with demand-side management capabilities. The software model constructed is implemented to represent the technical characteristics of a low-voltage, direct current network architecture and computational capabilities of a power management device. The main use-case of the model presented is based on serving representative, aggregated, household-level load profiles combined with simulated power output from solar photovoltaic modules and the kinetic operating constraints of lead-acid batteries at hourly timesteps over year-long simulations. The state-space for solutions is based on available solar module and battery capacities from distributors in Jharkhand, India. Additional work presented also extends to real-time operation of such isolated micro-grids with requisite local computation. First, for load disaggregation and forecasting purposes, clustering algorithms and statistical learning techniques are applied on quantitative results from inferred load profiles based on data logged from off-grid solar home systems. Second, results from an optimization approach to accurately parametrize a lead-acid battery model for potential usage in real-time field implementation are also shared. Economic results, sensitivity analyses around key technical and financial

input assumptions, and comparisons in cost reductions due to the optimization of solar and battery assets for decentralized micro-grids with demand-side management capabilities are subsequently presented. The work concludes with insights and policy implications on establishing differentiated willingness-to-pay, tiers of service, and dynamic price-setting in advanced micro-grids.

Thesis Supervisor: Professor Rajeev Ram
Title: Department of Electrical Engineering and Computer Science

Acknowledgments

I will be eternally grateful for having such a diverse set of rich — and humbling — learning experiences during my time at MIT. I am a better person for having been here, and going forward, I will always view coming to MIT to be one of the best decisions of my life.

First and foremost, I would like to thank Professor Rajeev Ram, my thesis advisor and mentor during graduate school. Professor Ram has been extraordinarily encouraging and patient throughout my research and academic pursuits; he is and will continue to be a role model not just for me, but I am undoubtedly sure for many of his previous, current, and future students.

In addition, I must thank the Tata Center for Technology and Design — from the Tata Trusts to everyone at MIT who has worked so hard to make the center's work and mission possible. In particular, I would like to thank Dr. Robert Stoner, who has supported me during my endeavors both at MIT and in India; his perception and sense of humor has led to many honest conversations. To Dr. Reja Amatya, for your steady hand and for being willing to go through the details of the code; and to Victor Lesniewski, for shaping my thinking on how to conduct effective research in the developing world with a sense of empathy.

I would also like to thank the many practitioners and experts I interacted with in India, specifically Huda Jaffer from the SELCO Foundation and Paras Loomba from GHE, for educating me on what it takes to actually install off-grid systems and showing me the realities on the ground. I must also profusely thank our partner organization, in the Tata Steel Rural Development Society (TSRDS) — Mr. Nandi, Mr. Debdoot, and Mr. Biren — for your time, resources, and commitment to the larger cause; I thoroughly enjoyed our interactions (especially those in Hindi), and I will always remember the high standard of respect and professionalism you all employ in working to improve the lives of the people of Jharkhand.

To the folks at MIT Energy Initiative, thank you to everyone for creating a thoughtful environment in which to work, from my friendly desk neighbors to the

generous staff. To Dr. Claudio Vergara, for your insatiable curiosity to understand the world around us — an incomplete list of which includes batteries, control systems, and rock climbing; and to Professor Ignacio Perez-Arriaga, who is committed to solving the challenges of electricity access both by teaching and by doing. I would also like to thank Vivian Li for your willingness to collaborate always without hesitation; to Ahmet Can Musabeyoglu, for having the best attitude in both the lab and in the field; and to Amy Rose, for being the best e4Dev co-president I could have asked for.

There are numerous other groups of people who have — knowingly or not — been absolutely critical for me to rely on as I faced the various challenges graduate school has presented. To my former colleagues at ARPA-E, our interactions are habitually intellectually stimulating; your accomplishments hold me to a higher standard and your collective drive reminds me to keep fighting the good fight. To my old friends, from UCLA and especially to those in DC: your abilities to enjoy life and to see humor in everything are thankfully contagious. There is a reason why I come to visit often — and it's not just for the N64. And to my new friends at MIT, it has been awesome to have shared this journey; I guarantee that I have learned something from each of you.

Lastly but most importantly, I would like to thank my family for your unconditional support since I embarked upon this opportunity. To my grandmother in Delhi and extended family in Mumbai, I loved the time we were able to spend together as a result of my research trips to India. And to my parents and brothers (which of course includes Tigger): thank you for always lending an ear and sharing thoughtful advice, including the unsolicited. Home truly never felt far away.

Contents

1 Introduction, Motivation, and Context **19**

1.1 Status and Market Opportunity of Electrification in India 20

1.2 Opportunity for Decentralized Micro-Grids with Demand-Side Management Capabilities 22

1.2.1 Review of Demand-Side Management & Intelligent Micro-Grids 23

1.3 Chapter Overviews and Literature Review 25

1.3.1 Review of Demand Modeling and Classification 26

1.3.2 Review of Battery Modeling 31

1.3.3 Review of Micro-Grid Design & Operation 37

1.3.4 Review of Micro-Grid System Techno-Economic Analyses . . . 40

1.3.5 Review of Policy Implications Related to Price, Reliability, & Quality of Service 43

1.4 Conclusion 47

2 Constructing Activity-Based Consumer Demand Profiles Based on Load Disaggregation and Statistical Learning Techniques **49**

2.1 Introduction 49

2.1.1 Examples of Quantitative Electricity Consumption Data Sets in Developing World Context 50

2.2 Data Acquisition Context, Process, & Calibration 52

2.2.1 Description of Solar Home System and Data Logger Configuration 53

2.2.2 Signal Processing & Calibration of Raw Data Sets 53

2.3 Methods for Separating Load from Spillage 56

2.3.1 Method 1: Directly Analyzing Solar & Battery Data 58
2.3.2 Method 2: Separating Combined Load & Spillage Data 63
2.3.3 Example Inferred Household Load Profiles 65
2.4 Appliance and State Combinations 66
2.5 Statistical Analysis and Feature Selection 68
2.5.1 Relating Lighting Usage to Time of Day 69
2.5.2 Relating Fan Usage to Ambient Temperature 71
2.6 Application of Machine Learning Algorithms for Load Disaggregation 73
2.6.1 Performance of K-Means and Gaussian Mixture Model Algorithms 75
2.7 Conclusion 80

3 Adaptation and Extension of Kinetic Battery Model in Simulation and for Real-Time Operation 81
3.1 Introduction 81
3.2 Kinetic Battery Model Implementation & Adaptation 83
3.3 Rainflow Algorithm Implementation for Counting Battery Cycles . . 90
3.3.1 Effect of Depth of Discharge on Available Cycles 94
3.4 Extension of Model and Methodology for Incorporating Voltage Response for Real-Time State-of-Charge Estimation Purposes 95
3.4.1 Battery Cycle Data Acquisition and Calibration Process . . . 96
3.4.2 Lead Acid Battery Chemistry Overview 98
3.4.3 Representative Equations and Selection of Diffusion and Resistance Battery Parameters 98
3.4.4 Battery Parameter Constraint Selection & Optimization Formulation 101
3.4.5 Optimization Results and Discussion 103
3.5 Conclusion 107

4 Technical and Economic Modeling Analysis for Optimizing Generation Asset Sizes 109

4.1 Introduction 109
4.2 Description of Load/Appliance Choice Scenarios for Demand Representation 111
4.3 Description of Selected Network Architecture & Devices 113
4.3.1 DC-DC Converters Model 117
4.3.2 Micro-Controller Power Consumption 120
4.3.3 Wiring Losses 120
4.3.4 Aggregated Load Profile 122
4.4 Solar Module Model 123
4.4.1 Solar Irradiance Resource Data 123
4.4.2 Solar Power Output 124
4.5 Matrix Population and Search Method for Generation Asset Selection Subject to Reliability Constraints 126
4.5.1 Further Analysis of Defined Level of Reliability 129
4.6 Choice of Battery and Solar Combinations Based on Distributor Availability & Economies of Scale 131
4.7 Greenfield Costs of Modeled Micro-Grid and Financial Analysis . . . 135
4.7.1 Key Micro-Grid Cost Inputs 136
4.7.2 Costs of Power Management Devices 136
4.7.3 Initial Capital Costs 137
4.7.4 Replacement Costs Based on Equipment Lifetime 139
4.7.5 Financial Model Overview & Results 140
4.7.6 Business Model Viability 141
4.8 Sensitivity Analysis to Key Model Inputs 143
4.8.1 Effect of Payback Period, Discount Rate, and Connection Fee on Monthly Payment and Internal Rate of Return 144
4.8.2 Effect of Maximum Depth of Discharge and Cycle Life on Levelized Cost of Electricity 146
4.8.3 Effect of Reliability Thresholds on Costs and Generation Asset Selection 148

4.9 Model Benchmarking & Cost Comparisons: Examples of Conventional Solar Home Systems & Micro-Grids 152
4.9.1 Tata Power Solar and SELCO Home Systems: Benchmarking Model with Generation Asset Size and Differences in Geographical Irradiance 152
4.9.2 Tata Power Solar and SELCO Home Systems' Costs 153
4.9.3 Mera Gao Power Micro-Grid: Generation Asset Sizing Example 155
4.9.4 Actual Micro-Grid System Costs in Jharkhand, India 156
4.9.5 Summary of Capital Cost Comparisons & Discussion 157
4.10 Comment on Developed Program's Computational Stability & Local Memory 159
4.11 Conclusion 160

5 Regulatory Recommendations and Social Implications of Dynamic Price Setting in and Interconnection of Micro-Grids with Demand-Side Management 163
5.1 Introduction 163
5.2 Current Regulatory Landscape & Challenges Faced By Distribution Companies in India 165
5.3 Interactions and Regulations Between Grid and Off-Grid Public/Private Companies and Services 166
5.3.1 Enabling Retail Competition in Off-Grid Areas & Roles of Regulators 168
5.4 Solar Subsidies & Load Coincidence Factor 171
5.5 Current Regulatory Approach for Tariff Setting & Relation to Micro-Grids 173
5.6 Incorporating Individual Users' Preferences & Determining Tiers of Electricity Service 177
5.6.1 Preference Differentiation Based on Survey Results near Patamda, Jharkhand 177

5.6.2 Conceptualization of Real-Time Pricing Based on Battery State-of-Charge Thresholds . . . 178
5.6.3 Extrapolation from Telecommunication Industry's Service Level Agreements . . . 182
5.7 Conclusion . . . 184

6 Conclusions and Future Work **185**
6.1 Introduction . . . 185
6.2 Conclusions on Data-Driven, Activity-Based Demand Profile Construction . . . 186
6.2.1 Generating Household Level Demand Forecasting Models . . . 186
6.3 Conclusions on Battery Modeling in Simulation & Real-Time Implementation . . . 190
6.3.1 Accurately Modeling Battery Degradation . . . 191
6.3.2 Integration of Battery Model within Control System Architecture . . . 192
6.3.3 Further Representing Micro-Grid Operational Dispatch and Demand-Side Management Algorithms . . . 192
6.4 Conclusions on Techno-Economic Analysis of Micro-Grid Design and Operation . . . 195
6.4.1 Including Topological Constraints, Larger Number of Households, & Productive Loads . . . 196
6.5 Final Concluding Remarks . . . 197

List of Figures

1-1 Comparisons of Costs and Examples of Off-Grid Electricity Access Options [1] 22

1-2 Example of Common Residential Appliance Patterns and Signatures [18] 28

2-1 Monthly Load Profile, Rural Feeder, Distribution Utility in Jharkhand, India 51

2-2 Layout of Data Logger Connection 54

2-3 Circuit Configuration for Data Acquisition 54

2-4 Distribution of One Household's Solar Current Digital Readings and Calibrated Values 57

2-5 Distribution of One Household's Battery Current Digital Readings and Calibrated Values 57

2-6 Example of Raw Solar Current and Voltage Readings (One Week) . . 59

2-7 Example of Raw Battery Current and Voltage Readings (One Week) . 59

2-8 Method 1: Example of Calculated Solar, Battery, and Spillage Power Data (One Month) 61

2-9 Method 1, Case 2: Spillage Correlation with Solar Power Production ($R^2 = 87.31\%$) 62

2-10 Method 2: Example of Combined Load and Spillage Data (One Month) 65

2-11 Example of a Weekly Load Profile: Method 1 and Method 2 66

2-12 Example of a Monthly Load Profile: Method 1 and Method 2 66

2-13 Frequency of Occurred States 68

2-14 Method 1: Non-Parametric, Bounded Joint Probability Distribution Fit of Lighting Use and Time of Day 70
2-15 Method 2: Non-Parametric, Bounded Joint Probability Distribution Fit of Lighting Use and Time of Day 70
2-16 Method 1: Conditional Probability Distribution Based on Non-Parametric Fit of Fan Use Given Temperature 72
2-17 Method 2: Conditional Probability Distribution Based on Non-Parametric Fit of Fan Use Given Temperature 72
2-18 GMM Clustering Results [Probabilistic Assignments] 78
2-19 K-Means Clustering Results 78

3-1 Kinetic Battery Model Concept Overview [35] 83
3-2 Example of Net Load Profile and KiBaM Variable Outputs 89
3-3 Example of Charging and Discharging KiBaM Constraints 89
3-4 Simulated Actual and Differential Battery State-of-Charge 91
3-5 Example of Daily State-of-Charge Over Entire Year 93
3-6 Example of Rainflow Algorithm Output [40] 93
3-7 Exponential Fit of MDOD versus Cycle Life for Select Lead-Acid Batteries 94
3-8 Data Acquisition Circuit for Battery Cycle Data 97
3-9 Charge & Discharge Cycle: Universal 100Ah Pb-Acid Battery 97
3-10 Notional Depiction of Functional Charging and Discharging Resistances 101
3-11 Output of IR Losses vs. Current Profile and Q1 SOC 105
3-12 Output of Predicted Final and Nernst Voltages vs. Measured Voltage 106

4-1 Example Total Fan and Lighting Load Conditioned on Ambient Temperature and Sunlight 114
4-2 Example of Total and Critical Yearly Load Profile for One Household 115
4-3 Example of Total and Critical Yearly Load Profile for Five Households 115
4-4 Modeled Architecture & Proposed Network Layout [91] 116

4-5 Measured Boost Converter Efficiencies and Simulated Network Losses [81] 119
4-6 Measured Buck Converter Efficiencies and Simulated Losses at Household [81] 119
4-7 Example of Wiring Losses in Network 122
4-8 Annual Average Global Horizontal Irradiance: India 123
4-9 Historical Average Solar Irradiance near Patamda in Jharkhand, India 125
4-10 Hourly Output of 300W Panel Based on Irradiance in Jharkhand, India 125
4-11 Total Reliability vs. PV and Battery Capacities 130
4-12 Critical Reliability vs. PV and Battery Capacities 130
4-13 Simulated Hourly Reliability: Total Load Profile (94.26%) 132
4-14 Simulated Hourly Reliability: Critical Load Profile (99.45%) 132
4-15 Exponential Fit for Unit Cost vs. Available PV Module Sizes 134
4-16 Exponential Fit for Unit Cost vs. Available Battery Capacities 134
4-17 Costs of Solar and Battery Asset Combinations 136
4-18 Distribution of Capital Costs of Optimized Generation Asset Micro-Grid Network 138
4-19 Yearly Cash Inflows and Outflow 142
4-20 Monthly Payment Based on Discount Rate and Connection Fee . . . 145
4-21 Monthly Payment Based on Discount Rate and Payback Period . . . 145
4-22 IRR Based on Discount Rate and Payback Period 145
4-23 Tradeoff Between MDOD and Cycle Life with Battery Selection and Replacement Costs 147
4-24 Effects of Reliability Thresholds on Cost Metrics 149
4-25 Proportion of Solar Costs Across Available Solar/Battery State-Space 150
4-26 Solar Module and Battery Capacity Choice Based on Reliability . . . 151
4-27 Comparison Between Solar Resource in Karnataka and Jharkhand [83] 154
4-28 Process Flow Diagram for Constructed Model 162

5-1 Overall Electricity Revenue Share in India [2] 166

5-2 Tariffs for Distribution Consumers by JBVNL [99] 175
5-3 Institutional Structure of India's Power Sector [2] 176
5-4 Qualitative Survey Results from Five Households 177
5-5 Example of ROBD-Adjusted Daily Electricity Balance Per Household Based on SOC Threshold 180
5-6 Simulated Battery State-of-Charge Over Entire Year 182

6-1 Use-Case for Hidden Markov Model [85] 189
6-2 Use-Case for Input Hidden Markov Model [85] 189
6-3 Representation of Battery Management System Architecture [103] . . 192
6-4 Depiction of Various Demand-Side Management Approaches [104] . . 193
6-5 Proposed Process for Forecasts, State Estimation, and Real-Time Dispatch [91] 195

List of Tables

2.1 Values for Current Channels Calibration Process 55
2.2 Appliance & State Combination 67
2.3 K-Means Centroid Results 76
2.4 K-Means Algorithm Performance 76
2.5 GMM Results, K=7 77
2.6 GMM Results, K=10 77
2.7 Data Set Length Effect on K-Means Performance 79
2.8 Data Set Length Effect on GMM Performance 79

3.1 Example of Number of Hours KiBaM Charge and Discharge Constraints Reached 88
3.2 Universal 100Ah Battery Capacity & C-Rate 99
3.3 Output of Optimized Battery Parameters for 100Ah Universal Battery 104

4.1 Demand Load Profile Inputs: Residential Load Scenario 113
4.2 State-Space Matrix: Available Solar/Battery Combinations 126
4.3 Key Cost Inputs 137
4.4 Lifetime of Equipment Assets 138
4.5 Key Financial Inputs 141
4.6 Comparison of Modeled Generation Asset Sizing for Tata Power Solar and SELCO Home Systems in Jharkhand and Karnataka 155
4.7 Summary of Capital Cost Comparisons 157

5.1 Solar Load Coincidence Factors (SLCF) for Fan Usage 172

5.2 Example of Daily Electricity Balance Allotment 179

Chapter 1

Introduction, Motivation, and Context

The concept and implementation of efforts relating to electrification dates back to when developed countries such as the United States enacted policies to achieve country-wide electricity access during the late 1800's and early 1900's. Given the advent of large-scale thermal power plants based on fossil fuels and the general acceptance of alternating current (AC) based equipment and networks, a centralized power system model took root. Over recent decades, mainly since the 1970's, utility institutional structures and electricity markets have gone through a process of liberalization. The introduction of regulation forced the unbundling of vertically owned and operated utilities (i.e. generation, transmission, and distribution). Regulation also paved the way for the formation of regional markets, enabling competition in generation and distribution; in the latter, rate cases of utilities as regulated monopolies began to ensure fair pricing and compensation of network investments for high quality of electricity service.

The importance of providing affordable options for electricity access cannot be understated. To-date, over 1 billion people live without basic access to electricity, and many who receive grid-connections are subject to low levels of reliability and poor quality of service. In India alone, it is estimated that around 300 million lack basic electricity access — nearly equivalent to the entire population of the United States.

Across academic disciplines, it is undisputed that electricity access is inextricably linked to human development, as is documented over a wide range of human indicators over the past two centuries in [1]. With the immediate challenges of minimizing greenhouse gas emissions from the power sector and serving increasing populations, governments in developing countries today are not faced with the same set of challenges in regards to providing electricity to their respective populations. Thus it is becoming an increasingly popular — and necessary — belief that the availability of affordable and distributed renewable energy sources will be required in order to achieve these transitions.

The term 'leap-frogging' is commonly used in reference to the opportunity developing countries have for widespread distributed generation and renewable energy deployment as opposed to centralized power systems primarily driven by fossil fuel-based thermal generation seen in the developed world. In the case of India, the country is still heavily reliant on coal as an import and as a source of fuel, and is likely to continue that trend given near-term demands of economic development. In order for a true 'leap-frogging' to take place for distributed, renewable energy generation to provide electricity access to the remaining and growing population demands, costs, business models, and quality of service must be superior to conventional approaches. Many aim to extrapolate the analogy of high penetration of cellular phones in the developing world as a 'leap-frog' over landline-based phone connections, but it was not until the convergence of convenience, costs, coverage, and pay-as-you-go strategies were implemented at scale was that transition truly able to take place [1].

1.1 Status and Market Opportunity of Electrification in India

To-date, India's central power system is still dominated by coal-based thermal generation — which accounts for roughly 60% of installed capacity [2]. India has made significant emissions reduction commitments and has put forth plans to increase in-

vestment and installations of renewables. For instance, the Jawaharlal Nehru National Solar Mission (JNNSM) outlines a 20 giga-watt (GW) target for solar, with 2GW slated for off-grid, by 2022 [3]. A number of states have also enacted renewable purchase obligations (RPO's) for public distribution companies, but are nominal and not strictly enforced to-date [2]. The political, economic, and technical interplay between electricity provision, fossil-fuel related emissions reductions, and investments required in centralized and distributed renewables will be a major plotline in India's development in the near and long term.

To address electricity access issues in the country, the Indian central government has established a number of efforts. The Rajiv Gandhi Grameen Vidyutikaran Yojana (RGGVY) initiative is focused on connecting hundreds of thousands of villages to the central grid, amounting to millions of people, based off of significant capital subsidies provided for connections. This approach is challenging given land rights issues, but more importantly, the financial insolvency of distribution companies; the high system losses and theft are politically perpetuated due to a lack of cost-reflective electricity tariffs, leading to low levels of cost recovery and revenue collection [4]. Concurrently, the Ministry of New and Renewable Energy (MNRE) in India has launched the Remote Village Electrification (RVE) program, with a focus on distributed solar systems [5]. RVE is targeting thousands of villages, again with significant capital subsidies to users. The delineation between the two programs is that RGGVY is focused on smaller villages (less than 300 inhabitants), while RVE is focused on larger villages — but it is unclear to what extent actual coordination takes place.

As shown on the left-hand side in Figure 1-1, the decreasing costs of solar combined with the prohibitive capital costs of grid extension is already helping to drive momentum towards distributed generation as a viable form of electricity access. In India, the market potential for off-grid electricity services is already significant and expected to grow, primarily in the form of individual solar home systems and microgrids. One projection has the solar home system market in India reaching $\sim$ 3 million units sold per year, with a market size of over $215 million by 2018; in the microgrid space (encompassing various capacities, sizes, and use-cases), a similar forecast

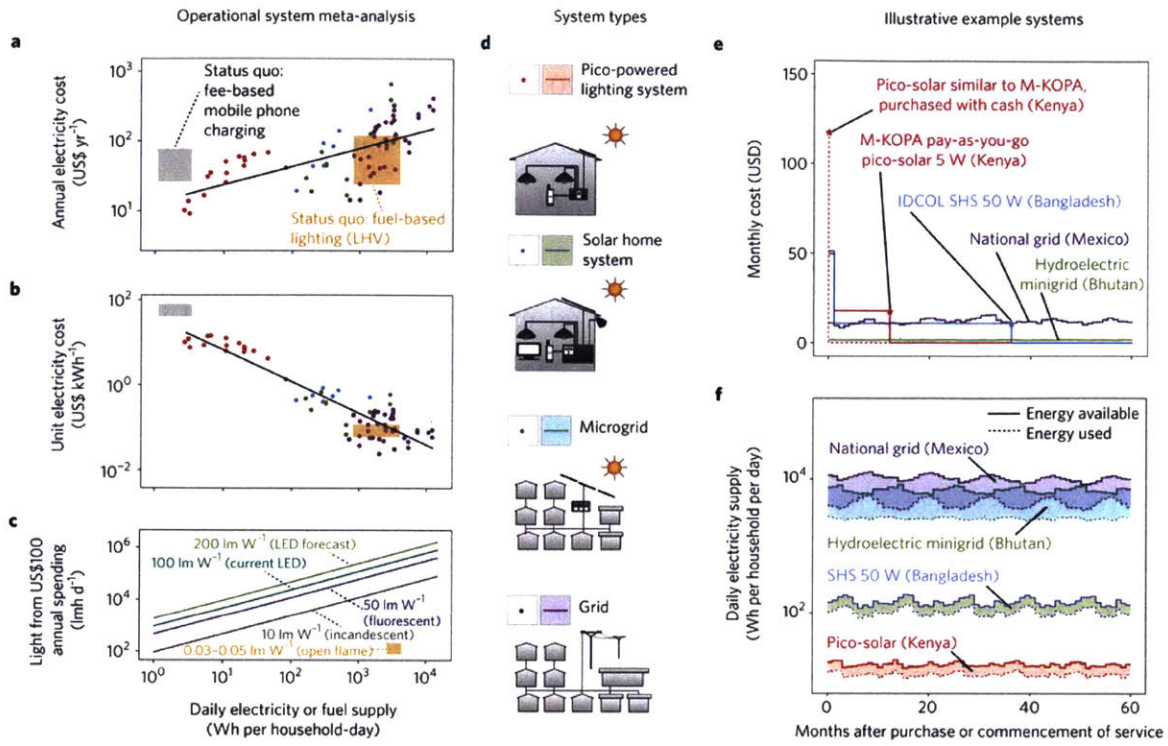


Figure 1-1: Comparisons of Costs and Examples of Off-Grid Electricity Access Options [1]

expects the market size to be over $150 million — with the potential to serve around 900,000 households by 2018 as well [6]. Private companies are starting to play a larger role in the off-grid electricity service space in India, with over 80 active companies (as equipment and/or electricity service providers) in both the solar home and distributed energy systems space [6].

1.2 Opportunity for Decentralized Micro-Grids with Demand-Side Management Capabilities

Despite significant cost reductions in solar panels in recent years due to efficiencies in manufacturing process and achievement of economies of scale, both solar home systems and micro-grids can still be cost-prohibitive for a number of reasons. Lead-acid batteries are most commonly used and are over-sized to ensure reliability and operation autonomy of these systems, which adds to overall costs. In particular,

utilization of smaller panels (higher per unit costs) and requirements for individualized maintenance in remote areas can also increase solar home system costs [1]. Similarly, micro-grids in remote villages typically require community buy-in, which forces a flat tariff on service providers and drives up costs of customer acquisition.

Thus, part of the focus of this modeling effort is to analyze decentralized micro-grids, meaning micro-grids on the order of 5-10 households connecting subsets of households in a particular village together. Part of the reason for this is to take advantage of economies of scale seen from connecting households to a central solar panel and battery — while potentially overcoming challenges of village-scale customer acquisition and site selection of solar panel arrays and battery banks common in conventional micro-grids [4]. This approach can also potentially enable new, bottoms-up business models for electrification — as with manageable costs and autonomous operation, individuals in off-grid areas can monetize investments in their own electricity infrastructure.

In regards to micro-grid system operation, it is becoming increasingly well-known of the challenges seen today; load curtailment/management, revenue collection, and theft monitoring are still major issues with status quo approaches and installations. To further catalyze the adoption, deployment, and financial sustainability of off-grid electricity services, technologies equipped as a "utility-in-a-box" solution can help alleviate issues seen today and have a significant impact in electrification efforts [7].

1.2.1 Review of Demand-Side Management & Intelligent Micro-Grids

The recent advent of intelligent devices and low-cost computation can enable such "utility-in-a-box" solutions in various ways, such as through demand-side management and network control [7] [8]. To-date, there are a number of research efforts and companies focused on designing and introducing various incarnations of demand-side management and intelligence. As is discussed in this section, the motivations for doing so include to mitigate electricity theft, enable pay-as-you-go strategies, and

curtail over-consumption at the household.

A number of private companies have began implementing various versions of demand-side management and intelligence today. For example, the company PowerHive, with a focus on micro-grids in Kenya, has developed a centrally-located meter; this meter handles pre-paid electricity transactions with daily energy consumption limits set at every household connected to the network. Other companies, such as Circuitor and INENSUS, similarly require pre-paid electricity transactions and overall daily energy consumption limits based on purchased amounts, albeit their approaches require credits to be physically added to activate each household's meter [9]. In addition, the company SparkMeter has developed a low-cost hardware and software platform, at the household level, for remote monitoring and control of electricity consumption, seemingly applicable in both solar home systems and micro-grids [10].

There have also been a number of academic efforts in this area. The SharedSolar concept, from Columbia University, uses a centrally-located meter that connects to the cellular network. This capability allows for customers to send scratch card codes via SMS to the central meter — and the operators receive a demand schedule via SMS as well. In Peru, the Huatacondo micro-grid integrates solar and diesel generating sources, and a diversity of heterogeneous loads in a village; this micro-grid requires on-site computation, and employs a rolling horizon strategy to forecast short-term consumption and to prioritize and schedule loads [11]. While in Bhutan, the GridShare device has been piloted in order to mitigate brownouts from peak consumption of rice-cookers in a micro-grid — which includes an LED indicator to convey the state of the system to each household. Exact cost numbers for such systems are typically not readily available, but as a reference point, the cost of the GridShare device at low-volume, which includes sensors, a micro-controller, LED display, a relay, and an enclosure, is estimated to be $93 [12].

Nearly all of these approaches require the integration of low-cost sensors for power consumption (i.e. current and voltage) and controllable switches to enable some form of demand-side management. However, aside from the Huatacondo micro-grid in Peru, current approaches lack on-site computation — necessary in order to disaggre-

gate, prioritize, and serve demand (in isolated micro-grids) and process signals from households in real-time. The ability for appliance- or household-level control paves the way to prioritize and curtail or serve loads. Such decisions require micro-controllers to conduct such computation, which have exponentially decreased in costs due to Moore's Law, in order to assess the current state of the micro-grid network, conduct load and generation forecasts, and then dispatch available electricity to serve demand. Yet, in such cost-sensitive environments initially designed for basic loads, the question still remains: what is the ability for value creation in the design and operation of decentralized micro-grids with demand-side management? The modeling approach herein is designed to answer this key question. For clarity, the term demand-side management in this work is defined to enabled through an intelligent power management device that consists of hardware and embedded software, specifically related to capabilities of power conversion and regulation, computational decisions, and communication signals; additional details are discussed in Chapter 4.

1.3 Chapter Overviews and Literature Review

In order to answer the questions related to the value of micro-girds with demand-side management designed for electricity access, the work presented herein is organized into four subsequent chapters as follows. Chapter 2 discusses the methods and statistical analytical techniques used in constructing household-level electricity demand profiles, a critical factor when considering design and operational approaches in power system simulations. Chapter 3 focuses on the adaptation of the Kinetic Battery Model (KiBaM) in a simulation environment and, based on acquired battery cycle data, also presents an extension of the KiBaM to take into account voltage effects for as required for using for real-time battery management. The first part of Chapter 4 then walks through the selection and implementation of the remaining technical aspects modeled in representing low-voltage, intelligent micro-grids — and the second part of Chapter 4 is a natural extension, discussing the systems cost, economic value, and financial viability of such micro-grid networks. To conclude, Chapter 5 discusses policy and

social implications of price-setting in such networks, and Chapter 6 provides a summary of the work and contributions shared herein, along with areas of future work. The rationale and explicit delineation of each chapter's contribution in relation to related research is discussed in the remainder of this introductory chapter.

1.3.1 Review of Demand Modeling and Classification

In any power system, the design and costs are directly related to the expected demand to be served in an area. In the context of the developing world, having accurate estimation of electricity consumption is of critical importance in order to inform both electrification planning efforts and real-time balancing of supply and demand — and is a consistent and recurring challenge faced by practitioners when planning electricity access in rural, off-grid areas.

Broadly speaking, there are two main methods —- qualitative and quantitative — for estimating demand profiles when designing power systems for rural electricity access. Furthermore, such methods can vary in their resolution, assumptions on appliance ownership, and incorporate effects of exogenous variables such as time of day. In more qualitative methods, one such approach is based on country- or regional-level demographics; previous work has used macro-economic indicators such as household income, population density, poverty levels, etc. to estimate and predict household electricity demand per year. In [13], the model developed outputs an aggregated demand for electricity at the national level, in the form of kWh per household per year; in [14], the focus is on household projections of fuel consumption at a regional level in India, again with the output being kWh-equivalent per household per year.

The MIT Design Advisor Model is based on inputting detailed assumptions of electricity consumption of basic temperature- and time-induced loads, such as HVAC and lighting. Estimates are made on building insulation characteristics and solar lighting insolance to come up with average monthly electricity consumption in a certain locale — specifically, a representative day (hourly) for each month of the year in watt-hours per meter squared [15]. Alternatively, instead of focusing on building occupancy, one can rely on individual survey questionnaires to obtain a baseline

understanding of income levels, power levels of appliances desired, typical daily usage patterns, etc. Once such information is obtained from individuals (such as through surveys), this data can be used to create average daily load profiles — which can then be extrapolated using basic randomization methods over a representative year, as is done in the Reference Electrification Model explained in [16].

In quantitative methods, raw data sets are acquired and more sophisticated inference methods and algorithms can be used to understand usage patterns, etc. In the developing world, high resolution (i.e. household level at sub-hourly time intervals ideally over months, if not years) data sets are rarely available but can be extremely useful. Such data sets can help validate conventional demand modeling approaches during design phases of electricity planning efforts, as over- or under-estimation of demand effects both cost and reliability of solar-based micro-grids or solar home systems. Based on data acquired from data loggers installed in solar home systems in the state of Jharkhand, India (over 222 days at 1 minute intervals, yielding over 18 MB per household), Chapter 2 presents the process undertaken in acquiring and calibrating household level energy consumption data sets.

In addition to comparing demand profile construction methods during the planning phase, such data sets can also be useful to test methods and abilities to disaggregate loads and generate an activity-based load profile. There is an established cost trade off between number of sensors installed and ability to monitor individual appliance electricity consumption. To generate an activity-based load profile for users, one option requires the installation of sensors at each appliance — which can be a costly and cumbersome effort [17]. The other option is to use a software-based algorithmic approach based on distinct expected power consumption durations, transients, or other signatures at the household level. Known as 'non-intrusive appliance load monitoring' (NIALM), the field initially focused on the need to acquire such data sets through installing sensors, and how to conduct basic load disaggregation of alternating current (AC) appliances based on cyclical patterns and transient signatures [18]. An example of common residential appliances in the developed world and their expected profiles and signatures are shown in Figure 1-2.

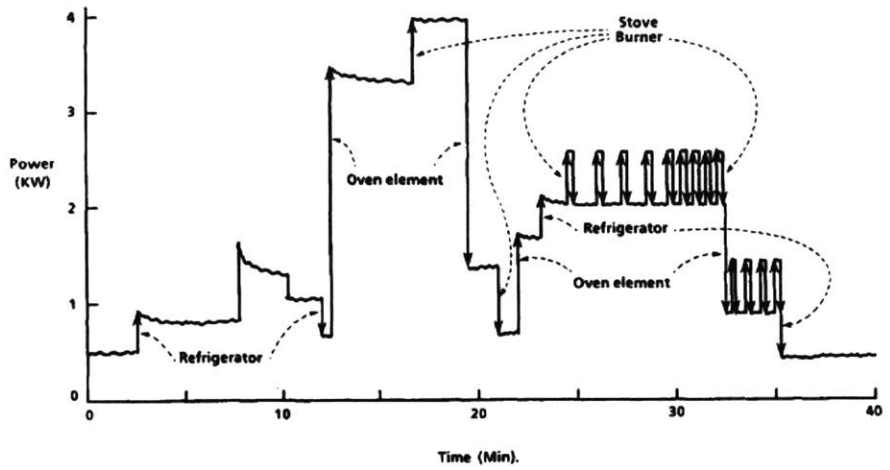


Figure 1-2: Example of Common Residential Appliance Patterns and Signatures [18]

Since the field's inception, numerous papers have been focused on analyzing various methods to disaggregate loads. Any method initially relies on acquiring data, which can vary based on spatial resolution (i.e. household vs. feeder level) and time resolution (i.e. hourly vs. minute). In the context of the developed world, there is a higher diversity of appliances in homes, such as televisions, computers, refrigerators, etc. — with most having different power levels during on and off states. With large data sets across a large number of consumers, and without any a priori information on appliances/loads, approaches such as identifying minimum sampling rates (frequency), probabilistic models, unsupervised clustering algorithms to learn potential number of appliances, combinations, and expected usage patterns have all been employed in various capacities. The papers subsequently referenced provide context on previous work focused on acquiring load consumption data at various time scales and resolution, along with the various application of machine learning techniques and load disaggregation algorithms — with a focus on developed world power systems, load profiles, and appliances given that are not many relevant examples in regards to electricity access and consumption in the developing world.

In [19], Patel et al., they develop a single-point sensing technique based on electromagnetic interference (EMI) detection from switched-mode power supplies for various loads that propagates through a household's wiring. Requiring installation of equip-

ment at the household level, the 'ElectriSense' method relies on the generation of continuous EMI, and institutes a Gaussian distribution over each appliance's switching frequency ($\leq$ 60 Hz, nominal system frequency). Each event is classified (for a particular appliance, at a particular time, etc.) using the K-Nearest Neighbor algorithm. Data sets were acquired across 7 households for over 6 months in the greater Seattle area, classifying over 2,500 events; thus, though information such as number of appliances and power consumption levels were known beforehand, this information were not used as inputs into the algorithms used.

In [20], Kim et al. assume that only low frequency measurements are available; the data sets acquired to test disaggregation algorithms are unlabeled across 7 households over a 6 month period as well. This work's focus is on extensions of Hidden Markov Models (HMM), such as the Factorial HMM. The advantage of FHMM's is that they can incorporate multiple potential sequences of states (i.e. activities) inferred from a sequential (i.e. time-series) data set (i.e. electricity consumption). This work also incorporates distributions of power consumption of appliances in both on- and off-states.

The work shared by Colter and Johnson in [21] includes a data acquisition process for household electricity consumption, open-source access to the data (15 kHz at household level across 10 homes for 119 days). The work also includes and implementation of a factorial Hidden Markov Model (FHMM) and an iterative HMM based on a more complex state transitions and higher order relationships between observed and latent variables. Their work tests both supervised and unsupervised implementations of the HMM variants — but only in the form of using the information on the number of consumers in the aggregated data set, not the number of appliances. Their analysis also relates disaggregated data sets to the time of day and temperature. While in [22], Jazizadeh et al. focus on a hierarchical clustering approach for unsupervised load disaggregation. This approach is meant to be data-set agnostic, with the goal of not knowing the number and density of clusters beforehand, and relies on using short-time Fourier transforms as the baseline for event detection and feature extraction. This technique is tested with 1 household's data set of current

and voltage measurements for only two weeks.

An application of a Dirichlet process mixture model on aggregated electricity data across commercial and residential sectors can yield insight and is used in [23]; such an approach is also attractive as it doesn't require a specification of the number of clusters beforehand (compared to other clustering algorithms such as K-Means). This work relies on hundreds businesses aggregated into datasets, available at 30 minute intervals in both the United Kingdom and Bulgaria. Their approach inherently does not rely on parameters being known beforehand, and uses the Chinese Restaurant Process to discover the number of embedded clusters in the data set. The drawback is that this approach lacks in specificity in its results, meaning that the exact activities aren't able to be extracted across households/businesses, but instead only clusters of power levels.

Chapter 2 establishes a method for activity-based load disaggregation from the data sets acquired, which consists of over 200 days of data measuring current and voltage of the solar panel and battery from three households' solar home systems in rural Jharkhand, India; it is expected that the approach shared herein can be useful in multiple ways. First, Chapter 2 provides methods for acquiring and analyzing large data sets with no labeled truth — which has impacts on interpreting current measurements due to quantization errors in measuring voltage across a sense resistor, and heuristics for separating load from spillage data.

Second, this approach lays the groundwork for feature selection in a load forecasting model at a household-by-household basis. Today, load forecasts are commonly used and regularly conducted by system operators at various timescales. For longer time scales, forecasts inform network investments and supply resource adequacy; for shorter timescales, forecasts inform real-time unit commitment, expected peak consumption periods, and grid operations. Inputs to such forecasts require historical consumption data, along with an understanding of the relationship of electricity consumption to exogenous variables such as time-of-day and temperature. In these cases, forecasts are typically conducted at feeder or nodal levels given the number of aggregated consumers; as a result, due to central power system's inertia, the effects of

an individual household's consumption patterns typically doesn't effect the grid in real-time. However, in a micro-grid setting, the fact that generation is reliant solely on renewables and storage and that the number of households (and appliances) is much smaller, the behavior of an individual household can affect the operation of the micro-grid. Thus, the work presented in Chapter 2 argues that capable power management devices, with the ability to learn users' electricity consumption behavior, can conduct forecasts at the household level — with analytics yielding insight on probability distributions associated with ambient temperature and fan usage along with with time of day and light usage.

And third, the work presented in Chapter 2 assesses the application of activity-based clustering techniques, using both K-Means and Gaussian Mixture Model algorithms, on rural household data sets. This effort is unique not just because of the context in which such techniques are applied, but in evaluating such algorithms' performance with a priori information on potential appliances/loads. The drawback of relying on conventional clustering techniques is their need to be initialized with the number of clusters — which in this case is the number of possible appliance combinations for an individual user (states). Chapter 2 also details the effect on initializing these algorithms with the expected cluster centers (centroids) given the possible available states for individual users. In relation to previous approaches, a reliance on more conventional clustering algorithms may be appropriate in a decentralized micro-grid with on-site computational capabilities, as the number of loads (and thus user states) are likely to be countable.

1.3.2 Review of Battery Modeling

One of the most important yet complex aspects to realistically simulate is the technical performance of batteries. In addition to representing solar power output and efficiencies/losses of electrical components in a micro-grid as described in Chapter 4, it is important to have access and an understanding of models representing battery performance — as batteries are costly and the critical component ensuring reliability in a micro-grid. As discussed in Chapter 3, of interest is to represent the underlying

electrochemical phenomena that depicts the real-time available capacity of batteries in a simulation environment. Having this capability allows for a better understanding of a battery's ability to respond under charge/discharge conditions expected in the operation of a micro-grid.

A key motivation for developing accurate battery models is to have an accurate as possible understanding of real-time availability of battery charge; inferring this value requires state estimation approaches — and having a battery management system reliant on accurate estimations is an important capability implemented in many battery installations, as it can better manage batteries and increase lifetime by limiting rates of charge/discharge and transient instances of over-charging/discharging. Real-time state-of-charge (SOC) estimation methods vary on the spectrum of simple to complex. The simplest SOC estimation approach is based on simple Coulomb counting, integrating the amount of current that has entered or exited the battery over a time interval and dividing that by the capacity; however, this approach can be inaccurate because the available capacity within a battery varies as a function of the charge/discharge rate. Furthermore, Coulomb counting does not use the battery voltage as a reference point, but calibrating the SOC with an open circuit voltage measurement when such measurements are available (which is typically after multiple hours of rest for concentration gradients of the chemical species in the electrolyte to reach a new equilibrium) can help increase measurement accuracy, given that open circuit voltage and SOC typically have a reasonable linear relationship in lead-acid batteries [24]. Yet this is also difficult, as there is no guarantee of obtaining periodic open circuit voltage measurements after hours of rest in a micro-grid, when a battery is expected to be relied upon throughout the day.

More complex approaches, which have been developed and tested for particular battery chemistries, include methods such as particle and extended Kalman filters for state estimation (due to non-linearities in battery dynamics), or conducting curve fitting via algorithmic techniques such as convolutional neural networks [24]. However, a common and recurring challenge with more complex approaches are that they are subject to over-fitting specific capacity curves, and these methodologies are typi-

cally not generalizable across even manufacturers (given slight differences in electrode materials, concentrations of active chemical species, etc.) let alone across battery chemistries [25].

The main categories of representative battery models fall into equivalent circuits, electrochemical, or analytical/mathematical. Equivalent circuit models are viewed as 'lumped' models, combining together underlying phenomena in the form of R-C (resistance-capacitance) networks. Most models view the battery as a voltage source, with various combinations of series resistances, look-up tables for voltage/resistance values as a function of the state-of-charge, and inclusion of series capacitance across individual cells. Some equivalent circuit models take into account transients through parallel R-C networks, or include diodes to represent differences during charging and discharging — as reviewed in [26] and [27].

Electrochemical models tend to be more complex, as their focus is typically on representing aspects such as reactions taking place across the cell (i.e. electrode-electrolyte interface, side reactions in electrolyte, etc.); such approaches aim to describe aspects such as diffusion, concentration gradients, and mass transport [25], [27] — and inherent is the presence of numerous parameters and partial differential equations. Electrochemical models and simulations aim to represent the "sequence of events [...] in the electrode reaction[s]", specifically the "transport of the reactant from the bulk to the electrode surface, the transfer of electrons at the electrode/solution interface, and the transport of the product away from the electrode" [28]. In [29], Park reviews and presents a detailed model describing equations for diffusion, kinetics as a function of temperature, ion drift velocities and flux, and current density — all dependent on partial differential values, constants, and battery-specific parameters for lithium-ion batteries. Another example is the 'single particle model' (SPM) for lithium-ion batteries, which reduces detailed representation of phenomena such as "local potential and concentration gradients" into a single dominant dimension, as opposed to taking into account three dimensional dynamics in a cell (which is less complex than the pseudo-two dimensional model). This is done by taking into account the flux (via Fick's Law) and the charge transfer of lithium ion intercalation at

the electrolyte-electrode interface (via Butler-Volmer equation), the latter of which dictates current density [30]. Yet key drawbacks of electrochemical-based models are that they require extensive parametrization, solving of complex, non-linear equations, and battery data — making them suffer from a lack of extrapolation and time consuming for both computation and analysis.

There has also been work on experimental validation of various battery models. In [27], Hu et al. test 12 battery models using a particle swarm optimization, comparing the root mean squared error between the predicted voltage outputs from optimized battery models with test data obtained for two different lithium-ion cells. While in [31], Tremblay and Dessaint assess the performance of the Shepherd Model, which includes a polarization constant and terms for fitting battery curves in the voltage 'exponential zones'. Their approach aims to be easily extrapolated across battery chemistries and shows accurate voltage response using the 5 parameters required — yet their approach relies on extracting (versus optimizing against acquired battery data) the parameters based on constant current discharge curves from manufacturer data sheets. Similarly, Ciez and Whitacre evaluate the cost-performance of different battery chemistries by establishing formulas for capacity losses as a function of cycle life based on data extracted from battery manufacturer's curves as well [32].

In terms of analytical and mathematical models, one of the first forays is the development of Peukert's Law, which was originally conceived in 1897 to relate the change in available capacity to the battery's charge rate (C-rate). The relationship is dependent on a dimensionless constant, which is specific to a particular battery chemistry and make [33]. However, the main challenge with relying on Peukert's Law is that it is not useful to represent dynamics of a battery under conditions that are not at constant current — typical when a battery is employed in the field [34].

As reviewed in [33], another battery model is the 'dual foil' FORTRAN program, which is based on solving six coupled, non-linear, differential equations that describe the potentials and current densities across a battery cell. Based on a load profile, the model outputs the battery's current and voltage over time — and requires detailed a priori knowledge about a battery and over 50 parameters (i.e. heat capacities,

electrode thickness, electrolyte concentrations, etc.) in order to do so. The Kinetic Battery Model (KiBaM), originally conceived by in 1993, is seen by many as the battery model with the balance of high accuracy and low complexity for modeling lead-acid batteries [33], [25]. The KiBaM was developed to mathematically represent the main electrochemical constraints of the input or output current of a battery as described above and originally conceived in [35]. Through the kinetic constraints of lead-acid battery, the KiBaM approach aims to realistically relate phenomena, specifically ion transport and diffusion during charge and discharge, by relying on a series of representative equations that discretize the available and bound charge at each time step.

Originally implemented in [35], the KiBaM can visually be thought of as a "two-tank model" to represent this concept of available and bound charge in real-time — intuitively showing the rate capacity and recovery effects of batteries. Furthermore, the KiBaM is used as the baseline for battery simulations conducted by both the National Renewable Energy Laboratory (NREL) [36] and in the HOMER software [37]. There have been additional incarnations of the KiBaM, such as modeling previous battery states using extended Markov chains or stochastic variants [33]. In one case, a spatial variant of the KiBaM is implemented to increase mathematical understanding of the effects of diffusion and migration [38], whine in another, a continuous version of the KiBaM by increasing the number of 'tanks' between the two electrodes [33].

Chapter 3 includes the details of the dynamic mathematical equations related to the real-time kinetic operating constraints (due to species diffusion and state of charge) originally developed in [35], yet the original presented in Chapter 3 is based on an adapted implementation of KiBaM. Specifically, the adaptation of the model shared here includes a method for determining the requisite input parameters for the KiBaM specific to lead-acid batteries available in India and includes constraints for maximum and minimum levels of the battery state-of-charge — a real-time battery management capability required in next generation micro-grids. The importance of estimating and managing battery state-of-charge and conveying that information to the user is of further discussion in Chapter 5.

In addition, Chapter 3 describes the evaluation and implementation of the rainflow algorithm for cycle counting in batteries, borrowing from a technique developed for the materials fatigue/degradation space as described in [39] and [40]. As discussed, approximating battery degradation is a regularly encountered challenge in the battery modeling field — but quantifying battery cycling is critical as battery cycling is directly related to battery degradation (in capacity fade) and lifetime (in cycles) [41] — and thus overall costs.

Lastly, Chapter 3 aims to address one of the shortcomings of the KiBaM, in that it doesn't explicitly take into account voltage effects and charging/discharging efficiencies, and therefore isn't reliable when considering real-time state-of-charge estimation for a battery. In the implementation of KiBaM, voltage is assumed to be constant (i.e. V=12 for lead acid batteries); this is not a realistic assumption when implementing a battery model and a state-of-charge estimation technique in the field. The original conceptualization of KiBaM does include a simple method for implementing a version of the model where voltage effects are important, but it requires knowing a handful of specific data points of a specific battery, i.e. minimum and maximum voltages during charging, discharging, and open circuit states [35]. These data points give an allowable range for the voltage values to be within during charge and discharge, and the voltage response is dictated by the ratio of the available capacity at each timestep versus the maximum available capacity — but is not a detailed enough approach to rely on.

Thus, a methodology is shared in Chapter 3, based on data acquired from a cycle of a lead-acid battery, for modeling an optimized voltage response for a given current profile — based on parameters that describe requisite IR losses and a re-evaluation of KiBaM input parameters. This approach is unique in that it can be utilized in other contexts (subject to the availability of battery cycling data). The description of the parameters and variables, brief derivation of the equations from [35], specific adaptation of the operating constraints in the model implemented, and the extension of the KiBaM as a technique for conducting real-time state-of-charge estimation are all shared in Chapter 3.

1.3.3 Review of Micro-Grid Design & Operation

For a certain level of expected demand, the work presented in Chapters 4 is critical in making a case for intelligent micro-grids designed for rural electrification; the first part of the chapter focuses on the technical representation of the remaining equipment/components in a low-voltage, isolated, DC micro-grid based on solely solar and batteries, while the second part of the chapter extrapolates the simulation to overall system costs. Depending on the task at hand, there is typically a trade off between the complexity, granularity, and the usefulness of power system models. One can start from the individual device level and physical system models to dynamically represent the state of devices/switches of a network under various operating conditions. This approach addresses issues such as understanding network stability, low-level control architectures, and appropriate sizing of components by utilizing software platforms such as Simulink and LTspice.

Operational simulation of power systems at a higher level is an active field of research, and numerous software programs and packages have been introduced in recent years that translate detailed engineering models to system design and overall economics. These software platforms, such as 'Hybrid Optimization of Multiple Energy Resources' (HOMER) and 'Distributed Energy Resources — Consumer Adoption Model' (DER-CAM), can be used to assess the sizing and model the performance of distributed energy technologies (such as fuel cells, diesel generators, photovoltaics, batteries, etc.) over a period of time in a specified geographic area.

In terms of approaches to sizing generation assets in micro-grids, there are a number of factors to consider — such as whether the micro-grid is completely isolated from the central grid, technology availability/selection, etc. In design manuals, such as presented in [42] and [43], conceptual formulations are shared on how to size micro-grid generation assets as a function of demand given expected daily and peak energy demand, battery depth of discharge, and days of autonomous operation desired. In [44], a rule-of-thumb is shared on how Mera Gao, a micro-grid company that started in Uttar Pradesh, sizes its solar and battery assets based on assumptions on average

daily demand and days of autonomous operation required (to ensure high reliability during times of low solar irradiance).

In [45], an iterative software program is developed to size the requisite generation assets in order to serve an anchor load in a micro-grid, a freezer that stores critical vaccines, with high reliability for every hour in a simulated year. Seemingly based on the data set available, this approach is based on months of data acquired of one freezer's load profile in Kenya. While in [46], another model is developed to increment solar and battery sizes if demand is not met (assuming fixed increments of 135W and 50Ah, respectively). This work includes detailed models on solar output, using an incremental conductance algorithm for maximum power point tracking (MPPT), and Simulink/PSCAD simulations for batteries and DC/DC converters — and also implements an economic model in MATLAB that makes assumptions on purchasing ability and assumes an organic topology for electricity sharing, using an example of a village in Kenya as a use-case.

Additionally, Koutroulis et al. have proposed a new methodology for optimally sizing hybrid wind, solar, and battery micro-grids using genetic algorithms and aim to more realistically represent technical characteristics associated with solar modules and wind turbines — such as tilt angle and installation height [47]. This work built upon previous work focused on optimally sizing generation assets subject to the constraint of supply meeting demand during every time period in simulation as outlined in [48] and [49]. Other approaches aim to take into account initial system costs and yearly maintenance and operation costs into the optimization of generation asset sizing [50].

In regards to operations, there has been a body of work focused on control strategies and dispatch algorithms in the context of micro-grids. For example, in [51], a new mathematical formulation is developed for operating micro-grids given uncertainty in renewable energy production using a combination of robust unit commitment with receding horizon control. And as mentioned previously, the Huatacondo micro-grid in Peru relies on a rolling horizon method that takes into account household-level preferences for prioritizing and serving a diversity of loads during 15 minute intervals [11].

With multiple generation source on a network, a number of control strategies can be employed — such as active load sharing, droop controllers, master/slave control, etc. As reviewed in [52], the efficacy of such control strategies are typically assessed using software packages that allow for implementation of equivalent circuits and detailed switching models, such as Simulink and PSCAD — but further analysis and simulations for an actual micro-grid are not included in this work. In [53], an energy management strategy is developed using adaptive fuzzy logic as the decision-making control technique, simulating agents behavior depending on the state of the system. Another approach by [54] represents automated demand response in a micro-grid, showing a simple yet idealized approach on how appliances would decrease consumption in response to a real-time electricity price in a micro-grid network.

Though insightful, there are several drawbacks in relying on these various models in designing and operating micro-grids. Most approaches lack in resolution in time-scale and ability to model aforementioned and differentiated capabilities of low-voltage, DC micro-grids with demand-side management capabilities. It is important to have a realistic representation understanding of the technical operating characteristics of a specified micro-grid software and hardware capabilities — such as the ability to illustrate electricity management system. In particular, the work presented in Chapter 4 represents the main capabilities of demand-side management — in differentiating critical/non-critical loads and providing different service levels.

Overall, this work and results presented in Chapter 4 builds and expands upon previous work in a number of additional ways. With the case study used in Jharkhand, India throughout this thesis, the simulation outputs are realistic and detailed enough to inform generation asset selection and technical operating constraints economics for the design and operation of a decentralized micro-gird with demand-side management designed for electricity access. Key and relevant technical characteristics of engineering assets in a low-voltage micro-grid network are taken into account, such as efficiency models for buck and boost DC/DC converters, wiring losses, solar module output, and battery operation.

1.3.4 Review of Micro-Grid System Techno-Economic Analyses

Analysis of system design, performance, and costs is an important area of research in the energy access space. The latter part of Chapter 4 explains how the results technical simulations for a decentralized micro-grid with demand-side management, including the optimized generation asset sizes, translates to an economic an financial analysis. There has been detailed discussion on challenges with the cost-competitiveness of conventional micro-grids cost in numerous analyses and reports, for example as conducted by the UN Foundation and others in [4]. Such analyses review micro-grid operations and costs in different geographies and countries — and are useful to assess various strategies employed by companies. Though having a qualitative and case-study based understanding is helpful for a general audience, these reports don't analyze a single micro-grid in detail, including aspects such as replacement costs, financial analysis, etc.

At a more academic level, a good portion of the literature does extrapolate technical simulations into economic analyses and financial results — again, as in HOMER and DER-CAM. As discussed in [45], the analysis on iteratively sizing generation assets in order to serve a critical load such as a freezer with high reliability does show the cost of providing higher quality of service — but doesn't fully extrapolate the analysis from an investment point of view for a company or entrepreneur. Another approach, as shown in [44], has been to use Monte Carlo simulations to illustrate the effects of level of demand, equipment and balance of system costs, and maintenance on financial viability of Mera Gao's operations, a micro-grid company in northern India [44].

Additional work has focused on optimizing selection of inverters and solar modules for AC micro-grids, as conducted in [55]. Based on a linear program, the model outputs the least-cost combination of equipment (i.e. inverter, array size, electronics, etc.) for an isolated solar system. In [56], Chaurey and Kandpal compare cost-effectiveness of solar home systems versus micro-grids. Their work highlights aspects

such as detailed cost tradeoffs (initial and operational) in implementing home systems versus micro-grids, appropriate capital subsidies from the government, and energy service company margin requirements — and rely on hourly simulation outputs from HOMER.

Furthermore, a number of research efforts have focused on analyzing techno-economic feasibility of micro-grids, ranging from purely renewable energy, isolated systems to hybrid, grid-connected systems. Many of these efforts analyze various combinations of generation technologies, levels of electricity demand, and cost sensitivities in a particular use case. For example, Han et al. develop a planning model that evaluates the economic performance of grid-connected micro-grids under various financial arrangements, specifically solar subsidies and tariffs, from the perspective of a micro-grid operator [57].

In terms of case studies, Akinyele and Rayudu analyze the production, reliability, and economics of numerous solar-based micro-grids in Nigeria — incorporating a yearly demand growth factor of 2% into their analysis [58]. While Thomas et al. conduct hourly simulations for a year (8760), creating synthetic solar irradiation data sets and notional estimates for demand, for various configurations of a hybrid wind-solar-battery-diesel micro-grid serving communities in an island off the coast of Greece — using HOMER to evaluate the state-space of possible configurations [59].

In addition, Bhatt et al. analyze a hybrid micro-grid system (i.e. micro-hydro, solar, biomass, biogas, diesel, and battery) in Uttarkhand, India. Using HOMER, their results show various configurations and sizes of generation technologies, serving five villages' demand — which include seasonal and productive loads such as mills [60]. Relatedly, Alireza et al. also look at the techno-economic feasibility of a hybrid micro-grid in rural Colombia. Using HOMER as well, their work focuses on a hybrid solar and diesel combination for a particular village, and share demand estimation and cost sensitivities for electricity service provision [61].

As is clear from the discussion above, there has been significant work in techno-economic modeling for micro-grids to-date, but most approaches either rely on existing micro-grid modeling software and apply them to a specific use-case, or are not

holistic in their approach in the design and simulation of a micro-grid's performance. To the former point, the optimization of sizing the generation assets (i.e. solar panels and battery capacities), and associated costs, are calculated in a transparent manner herein, and with an understanding of sensitivities in the assumptions made — technical, economic, or financial. To the latter point, approaches today make notional assumptions of electricity demand and desired (versus realistically available) distributed generation sources in a certain region, which is inherently less realistic.

The work presented in Chapter 4 aims to address these issues and highlights key results. In order to understand the value of micro-grids with demand-side management in the context of electricity access in the developing world, Chapter 4 takes and then extrapolates the technical simulations into system economics in order to highlight specific aspects in more detail and answer questions of interest. The combination of both real-time operation and optimization of generation asset sizing for such micro-grids is the novelty of the approach taken herein. In addition, Chapter 4 takes into account the effects economies of scale of larger solar panels and batteries have on costs —- in $\$/W$ and $\$/kWh$ respectively — based on an exponential fitting of values seen by distributors in Jharkhand, India. As opposed to static per-unit prices, this is a key parameter to include in order to fully realize the cost benefits embedded in a realistic modeling approach built around the idea of minimizing solar and battery asset costs in micro-grids — an aspect also included in [44].

As explained in Chapter 4, the output of the technical simulations of available solar/battery combinations is then fed into an optimization heuristic; through a search methodology, this process selects the cheapest available solar module / battery capacity combination for installing a micro-grid with demand-side management based on requisite reliability constraints (thresholds) for serving both critical and total load profiles over hourly time-steps for a simulated year; this is a key assumed capability embedded in power management devices in the form of load disaggregation, sensors, and communication. The final results show that for a given set of cost/financial assumptions, how the economics of such advanced micro-grids enabled through power management devices compare to readily available technologies in solar home systems

and conventional micro-grids. Furthermore, the work herein uses the state of Jharkhand, India, specifically the rural areas surrounding the city of Jamshedpur, as a reference point for analyses, but the structure of this comprehensive techno-economic modeling approach can be extrapolated to other contexts given changes in input assumptions such as solar irradiance, demand profiles, and equipment availability; a version of the entire model is made available online for use by interested parties and practitioners by following instructions in [62].

1.3.5 Review of Policy Implications Related to Price, Reliability, & Quality of Service

With the context of the technology, model, and system economics in mind, Chapter 5 focuses on the social and policy implications of price setting in such electricity networks designed for rural electrification. As is discussed at length, the notion of implementing electricity tariffs that are cost-reflective is far from reality in India — and the need for significant price reform and for implementation of regulatory unbundling as outlined in India's Electricity Act of 2003 has been studied and argued by many, such as in [63],[64], and [2].

Another capability of next generation power management units is to be able to convey information, i.e. the state-of-the-system to the end-user along with some notion of a real-time electricity "price" or "balance", and to receive signals from end-users. There has been a fair amount of previous work understanding users' ability and willingness to respond to a signal in advanced micro-grids in the context of the developing world. In the case of using rice-cookers in Bhutan [12], the GridShare project included an LED indicator, based on the bus voltage, to convey whether the system was strained during periods of peak demand (caused by the usage of electric rice cookers). In the Huatacondo micro-grid in Peru, a demand-side interface was installed at every household to similarly convey the state-of-the system to the user (i.e. voltage, frequency deviations from nominal set points) — and the rolling horizon approach implemented takes into account potential shifts in electricity consumption

due to a behavioral response from the signal [11].

Given the small number of users in micro-grids and the potential for such power management devices devices to be installed at the household level, notions of household-level reliability preferences are critical questions that remain to be understood for the successful operation of micro-grids with demand-side management capabilities. The successful implementation of such a dispatch strategy, especially one relying on a behavioral response from the user, inherently relies on understanding load prioritization, notion of demand elasticity, and willingness-to-pay. Access to this information will require preferences at the household level within each village, and has been the subject of related work.

The concept of demand elasticity at the household level (versus a macro-economic understanding based on longer term trends such as GDP, population growth, etc.) in relation to electricity is important to understand, as a rigorous understanding can shed insight on cross-price elasticities (i.e. kerosene, LPG) and the effects of aspects such as income, region, household size, etc. on consumption. Not only is this concept important in micro-grids, it is also important to understand as distribution utilities in India hopefully moves towards variable tariffs that are cost-reflective. Filippini et al. acquired data on 30,000 urban households and estimated the econometric effects of parameters such as season, income, and household size on electricity consumption. Their results found that a 1% increase in income had a a stronger effect on consumption than a 1% increase in price — but that both variables were relatively inelastic [65]. In related work, Haipriya sampled data from 100,000 households and examined the price and expenditure elasticities across energy types (i.e. wood, fuels, electricity), urban versus rural, and income strata [66].

Additional work has focused less on large quantities of aggregated data, but on a more nuanced understanding through focused surveys to gain insight on user experiences, reliability preferences, and willingness-to-pay. TERI conducted an analysis in the Indian states of Haryana and Karnataka to assess industrial, manufacturing, and agricultural consumers' quality of service and the cost of non-served energy. Understanding the cost of non-served energy can be a useful proxy for valuation of reliability,

and can be estimated by valuing the production lost per kWh not served, the cost of alternative energy sources, and the willingness-to-pay for reliable electricity supply. Through a survey of 500 manufacturing companies and 900 farmers using electric water pump sets, TERI estimated Rs./kWh in cost of non-served energy across the three methods — and extrapolated them to economic losses at the state level [67].

With more of a rural residential focus, Gunatilake et al. surveyed over 2,000 households in Madhya Pradesh (across 40 villages in 2 districts) — both grid-connected (roughly 8 hours per day of service) and off-grid. The main challenge in Madhya Pradesh, as in many states, is that a transition towards cost-reflective tariffs requires a separation of agricultural (for water pumping) and residential feeders along with an understanding of willingness-to-pay for higher quality of service. A detailed understanding of willingness-to-pay in the context of a village requires a rigorous academic approach, such as the utilization of contingent valuation methods. As seen in previous work, the work shared in that effort uses a regression to identify impact of explanatory variables on willingness-to-pay [68].

Regarding assessing existing off-grid electricity service, Columbia University conducted a randomized control trial of 1,500 households in the Barabanki District in Uttar Pradesh, an area where the company Mera Gao has a number of micro-grid electricity service subscribers (2 LED's and 1 mobile charging point for Rs. 100 / month). Of interest that for the households surveyed that were existing subscribers, all of them chose Mera Gao's service due to the quality of lighting (and less so for mobile charging or saving fuel); furthermore, over 70% of the lighting usage was for outdoor lighting — and that majority of current subscribers wanted additional services such as fans and television sets, but for the most part were not willing to pay for additional services [69].

In addition, in [70], willingness-to-pay surveys and activity preferences analyses were conducted in Ghana to show the differences in proportion of income spent on electricity across income groups, and the variance of activities and individualized use-cases of electricity. And in [71], the argument is made based on the implementation of a hybrid micro-grid in Andhra Pradesh that both subjective (i.e. contingent valuation,

price-response surveys across literacy and income levels in a particular locale) and objective (i.e. substitution costs, avoided costs, demand curves) methods need to be combined to properly assess both ability and willingness-to-pay.

There has also been work focused on surveying users' preferences across appliances and tiers of service. For example, in a 120 kW solar micro-grid in West Bengal serving nearly 200 households, Kobayakawa and Kandpal analyzed load consumption data based off of the two tiers of service; one tier had a 3-point connection with an initial payment of 1,000 Rs. and a monthly payment of 100 Rs., while the other tier had a five-point connection with an initial payment of 1,500 Rs. and a monthly payment of 150 Rs. Their work identified consumption patterns based on a number of factors, but were unable to assess the impacts on having a variable (versus flat) electricity tariffs [72]. In Senegal, Camblong et al. surveyed 34 villages across 3 regions to identify willingness-to-pay across four service levels, ranging from 2-3 CFL lamps and a radio, to 8 lamps, a radio, a television set, and other devices [73].

Chapter 5 focuses on the regulatory and political economy challenges associated with India's public distribution companies, in regards to quality of service and electricity tariffs — and the need for clear interconnection policy to further encourage private sector activity. Chapter 5 also dives into the concepts relating to how next generation micro-grids can compute and convey some level of a dynamic electricity 'price', potentially pegged to the battery's state-of-charge. A detailed price-elasticity analysis at a household level may be difficult to acquire and utilize in terms of dispatching electricity in a micro-grid with demand-side management capabilities in real-time; however, the provision of tiered electricity service based on load prioritization and incorporating willingness-to-pay / pay-as-you go strategies may be a more feasible approach. Furthermore, similar to automated demand response efforts taking place in developed world power systems, such an approach could focus on integrating appliance/activity level preferences in forecasts, scheduling, and dispatch. As analyzed in Chapters 2 and 4, the ability to disaggregate loads and provide levels of reliabilities across critical and total demand profiles can lower the costs of micro-grids, so aiming to answer the realities of how these questions play out on the ground is

necessary to further support — or challenge — the value of decentralized micro-grids with demand-side management. From a social science perspective, sensitivities on the effects of curtailment, ability for users to understand signals that convey the state of the system, and individual appliance preferences all need to be further understood.

Chapter 5 also extends the concept of tiered electricity services in isolated micro-grids by relating the available charge in the battery. Similar to the concept of conducting unit commitment based on least-cost generation in centralized power systems, the available state-of-charge range of a battery can be broken up into thresholds; during periods when the state-of-charge is low lower, the system is more strained, and less available energy is allocated to each household. Chapter 5 also imports relevant concepts from the telecommunications industry for consideration. At the onset of information and communication technology services decades ago, internet service providers offered various service offerings for customers to choose from based on willingness-to-pay [74]. Analogous to discussions in demand growth in the electricity access field, users had the option to increase their service demand (i.e. bandwith, speed) over time, and ISP's responded by allocating available resources to meet service level requirements demanded by consumers [75], [76].

1.4 Conclusion

The work presented in the subsequent chapters is designed to generate insight on the design and operation of next-generation, decentralized micro-grids with demand-side management capabilities. As this chapter discusses in detail, there are numerous previous research efforts across relevant topical areas, such as demand modeling and micro-grid techno-economic analyses. In relation to previous work in demand modeling and classification, Chapter 2 presents a methodology for acquiring, calibrating, and analyzing load profiles based on electricity data from home systems in rural Jharkhand. The work both extends activity-based models at the household level to feature selection in load forecasting models, and assesses the performance of using clustering algorithms for conducting load disaggregation. Chapter 3 focuses on adapting

and extending a popular battery modeling framework, in the Kinetic Battery Model (KiBaM) for lead-acid batteries. This builds upon previous battery modeling efforts in adapting the KiBaM to include battery management constraints to mitigate periods of over charging or discharging — an important capability assumed in micro-grids with demand-side management. Furthermore, an extension of the KiBaM for use in real-time battery management systems based on an optimization technique of parameters that accurately reflect the voltage response of the battery given a current profile.

For a certain level of expected demand, Chapter 4 discusses the integration of the remaining technical components, network architecture, equipment costs, and financial analysis in determining the value of decentralized micro-grids with demand-side management capabilities — a unique contribution in relation to previous system-level analyses on micro-grids. Again, the main reason for choosing a decentralized approach for micro-grids, on the order of 5-10 households, is to consider bottoms-up electrification where individuals can potentially invest (and earn) in their own electricity infrastructure. However, this only makes sense to do so if there was a cost advantage and autonomous operation — two aspects aimed to be shown in simulation, with key results shared in Chapter 4 for a use-case in rural Jharkhand, India.

With the model framework and results presented, Chapter 5 outlines key policy and social issues that need to be addressed and understood in order to enable such micro-grids in the context of off-grid electrification — with a focus on the state of Jharkhand, India. Though the value for incorporating demand-side management, in load differentiation, prioritization, and curtailment, is presented in Chapter 4, the social impacts of real-time operation are yet to be fully understood and need to be rigorously tested. Furthermore, a number of regulatory hurdles need to be addressed, such as the potential for dynamic 'price' setting and eliciting user responses, in such micro-grids. And lastly, Chapter 6 concludes with a summary of the work presented herein, along with areas for future work.

Chapter 2

Constructing Activity-Based Consumer Demand Profiles Based on Load Disaggregation and Statistical Learning Techniques

2.1 Introduction

Expectation of electricity demand to be served is the key driver in design choices in any power systems, as it dictates the sizing of generation assets and real-time operation. Access to electricity demand data at any resolution has proved to be relatively challenging in any context. Though various metering technologies and initiatives are prevalent throughout the developed world, access to data sets from utilities are limited, likely for privacy and security reasons. As this Chapter will discuss in more detail, there are two main methods for constructing load profiles. One is a more deterministic approach, based on extrapolation of qualitative surveys — which is a standard approach relied upon in the electricity access community today. Another approach is to take historical electricity demand data, but key aspects related to temporal frequency, duration, and resolution (i.e. feeder, household, etc.) dictates

its usability and the types of inference and information that can be learned from such data sets.

2.1.1 Examples of Quantitative Electricity Consumption Data Sets in Developing World Context

In the developing world, access to logged historical electricity consumption data sets at a household level and at a high enough temporal resolution are rarely available. Utilities in India undoubtedly have some information on electricity consumption, but this is a function of the utilities' competence, technology infrastructure, time/spatial resolution, and back-end data processing techniques; to-date, many utilities' data are read manually and transcribed by hand. As an example, Figure 2-1 shows an example of feeder-level data at a monthly timescale from a distribution utility in Jharkhand, India; the figure shows monthly energy consumption levels across connections to this particular local feeder, which includes a local college (the largest consumer), temples, and numerous households. The ideal use cases of such data at such scales for distribution utilities are to identify theft, bill consumers, inform electricity procurement decisions, and plan for future supply adequacy.

In the electricity access space, there are a number of use cases for logged electricity consumption data; for example, equipment providers are interested in understanding whether home systems are over- or under-sized (or over-/under-utilized). Conducting household level analysis is useful to understand appliance usage patterns; in contrast, the sheer number of consumers connected to a distribution feeder makes such analyses challenging. However, micro-grids typically have a countable number of consumers connected, along with the number of appliances — meaning that there is likely an increase in heterogeneity across users' consumption patterns, and an individual user's load activity can affect the operation of the micro-grid. Furthermore, isolated micro-grids solely dependent on renewables such as solar are unable to rely on 'slack' power back-up that would be available from an interconnected grid. The potential for integrating demand-side management and network control (through sensors, commu-

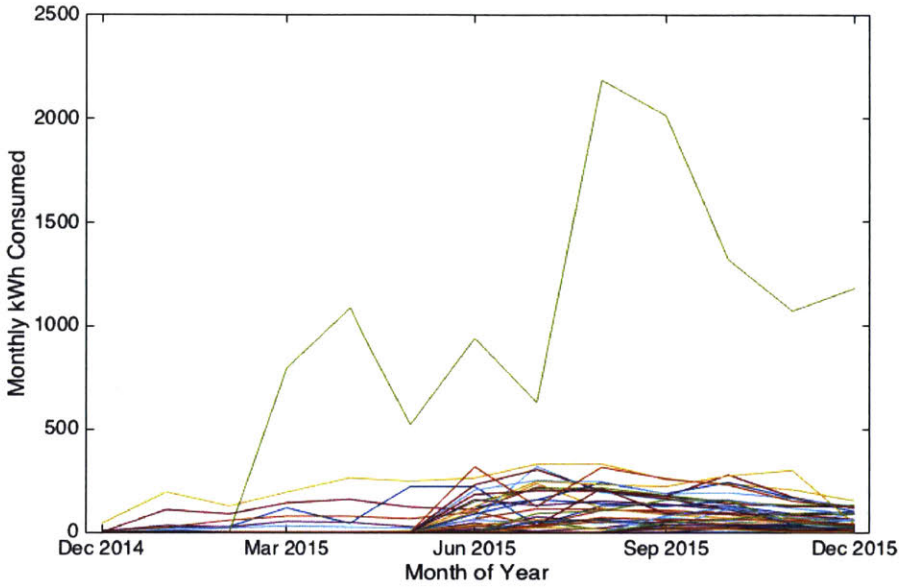


Figure 2-1: Monthly Load Profile, Rural Feeder, Distribution Utility in Jharkhand, India

nication, power management, and algorithms for load forecasts/electricity dispatch) can help mitigate such issues expected in real-time micro-grid operations.

Data sets on electricity consumption in the developing world, especially in rural, off-grid areas, has been the subject in related work, such as with a freezer anchor load in [77] and the development of a remote monitoring software/hardware platform for solar home systems in [10]. On average, data sets on electricity consumption are not widely available; thus, along with the aforementioned points, these were the driving motivations in acquiring raw electricity consumption data sets. In coordination with Tata Steel's Rural Development Society (TSRDS), data loggers were installed in protected enclosures and connected to solar home systems (powering lights and fans) in three rural households without electricity access outside the city of Jamshedpur, located in the Indian state of Jharkhand. The remainder of this chapter focuses on the data acquisition process and analytical techniques used to gain insight on activity-based electricity consumption based on load disaggregation clustering algorithms.

2.2 Data Acquisition Context, Process, & Calibration

In this work, over six months of both solar panel and battery current and voltage, plus the ambient household temperature data were acquired with a temporal resolution of 1 minute. These data sets are used in the analysis conducted and presented herein; for simplicity, one of the three household's datasets is analyzed for the purposes of this paper. To facilitate others to apply other or similar techniques to these or larger data sets, the MATLAB code for loading, visualizing, and conducting basic analysis on the household datasets is available online via accessing [78] or [79]. Due to the fact that only three data loggers were installed in solar home systems in one particular village, any sort of statistical significance or generalized claims on consumption or behavioral patterns associated with users' demand profiles are not claimed; rather the goal of this effort is that the data acquisition process and insight gained will be of value to other practitioners. Furthermore, only one household's data set is analyzed and presented herein, though similar methods can be applied on the other two households' data sets. At the onset of this analysis, it is important to explicitly point out that the load profiles for each household were not measured directly, but rather had to be inferred based on the available solar and battery data; this presents some challenges in identifying what was truly electricity consumption versus spillage from solar power production (or self-discharge from the battery) that is addressed in detail in the following sections.

Each household wherein a data logger was installed was constructed of dried mud with corrugated metallic rooftops and was without windows; this allowed the interiors of the house to be slightly cooler than the ambient air temperature but also made the homes quite dark throughout the day. In terms of size, each of the households were no more than 100 feet squared — essentially one large room — mainly consisting of a wooden bed and in some cases, shelves for storage. And in terms of location within the village, most of the households only door opened into an outdoor common area that

was rectangular in shape and surrounded by 5-6 households of similar dimensions; these common areas, seen throughout this and other villages in the area, is where a hamlet of neighbors and families could congregate for cooking, drying food crops, or manually milling grains/rice into flour. These details are important to keep in mind as these qualitative aspects likely influence the placement and usage patterns of the appliances.

2.2.1 Description of Solar Home System and Data Logger Configuration

The solar home systems installed in these rural households were designed and made by Tata Power Solar, which is a provider of off-grid solar home systems in India. The system installed in each household included with a 70W (12V) solar panel, a 75Ah (12V) battery, four 9W CFL lights, and one 14W fan — all operated in DC (direct current) and connected to an analog-based charge controller hung from the wall in each household. As depicted in Figure 2-2, each data logger used for this research purpose was an off-the-shelf 16-bit voltage analog-to-digital data logger, equipped with ample memory and battery storage to power operation and with a +/-20V range. The data logger was acquired *CAS Data Loggers*, specifically the VersaLog DCV-2 voltage data logger; additional details of the data logger can be found in [80].

In order to measure current, 20 $m\Omega$ sense resistors were used in series with each household's solar panel and battery — and converting from the 65,536 (2^{16}) available digital reading values gave a resolution of $\sim 0.31mV$. Given that the nominal voltage of the system was 12V, a voltage divider was not required given the voltage input range of the data logger used here.

2.2.2 Signal Processing & Calibration of Raw Data Sets

Current and voltage were recorded for both the solar panel and battery, along with an on-board thermistor to measure ambient temperature — utilizing 5 analog input channels of the data logger. The layout of the connections of the four analog input

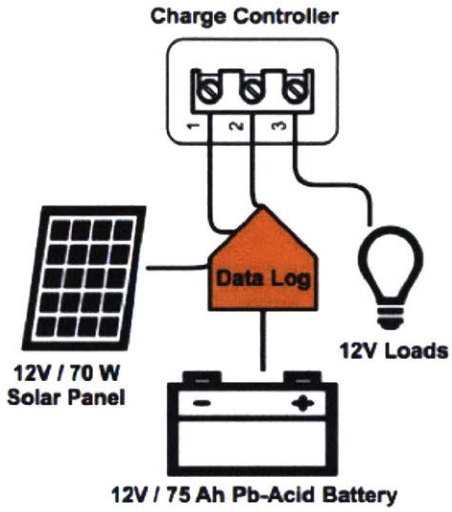


Figure 2-2: Layout of Data Logger Connection

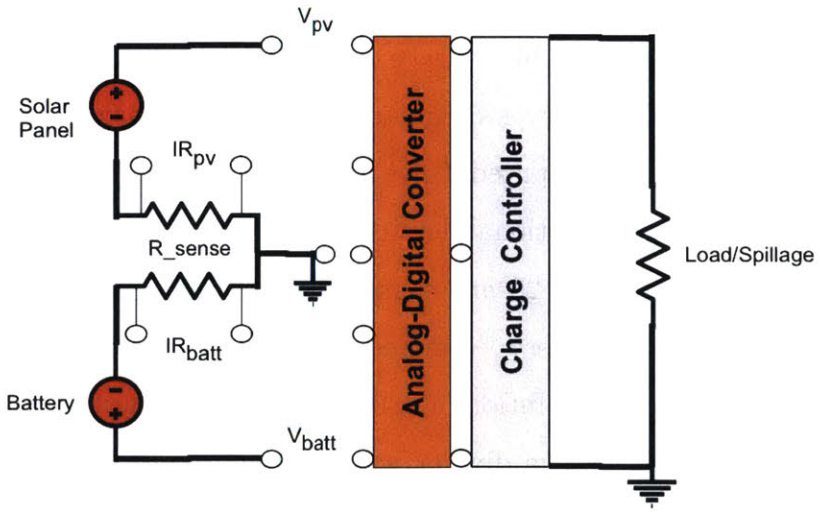


Figure 2-3: Circuit Configuration for Data Acquisition

House Number	1	2	3
Solar: ZV	32786	32776	32771
Solar: Δ	-0.0181098	-0.018034	-0.0184049
Battery: ZV	32785	32777	32771
Battery: Δ	-0.01779	-0.01845	-0.018519

Table 2.1: Values for Current Channels Calibration Process

channels for current and voltage, including the sense resistor, is shown in Figure 2-3. From the raw data sets, the power values (in watts, at each time step of one minute) could be determined by first multiplying the respective instantaneous current and voltage measurements from the solar panel and the battery. The digital values outputted from the channels for the solar and battery could be directly read in as voltage values, but the current channels needed to be calibrated based on the voltage drop across the sense resistor at different currents. Before data logger installation, a series of experiments were conducted before to determine the conversion from digital readings to Ampere values for each channel used to measure current, and thus for each data logger.

Each analog-to-digital (ADC) input channel reading current (2 channels per data logger, and 3 households total, making for 6 channels), were measured against 4-5 current draws (including a reference zero value) to develop a linear relationship from the digital reading from the data logger to a usable current value in advance of installation; the values obtained and used in the calibration process are shown in Table 2.1, with the final current value ($I_{i,c,n}$) calculated based on the difference between the digital reading ($DR_{i,c,n}$) and the zero value ($ZV_{c,n}$), multiplied by the slope ($\Delta_{c,n}$, change in current value over the change in digital value) — per data point (i), per channel (c), per household (n):

$$I_{i,c,n} = (DR_{i,c,n} - ZV_{c,n}) \times \Delta_{c,n} \tag{2.1}$$

It is important to note the slight difference in the approximate slope and the selec-

tion of zero values for the current channels based on the experimental readings taken before installation; regarding the zero value, for a 16-bit data logger, it should ideally be in the middle of the available digital range, $2^{16}/2 = 2^{15} = 32,768$. Quantization errors may be present in any analog-to-digital signal process, as the analog-to-digital data converter (embedded in the data logger) is processing continuous-time variables into discrete values across the available range. For explicitly analyzing the choice of the latter value, this can be done via the solar panel's output current, given that the current should only be positive. An example of a household's solar current readings are shown in Figure 2-4; the top histogram illustrates that there is clearly a skewed distribution around both sides of the selected zero value of 32,786 — re-enforcing it's approximation for the true zero value and that the digital values are, for the most part, on one side of the zero value given that the solar current is expected to be only positive.

After calibration, this translates to a similar distribution around the zero current value, with a minimum value at -0.4 Amperes. For the purposes of this analysis, any values greater than 32,786 (which would translate to negative current values) were not removed, but rather replaced with 32,786 given that any subsequent analysis relying on negative values for the solar panel's current would not make sense. A similar approach can be taken to analyze the battery values, with the same outputs shown in Figure 2-5; given that the battery current fluctuates between positive and negative for charging and discharging, the distribution of digital and calibrated current values are multi-modal and on both sides of the zero value — making it more challenging to analyze the selection of the referenced digital zero value.

2.3 Methods for Separating Load from Spillage

As described above, after the calibration process for the current channels, the energy values were determined by multiplying the respective solar and battery current and voltage. Though the consumption from the loads was not measured directly, it could be inferred given these two values and subject to some assumptions and methods

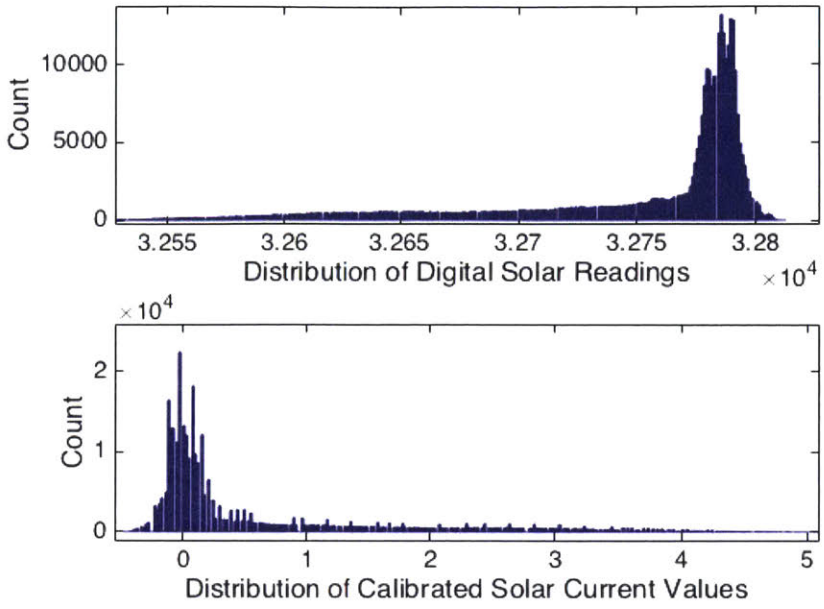


Figure 2-4: Distribution of One Household's Solar Current Digital Readings and Calibrated Values

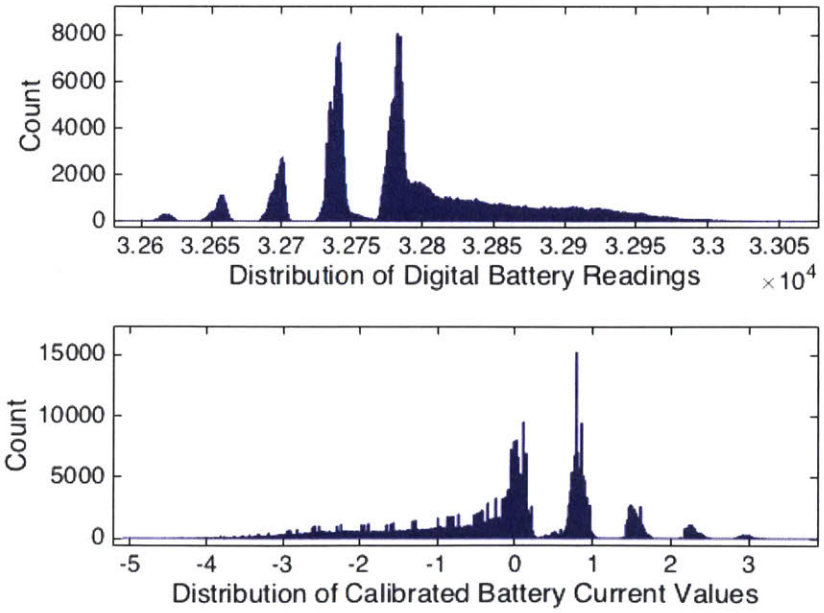


Figure 2-5: Distribution of One Household's Battery Current Digital Readings and Calibrated Values

further explained here. To determine the amount of load at any given data point, the amount of load needs to be extracted from the solar and battery data sets; for reference, an example of calibrated current and raw voltage readings, for both solar and battery, are shown over a week in Figure 2-6 and Figure 2-7 — and for simplicity, consistency, and interpretation purposes, examples from the July-August 2015 time frame of the data sets are shown in subsequent plots (as opposed to the entirety or random slices of the data set).

This section proposes two different methods for separating the load from the spillage. The first method is based on analyzing the solar and battery data — and is a more direct approach and will be referred to as Method 1 for the remainder of this chapter. However, a second method is also considered, in this case assuming that the solar and battery data sets are unable to be separated; if the data was not separated at the onset, this method requires basic assumptions to be made about the load consumption habits and knowledge on the appliances. Both of these methods for determining and then separating spillage are described in this section, with the comparative effects on the shape of probability distributions associated with appliance usage described in the subsequent section. Note that the possibility of self-discharge from the battery is neglected as this typically happens when a battery is sitting idle and not in use for extended periods of time — which is not the case as these batteries were cycled nearly daily as shown in Figure 2-7.

2.3.1 Method 1: Directly Analyzing Solar & Battery Data

For Method 1, Equation 2.2 is used as a baseline to separate whether the power (in watts, with a time step of one minute) from the solar (PV_n) or the battery (B_n) was consumed by the loads present in the home system (L_n), or if the energy was spilled (S_n, 'spillage'), per data point (i) per household (n).

$$PV_{i,n} + B_{i,n} = L_{i,n} + S_{i,n} \tag{2.2}$$

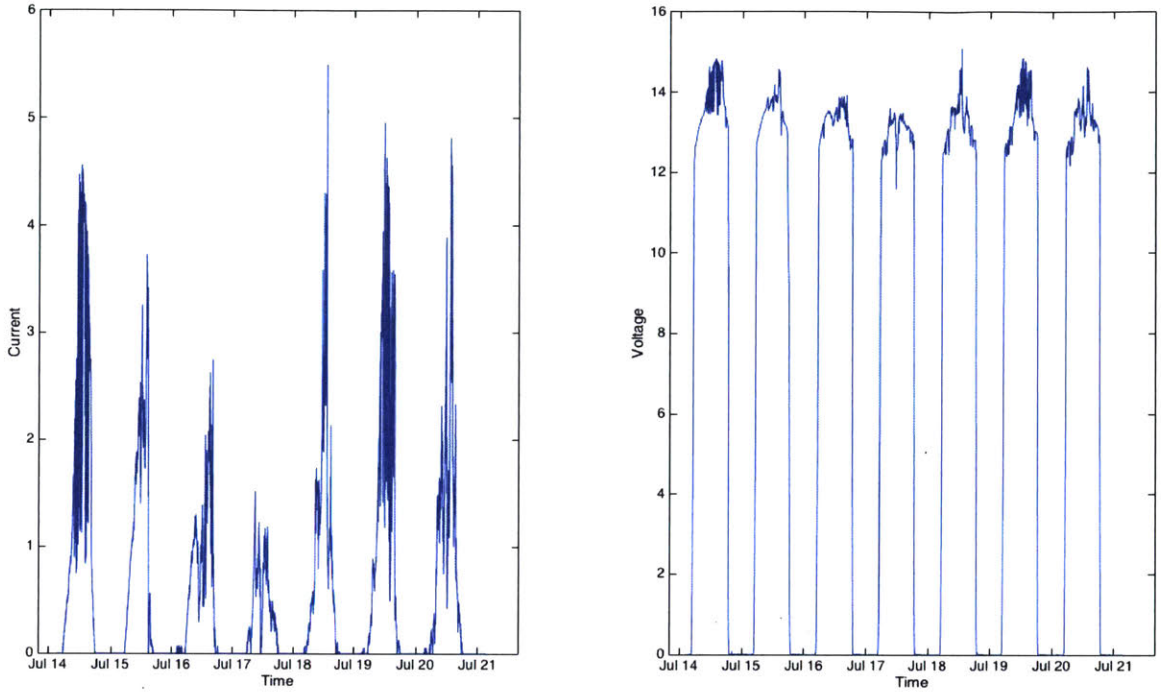


Figure 2-6: Example of Raw Solar Current and Voltage Readings (One Week)

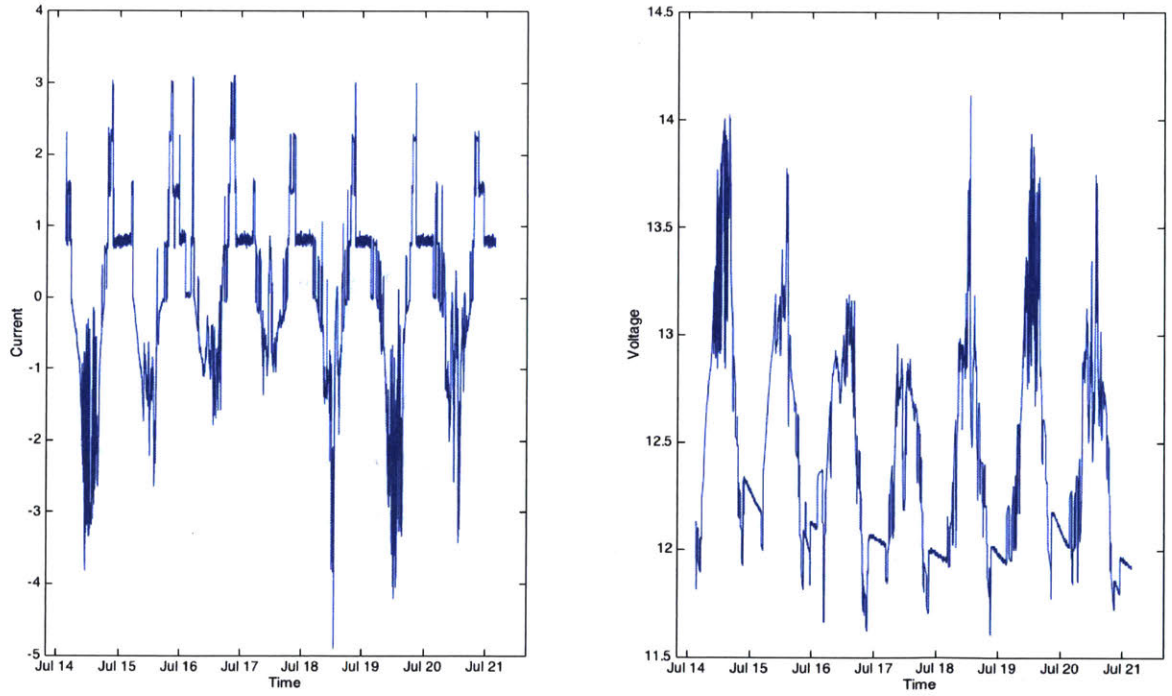


Figure 2-7: Example of Raw Battery Current and Voltage Readings (One Week)

Equation 2.2 can be interpreted in four distinct cases, noting again that the solar panel energy values could only be positive, and that the battery energy values could be positive (discharging) or negative (charging):

- **Case 1:** $PV_{i,n} > 0$, $B_{i,n} = 0$: None of the solar energy being produced is entering the battery, either because of the presence of a daytime load or that the energy is being spilled.
- **Case 2:** $PV_{i,n} > 0$, $B_{i,n} < 0$: Solar energy is being produced and is charging the battery. If these two values are equal, then there is no spillage or load — but if these two values aren't equal, then there is spillage present.
- **Case 3:** $PV_{i,n} > 0$, $B_{i,n} > 0$: Solar energy is being produced (potentially at low levels) and the battery is also being discharged into the load.
- **Case 4:** $PV_{i,n} = 0$, $B_{i,n} > 0$: No solar energy is being produced, and the battery is being discharged into the load.

In order to fully separate the load from the spillage, Cases 1 and 2 need to be addressed, as Cases 3 and 4 can directly be classified as load when the battery is discharging. Figure 2-8 shows an example of a month of both the calculated solar and battery power data in the top plot, and the classified spillage in the second plot based on the criteria identified for Case 1, and the third plot for Case 2. Without labeled truth for these data sets, Cases 1 and 2 present a challenge as they can either be spillage, or solar power instantaneously serving a day-time load. For the example month time frame plotted, Case 2 follows the shape and expected hours that solar power is being generated — and does clearly not equal the amount of power charging the battery — making it more likely to be spillage. However, this is less clear for Case 1, as it follows a less regular pattern (if any).

To assess this claim, the relationship between solar power and Case 2's spillage (via a linear regression) is plotted in Figure 2-9. With a correlation coefficient of 87.31% (R^2), this figure shows that there is a strong relationship between the solar power production and the values classified as spillage in Case 2. In contrast, the R^2

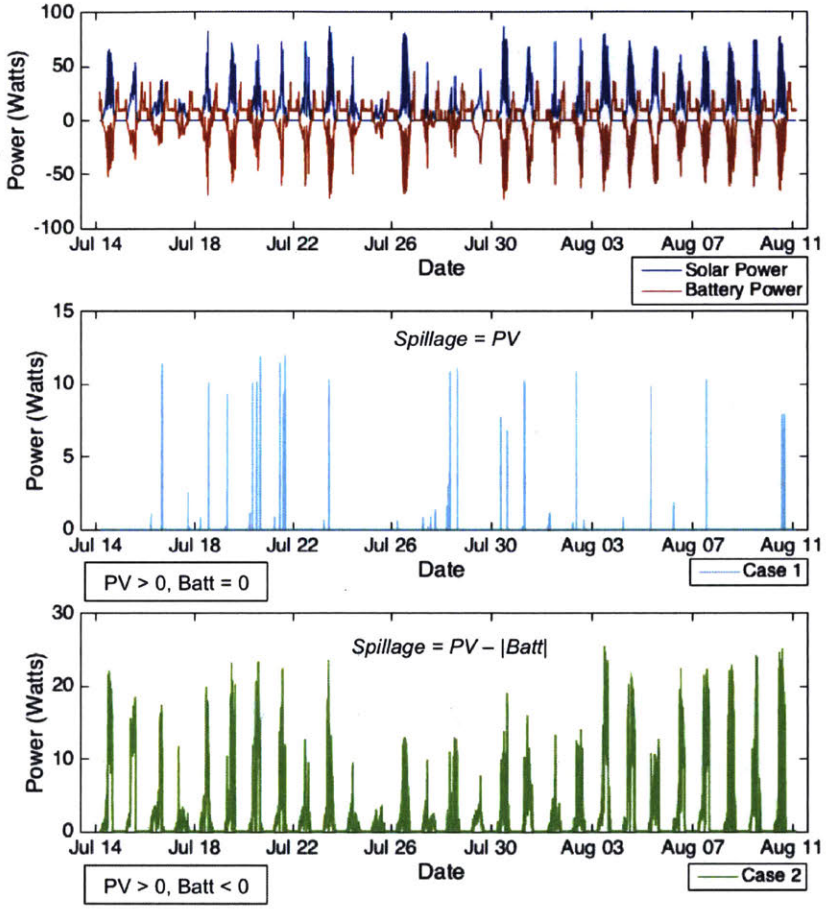


Figure 2-8: Method 1: Example of Calculated Solar, Battery, and Spillage Power Data (One Month)

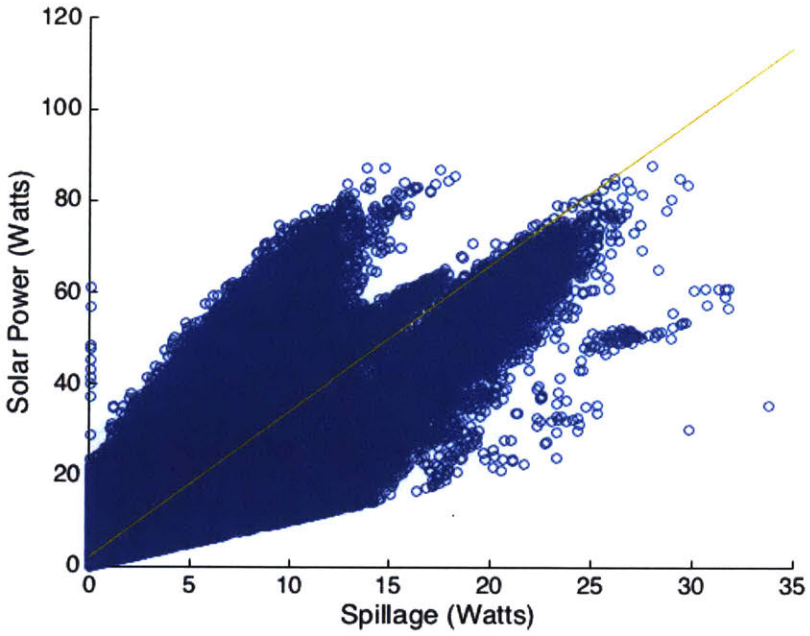


Figure 2-9: Method 1, Case 2: Spillage Correlation with Solar Power Production ($R^2 = 87.31\%$)

value for Case 1 is -0.66% — essentially no relationship between the periodic nature of the solar power production and the generation of Case 1's spillage. And in aggregate for Method 1, integrating over the entirety of the data set, 1.2691×10^4 watt-hours were spilled — with 99.55% of the spillage coming from Case 2. This shows that Case 2 not only has the strongest relationship in reference to the solar production, but it also accounts for nearly all of the spillage. For clarity and for the purposes of the subsequent analysis, the load profile data for Method 1 is separated from both the Case 1 and Case 2 results of spillage.

Without empirical evidence, there could be two logical explanations for this amount and pattern of spillage shown in Case 1. First, as shown in Figure 2-3, the power from the solar panel is measured in advance of the charge controller and thus the measurements on hand are not taking into account efficiency losses associated within the charge controller. The efficiency of any converter is a function of a number of factors, with an example of DC/DC converter efficiencies discussed in Chapter 4. As an example, a well-designed, off-the-shelf charge controller, with on-board maximum power point tracking to optimize battery charging current, is on the order of 90%-95%

[81] [82]. Second, the charging efficiency of the battery can be another source of this mismatch. As explained and analyzed in Chapter 3, a battery's charging resistance increases as a function of the state-of-charge — and the battery is more likely to be at a high state-of-charge during periods when the sun is shining. Furthermore, the ability for a battery to store energy is also a function of the charge rate (C-rate) due to internal electrochemical dynamics of a battery. If the battery is seeing a relatively high C-rate, which is likely the case during periods when the sun is shining, not all of the energy will be able to be stored — especially with a sub-optimal design of the charge controller, which may have been the case in such older solar home system models. More detailed explanations, models, and simulations of lead-acid batteries are discussed in Chapter 3.

2.3.2 Method 2: Separating Combined Load & Spillage Data

Given that the focus here is to analyze the load profiles, another potential option worth considering as a secondary check is if only the load and spillage data were aggregated together; this would be relevant in instances without previous information on the raw solar and battery data sets, i.e. the right-hand side of Equation 2.2. In this situation, and given the lack of labeled truth to these data sets, another heuristic needs to be used based on information known about the loads. As discussed in the subsequent sections and shown in Table 2.2, the loads in these home systems (and thus potential combinations) are known beforehand — specifically in light and fan expected power consumption levels. The key goal is to separate the day-time load usage from the spillage, which only happens during the day.

The solar energy data set measured can be used to *roughly* back-calculate the solar irradiance, which could be determined as the nameplate panel capacity ($70W$), efficiency (15%), and thus area ($\sim 0.467m^2$) were all assumed to be known for this system. However, this inferred irradiance may be inaccurate due to reasons such as sub-optimal positioning, angle of solar incidence, cell temperature, and potentially shading. Using a historical average solar irradiance data set obtained from NREL for Patamda, Jharkhand (the nearest peri-urban area to the village) over the exact

same time period (i.e. June—February) [83], the next step was to integrate across the both data sets to obtain total solar energy incident over the same time frame. The ratio of these values, in the total incident irradiance from NREL (IR_{NREL}) and the inferred irradiance from the solar data set (IR_{PV}) from June to February, gives an adjustment factor; multiplying the the inferred irradiance by the adjustment factor gave an adjusted irradiance (IR_{adj}). This adjustment factor could approximate how much the inferred solar irradiance from the original dataset underestimated the expected total solar irradiance over the same time period.

$$IR_{adj} = IR_{PV} * \frac{\Sigma IR_{NREL}}{\Sigma IR_{PV}} \tag{2.3}$$

With the adjusted irradiance (IR_{adj}) in hand, the following heuristic was used to separate the potential day-time loads from the spillage. Note that as discussed in subsequent sections, a range is used to classify whether a power reading corresponds to a particular load — and this range is calculated, in the absence of labeled truth, by taking the means of the adjacent expected appliance power consumption levels as lower and upper bounds, as shown in Table 2.2. With this approach, relying solely on the combined load and spillage data ($LS_{i,n}$) along with data on the appliances (light power consumption range, CFL_{lb}, CFL_{ub}, and fan power consumption range, (F_{lb}, F_{ub}), the two cases for separating spillage are as follows — for each household, n, and for each data point, i:

- **Case A:** $IR_{adj,i,n} > 0.05W/m^2$, $LS_{i,n} \notin \{CFL_{lb}, CFL_{ub}\}$**:** If the adjusted solar irradiance is above a threshold *and* the value is not within the expected range for a light to be used, then this value is classified as spillage.

- **Case B:** $IR_{adj,i,n} > 0.05W/m^2$, $LS_{i,n} \notin \{F_{lb}, F_{ub}\}$**:** If the adjusted solar irradiance is above a threshold *and* the value is not within the expected range for the fan to be used, then this value is classified as spillage.

Figure 2-10 shows the results for classifying spillage using Method 2, with the top

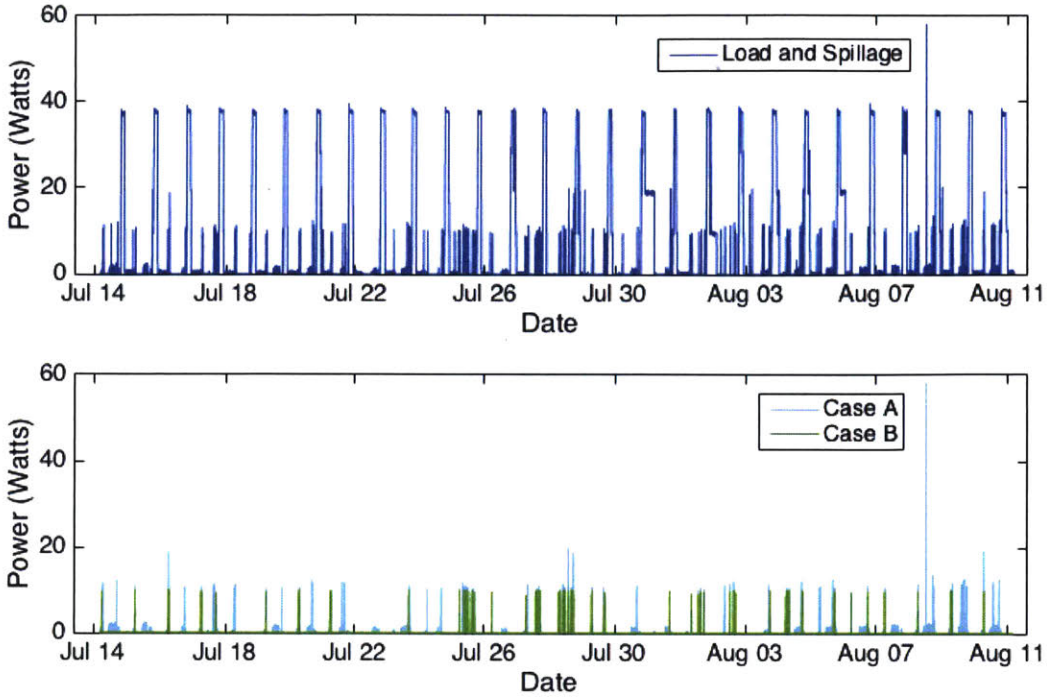


Figure 2-10: Method 2: Example of Combined Load and Spillage Data (One Month)

plot showing the combined load and spillage data, and the bottom plot showing the values for Cases A and B as described above. In comparison to Method 1 (specifically Case 2), results shown in Figure 2-8, the results in Method 2 seem not to follow as regular of a pattern following the solar irradiance. This difference is important to keep in mind, as the addition or subtraction of values from the load profile data set can change values in the data set assigned to particular user states (appliance combinations) and affect the interpretation of subsequent analysis of probability distributions associated with appliance usage.

2.3.3 Example Inferred Household Load Profiles

After these initial processing steps, the load profiles at each household is determined using both methods. Examples of data at one household over different time frames and across both methods are shown in Figure 2-11 for an example week, and Figure 2-12 for an example month. Both of these figures show that there is a periodic but

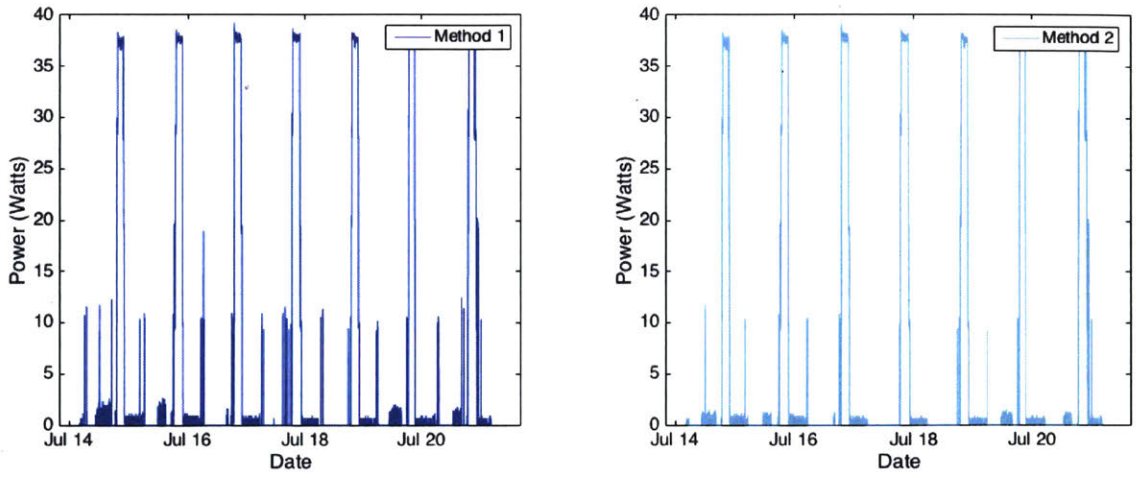


Figure 2-11: Example of a Weekly Load Profile: Method 1 and Method 2

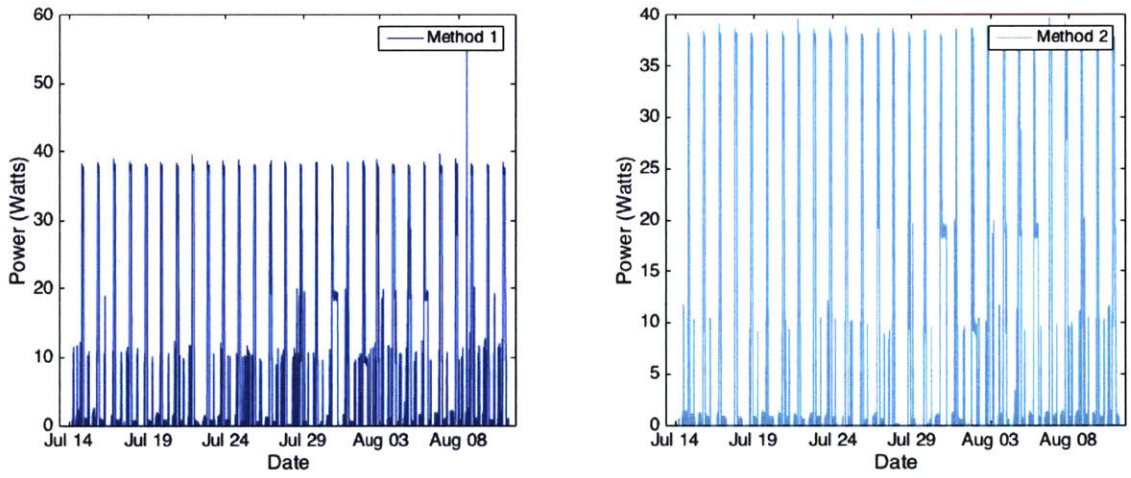


Figure 2-12: Example of a Monthly Load Profile: Method 1 and Method 2

irregular load profile (across both methods), which is important to keep in mind when understanding usage of appliances associated with the time-of-day or temperature.

2.4 Appliance and State Combinations

Regardless of the context, when considering disaggregation approaches based on load data, key parameters such as AC versus DC,sampling rate, and data resolution (i.e. appliance, household, or feeder) must be taken into account. In the situation at hand, the number — and thus potential combination — of appliances is known and the

State	Expected Mean Power (W)	Appliance Combination
1	0	None
2	9	1 CFL
3	14	1 Fan
4	18	2 CFL's
5	23	1 CFL + 1 Fan
6	27	3 CFL's
7	32	2 CFL's + 1 Fan
8	36	4 CFL's
9	41	3 CFL's + 1 Fan
10	50	4 CFL's + 1 Fan

Table 2.2: Appliance & State Combination

network operates on DC; what is not known at this point is the standard deviation of each appliance. The goal is to identify the user's state (i.e. combination of appliances that is on) given a power consumption reading:

In order to relate exogenous variables to the user's state and assess performance of clustering algorithms, a proxy for labeled truth needed to be generated for this data set at the minute level. As discussed previously, Table 2.2 is organized in increasing magnitude of power consumed / number of appliances on, and labeled truth is generated by using a method in taking the means of the adjacent states as upper and lower bounds; having this range allows for values to be classified based on the power readings into its equivalent state at each minute, and doesn't allow for overlap between state boundaries which would yield vague and uninterpretable results. This relatively simple classification process is done with the original data set with one minute resolution, as conducting this process after taking hourly average would lose not only granularity, but also distort power levels to be unexpected values or perceived as alternate states. It is worth mentioning that there may be multiple reasons why the logged power consumption may not exactly equate to the rated power consumption of the appliance — such as due to calibration mismatch with the current measurements (as discussed in the previous sections) and even quality of the appliances themselves.

As shown in Figure 2-13, the number of possible states with the data sets at hand is 10 for one particular household (based on the Method 2 load profile here).

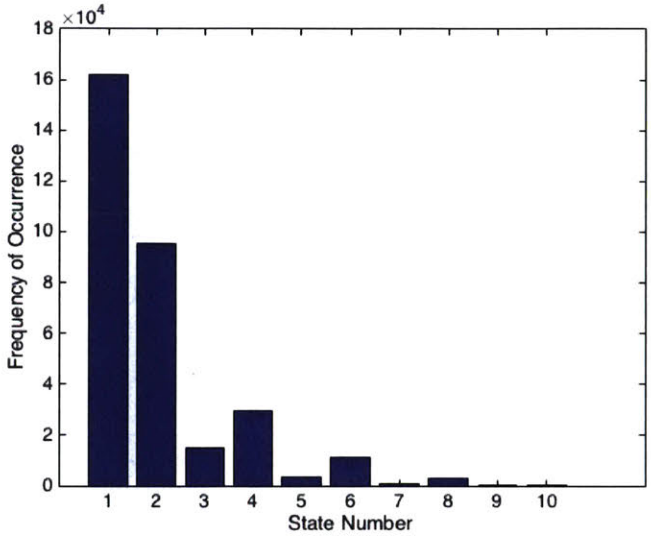


Figure 2-13: Frequency of Occurred States

However, plotting the frequency of states occurred based on the generated truth data, its important to note that users may not reach all of the possible states — some without any sort of frequency or recurrence. Specifically, three to four states are rarely, if ever, reached for any of the households (such as states 7, 9, 10 as defined above in the case of this particular household). The reasons for this may be part preferential, in that there may be few instances when all the lights and the fan are used at the same time, or part technical, in that the battery may be unable to supply the requisite discharge rate of current to reach these higher power states.

2.5 Statistical Analysis and Feature Selection

As discussed, one of the main reasons having a disaggregated dataset of energy consumption data in place is useful is that decisions can be made in a real-time setting — which can help determine load criticality, deferability, etc. Furthermore, when predicting future energy consumption at an hour- or day-ahead timescale, a disaggregated dataset has more information, and thus more ability to relate to exogenous variables impacting the user's state. In these particular cases, having a disaggregated data set at each household allows for more detailed probability estimates in relating

the lighting usage to the time of the day and the fan usage conditioned on the ambient temperature. Again, this type of analysis is made possible by the fact that a priori information on the appliance states and power level are known beforehand. Without this information, it would likely require more computational effort to understand which states (and thus power levels) correlate to exogenous variables of interest such as time of day and ambient temperature.

2.5.1 Relating Lighting Usage to Time of Day

For both Methods 1 and 2, the histograms shown in Figures 2-14 and 2-15, there seems to be multiple ranges of hours for when the light(s) — which could mean any combination from one to four available lights — are on for this household. The x-axis is labeled in minutes after midnight over a 24-hour period (1,440 minutes in a day), and the y-axis is labeled as the probability density; both plots include a non-parametric probability distribution fit.

For both methods, there seems to be a good amount of morning evening and late-night light usage (potentially for lighting outdoor common and cooking areas, reasons of convenience, or to illuminate darkness indoors irrespective of the time of day). This type of insight challenges conventional expectation, such as the reliance on qualitative surveys, that in networks without controllable switches or signals being conveyed to users, lights may not solely be used during the evening hours. However, for Method 2, there seems to be some light usage seen throughout all the hours of the day; this discrepancy with Method 1 may be due to heuristic discussed previously misclassifying values of spillage as load, as the uptick is seen during the middle hours of the day — when there is likely to be more solar incidence. As previously explained, Method 1 suppresses the probability that the lights may be on during the middle of the day.

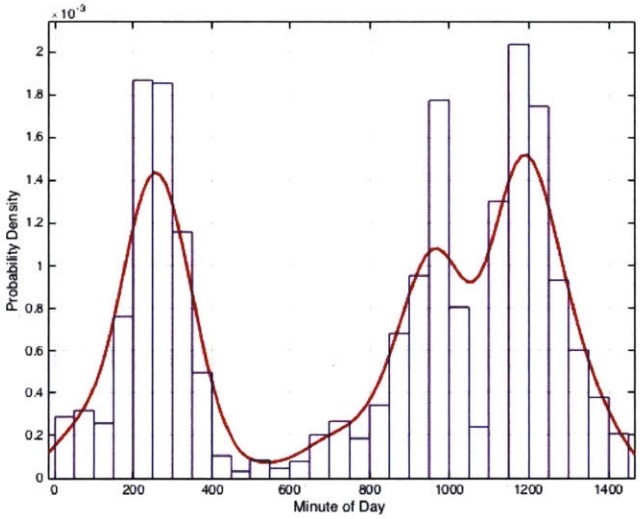


Figure 2-14: Method 1: Non-Parametric, Bounded Joint Probability Distribution Fit of Lighting Use and Time of Day

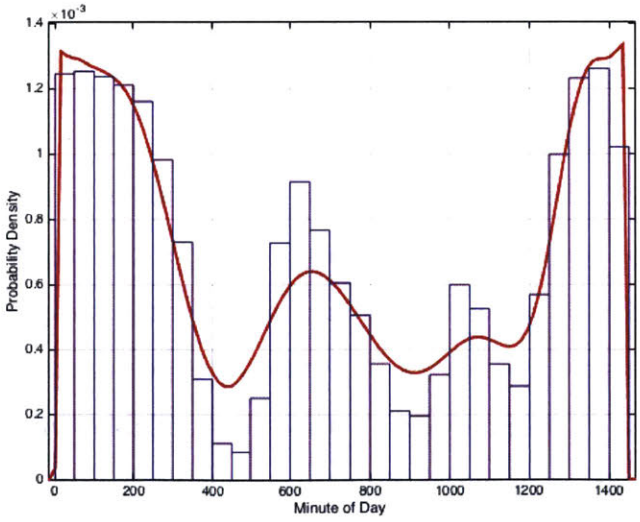


Figure 2-15: Method 2: Non-Parametric, Bounded Joint Probability Distribution Fit of Lighting Use and Time of Day

2.5.2 Relating Fan Usage to Ambient Temperature

In regards to the fan usage, Figures 2-16 and 2-17 show the conditional probability that the fan was on given the ambient temperature for both Methods 1 and 2 — again, which could mean any of the states where the fan usage is present. Here, the x-axis is the temperature (again, which was measured with the on-board thermistor in the data logger) in Celsius, and the y-axis is the probability density. As seen in both plots, there is undoubtedly a distribution of temperatures for which the fan is on over the duration of the data set. Both figures illustrate that the fan may not turn on at an exact temperature threshold — and also show that the probability of fan usage does increase with increasing temperature. Method 2 does seem to have a larger range of temperatures, and a clear uptick at lower temperatures. Similar to the discussion in with the lights and the time of day, this suppression of this uptick at lower temperatures for Method 1 versus Method 2 is likely due to the misclassification of spillage values as load.

Note that as opposed to the previous case with the lights and the time of day, the conditional probability of the fan usage given the temperature is use as opposed the joint probability. This is done in order to essentially normalize the joint probability distribution by all the distribution of the temperature throughout the data set — regardless of whether the fan was on or not. Based on the disaggregated data set, what is known is the joint probability and the marginal probability (of the temperature), so using Bayes Theorem, the conditional probability distribution was determined by:

$$P(Fan \,\&\, Temperature) = \frac{P(Temp \mid Fan)}{P(Fan)} \tag{2.4}$$

$$P(Temp \mid Fan) = \frac{P(Fan \,\&\, Temperature)}{P(Fan)} \tag{2.5}$$

And presented in the aforementioned figures, the relationships between the exogenous variables to user activities do not represent conventional, parametric probability

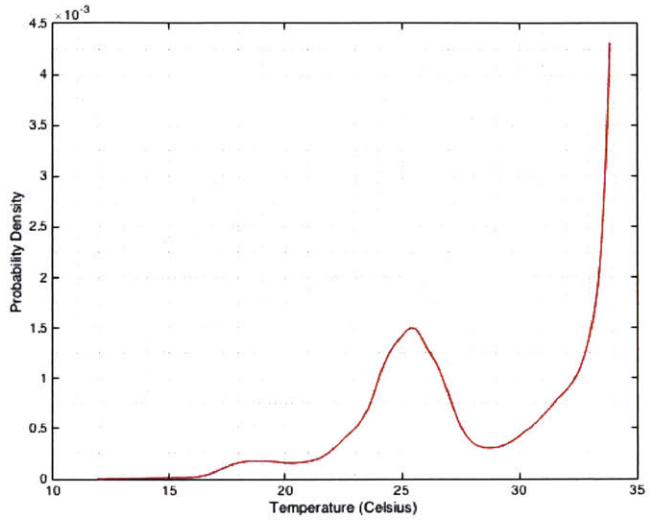


Figure 2-16: Method 1: Conditional Probability Distribution Based on Non-Parametric Fit of Fan Use Given Temperature

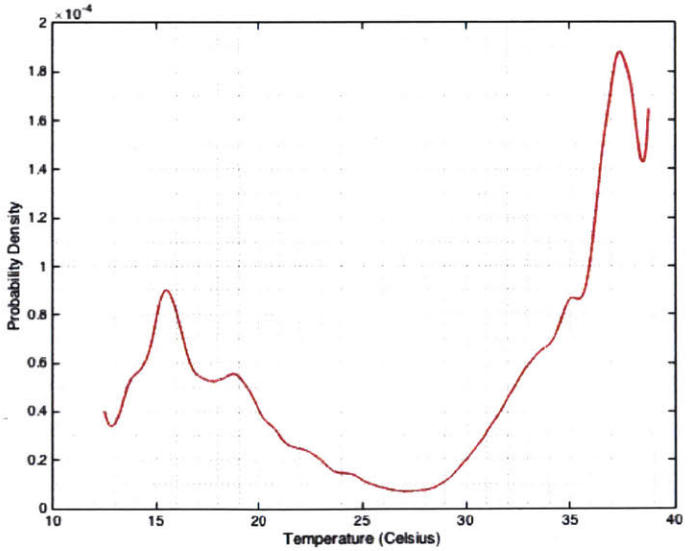


Figure 2-17: Method 2: Conditional Probability Distribution Based on Non-Parametric Fit of Fan Use Given Temperature

distributions based on the data sets acquired — which may or may not be consistent across other data sets or load profiles. Thus, the fitted probability density functions represent a non-parametric fit to these disaggregated data sets of lighting and the time-of-day, and the resulting conditional probability of fan usage given the temperature. Similar to the determination of bin centers and widths in histograms, 'kernel density estimators' use a smoothing function and bandwidth value to generate a fitted probability density curve, and in order to avoid discontinuities, the fits of a normal kernel smoothing function are shown here [84]. Again, this is the result of a conducting a density estimator after seeing six months of disaggregated, electricity consumption data; for such an approach to be relied upon in more real-time forecasting settings, utilization of non-parametric Bayesian approaches may be necessary in order to update distribution fits with incoming data points [85].

Both methods in terms of load profile determination yield interesting results using comparing the disaggregated data sets to exogenous variables such as time of day and temperature. However, as discussed, the approach used in Method 1 seems to yield more logical and insightful results when compared to Method 2. Furthermore, it is clear that interpreting results from disaggregation is sensitive to how the load profile is determined when not measured directly.

2.6 Application of Machine Learning Algorithms for Load Disaggregation

The previous analysis depended on the classification of power consumption readings to an associated state (appliance combination). With the power readings, it is also worth assessing the performance of clustering algorithms — to assess their ability in identifying the 'centers' of each state (in terms of watts). In machine learning, clustering algorithms are used to identify grouping and assign labels to data points. However, one challenge with clustering algorithms is the need to know the number of possible clusters (or in this case, states) in advance of applying the clustering

algorithms.

K-Means and Gaussian Mixture Models (GMM) are two common techniques used in machine learning to partition or appropriately cluster data sets, and the description of the underlying mathematical principles behind K-Means and Gaussian Mixture Models are adapted from [85]. A prerequisite to use these approaches is the requirement to know the number of clusters, denoted as K, beforehand; in the case at hand, K can be considered as the number of possible states, while u_k can be considered as the center of each cluster (i.e. power consumption of each state), and n is the number of data points on hand.

In K-Means, each data point x_n is assigned only to one cluster (denoted by $r_{nk} = 0$ or 1), whereas in Gaussian Mixture Models, a probability of assignment to a particular cluster is given to each point. Thus, the objective function is to minimize the overall distances, squared, between the data points and the cluster centers as shown in Equation 2.6.

$$W = \sum_{n=1}^{N} \sum_{k=1}^{K} r_{nk} ||x_n - u_k||^2 \tag{2.6}$$

K-Means relies on a two-step iterative approach to minimize J, known as the Expectation-Maximization algorithm (common for identifying maximum likelihood solutions for "models with latent variables"), until there is no change in cluster assignments or a pre-determined maximum number of iterations is reached [85].

In GMM, the latent variable z_k is a value between 0 and 1, and the $\sum_k z_k = 1$; furthermore, the probability of the assignment of z_k is described by the mixing coefficient π_k, a value between 0 and 1 and $\sum_{k=1}^{K} \pi_k = 1$; this method denotes the proportion of data points assigned to the clusters (or states). The utilization of the Expectation-Maximization algorithm in GMM is more arduous than in the K-Means case — requiring more computation due to the presence of mixing coefficients and covariance matrices (along with the means in cluster centers) [85].

The interpretation for the data set at hand can be viewed as minimizing the

distance, in watts, between the power consumption values of various appliance combinations (states). Again, the presence of noise in the data acquisition process and the reality that the actual power consumption of the appliance may be different from the rated power consumption are reasons for why the actual cluster centers seen in the data may deviate from the expected cluster centers.

2.6.1 Performance of K-Means and Gaussian Mixture Model Algorithms

Both K-Means and Gaussian Mixture Models (GMM) are applied to the load profile data set at the household level using the Machine Learning Toolbox in MATLAB [86]; note that the results shared in this and subsequent sections are based on Method 2, but similar methods can be applied to Method 1. The K-Means algorithm is used to identify clusters embedded in data sets and assign data points to a particular cluster, but is non-probabilistic in its nature. The algorithms objectives are to minimize the total sum of the square of distances between each data point and its assigned cluster. GMM is related but different in that the clusters are probabilistic and normally distributed around cluster centers; thus, each data point is assigned a probability that it belongs to a given cluster. Again, both of these algorithms do not have closed-form solutions, and rely on the iterative Expectation-Maximization (EM) algorithm to recursively determine the cluster centers (and associated mixing coefficients in the case of GMM) until a convergence criterion is reached [85]. As the results below indicate, the algorithms are used in a number of different scenarios to assess their respective performances in assigning user states (i.e. combination of appliances on) based on reading in a power consumption level. First, Table 2.3 show how the K-Means algorithm performs when used with 7 or 10 clusters, and with or without initialization of centroids. For K=10, initialization does help the algorithm converge towards centroid values that are expected for each of the states — and to a lesser extent for K=7.

Comparing between K=10 and K=7, Table 2.4 shows that the algorithm had the

State	Expected Mean	K=10 Centroid	K=10 Centroid (w/ initialization)	K=7 Centroid	K=7 Centroid (w/ initialization)
1	0	0	0	0	0
2	9	8.06	9.09	8.51	9.08
3	14	9.54	11.23	10.15	11.23
4	18	10.87	17.96	12.36	17.96
5	23	13.14	19.62	18.81	19.62
6	27	18.81	27.49	27.49	27.49
7	32	27.49	34.59	35.52	35.52
8	36	34.60	36.29		
9	41	36.32	40.85		
10	50	43.45	44.05		

Table 2.3: K-Means Centroid Results

	Num. Iterations	Total Sum of Distances
K=7	32	8.8×10^4
K=7 (w/ initialization)	23	1.2×10^5
K=10	66	4.2×10^4
K=10 (w/ initialization)	23	1.1×10^5

Table 2.4: K-Means Algorithm Performance

least aggregate sum of distances — and number of iterations required for convergence – from points to centroids when initialized for K=10. This result was initially unexpected, such as states with expected higher magnitude centroids such as 9 and 10, are rarely ever reached. However, given that the majority of the states are reached in lower magnitude centroids, such as states 1 through 4, having more clusters available allow for the algorithm to space out the centroids – which makes them closer to the expected centers when compared to K=7.

Second, Tables 2.5 and 2.6 indicate how the Gaussian Mixture Model (GMM) performs; the key difference with K-Means is that here, the algorithm assigns a probability that a given point belongs to a cluster that is normally distributed around its center. With K=7, Table 2.5 shows the difference in expected centers and mixing proportions when the GMM is or is not initialized with expected mean values.

It's clear that initialization has a substantial impact on the algorithm's performance — as the GMM centers and mixing proportions are very similar to the ex-

pected values. Without initialization, the majority of the GMM centers hover around zero, with the sum of the mixing proportions of the first five centers equating 0.513, which is the expected mixing proportion for one centroid expected to be at zero. For K=10, a nearly identical story holds in Table 2.6, illustrating the importance of initialization and the tradeoff of maximizing the distance between centroids – while minimizing the total distance between data points and centroids.

Table 2.5: GMM Results, K=7

State	Expected Mean	Original Mixing Proportions	GMM Centers (w/ initialization)	GMM Mixing Proportions	GMM Centers (w/o initialization)	GMM Mixing Proportions
1	0	0.5107	0	0.4882	0.0323	0.1113
2	9	0.3528	9.09	0.3167	0.0323	0.1113
3	14	0.0422	13.79	0.0726	0.0323	0.1113
4	18	0.0727	18.27	0.0725	0.0323	0.0849
5	23	0.0027	22.47	0.0204	0.0323	0.0942
6	27	0.0342	27.23	0.0021	11.44	0.4393
7	32	0.0018	34.05	0.0075	29.08	0.0479
8	36	0.0097				
9	41	0.0003				
10	50	0.0000				

Table 2.6: GMM Results, K=10

State	Expected Mean	Original Mixing Proportions	GMM Centers (w/ initialization)	GMM Mixing Proportions	GMM Centers (w/o initialization)	GMM Mixing Proportions
1	0	0.5107	0	0.5107	0	0.1021
2	9	0.3528	9.39	0.2835	0	0.1021
3	14	0.0422	11.83	0.0844	0	0.1021
4	18	0.0727	18.35	0.0506	0	0.1021
5	23	0.0027	19.74	0.0248	0	0.1021
6	27	0.0342	27.49	0.0349	9.18	0.1391
7	32	0.0018	34.75	0.0069	10.10	0.2045
8	36	0.0097	36.38	0.0039	13.11	0.0244
9	41	0.0003	41.98	0.0001	18.81	0.0753
10	50	0.0000	44.26	0.0002	29.42	0.0460

As the Tables 2.5 and 2.6 indicate, the performance of the clustering algorithms in terms of the centers' proximity to expected mean power levels of states is far better when initialized with the expected power consumption levels of each state; without this, the algorithms tend to congregate near zero, given that is where over 50 percent of the power readings lie (for this particular household, though similar results hold for the other two households). This is a rational enough conclusion with a labeled data

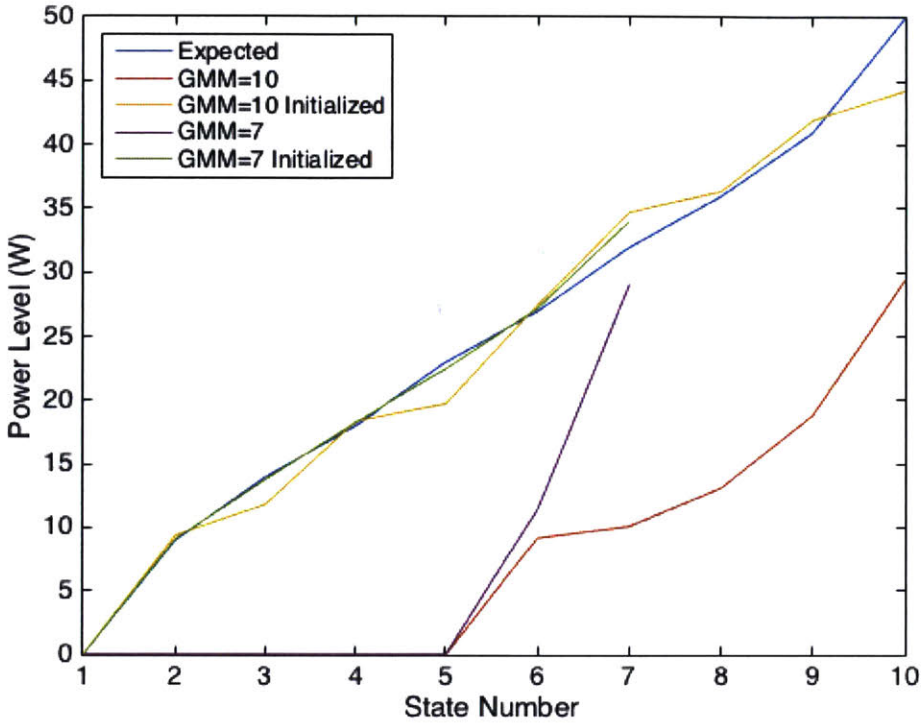


Figure 2-18: GMM Clustering Results [Probabilistic Assignments]

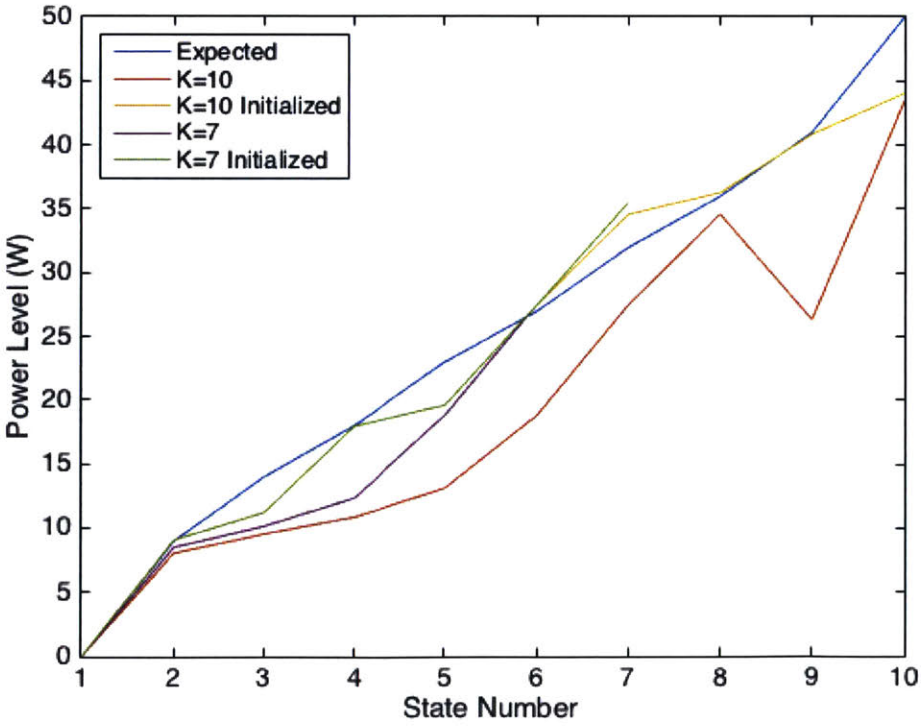


Figure 2-19: K-Means Clustering Results

	One Day	One Week	One Month
No. of Iterations	11	14	13
Centers	0	0	0
	9.309	9.12	9.19
	13.72	13.25	12.90
	19.05	19.12	19.25
	28.18	20.57	22.34
	37.33	27.99	28.33
	49.04	28.64	31.17
	50.69	37.28	37.44
	52.18	47.97	48.24
	53.98	53.84	53.80

Table 2.7: Data Set Length Effect on K-Means Performance

One Day	Mixing Proportion	One Week	Mixing Proportion	One Month	Mixing Proportion
0	0.613	0	0.711	0	0.706
9.31	0.183	9.14	0.098	9.21	0.99
13.72	0.012	13.34	0.016	12.93	0.043
19.05	0.043	19.13	0.034	19.26	0.019
19.06	0.000	21.23	0.000	22.52	0.001
28.18	0.033	28.18	0.027	28.33	0.025
28.19	0.000	30.32	0.000	31.38	0.001
37.33	0.074	37.28	0.084	37.44	0.093
37.39	0.000	47.04	0.005	48.25	0.009
52.43	0.042	53.83	0.024	53.82	0.006

Table 2.8: Data Set Length Effect on GMM Performance

set and knowledge of appliance states beforehand. Note that the above analysis is based on the algorithms' performance over the entire data set of length 319,680 data points (222 days x 24 hours x 60 minutes). For situations in the field where neither the expected power consumption of the appliances or the number of appliances is not known in advance, different algorithms may be required. But another point to understand is how the algorithms fare after seeing subsets of the data – after just a day, a week, or a month. Tables 2.7 and 2.8 indicates the performance of GMM for K=7 and K-Means for K=10, both with initialization of centers, after seeing data sets of length 1,440 (24 hours x 60 minutes), 10,080 (24 hours x 60 minutes x 7 days), and 40,320 (24 hours x 60 minutes x 7 days x 4 weeks) values:

2.7 Conclusion

The above analysis yields insight on a number of timely and important topics. First, a process for data acquisition of residential load profiles is shared herein, which can be replicated by practitioners aspiring to get a better understanding of electricity consumption patterns in rural, off-grid contexts. This is supported by methods to analyze the data sets, from the raw digital readings to the separation of the load profile from spillage (a combination of both empirical and inferred methods), when the load profile is not measured directly.

Second, assuming the capability for load disaggregation is in place, this paper shows the potential for deeper insight in to users' electricity consumption patterns. More specifically, once the appliance combination is known, joint and conditional probability density relationships with exogenous variables such as time of day and temperature can be made — which provides a starting point for making probabilistic load forecasts. Again, based on the inferred load profiles from the data sets acquired in this effort, the probability density functions generated at the household level for appliance usage are sensitive to the classification of spillage.

Thirdly, the analysis applies and compares a pair of clustering algorithms in load disaggregation, commonly used in the field of machine learning. A key learning is the effect of initializing the algorithms with expected cluster centers — as the combination of the noise embedded in the raw data and that appliances are not on during the majority of the time adversely effects the algorithms' performance. Furthermore, understanding of these techniques' convergence based on the amount of data they receive, along with the effect of the number of clusters, are also shared.

Chapter 3

Adaptation and Extension of Kinetic Battery Model in Simulation and for Real-Time Operation

3.1 Introduction

In India, lead-acid still remains the most widely available, well-understood, and popular battery chemistry across many applications (i.e. uninterruptable power supplies (UPS), urban power back-up, etc.), hence its choice for modeling purposes. Even with the advent of newer battery chemistries such as lithium-ion, based on conversations with practitioners in India, it is expected that it will take years for other battery chemistries to reach the scale, penetration, and operational know-how in micro-grids — especially in peri-urban and rural areas. Thus, the focus of the work presented in this chapter is on simulating and modeling lead-acid batteries.

Depending on the available capacity, the concentration of water and sulfuric acid varies (see following sections for discussion on lead-acid battery's chemical reactions). The ability for ionic species to flow through the electrolyte directly dictates the rate at

which current can flow in or out of the battery. Thus, the conductivity of ionic species through the electrolyte is driven by a number of transport processes such as kinetic diffusion, concentration gradients, and resistive losses — and all are key aspects that constrain the performance of lead-acid batteries in responding to demands to store energy or serve load. In lead-acid batteries, oxidation and reduction reactions take place at the electrodes, which are immersed in the electrolyte. The key reason that a battery's available capacity is a function of of the charge or discharge rate is because of the development of a concentration gradient — with a higher concentration of ions near the electrode where the oxidation (discharge) or reduction (charge) reaction is taking place. Thus, if the concentration of available ions near the electrode depletes at a fast rate, ionic species that are further away are not available; and when a battery returns to an open circuit state, the voltage recovers as the concentration of ionic species in the electrolyte becomes more uniform [25].

As discussed in Chapter 1, battery modeling has and will continue to be an important area of research. There are many reasons to develop accurate battery models, such as in order to develop state-of-charge and state-of-health estimation methods — and there are a handful of approaches one can take to modeling batteries in order to represent detailed physical interactions between chemical species and approximate issues such as degradation and cycling effects. Previous work has relied on methods such as directly observing such physical phenomena experimentally, acquiring current/voltage data from battery cycling, or extrapolating data made available from battery manufacturers.

The work presented in this chapter focuses on the adaptation for simulation and extension for real-time operation of the Kinetic Battery Model (KiBaM). Specifically, this chapter discusses the implementation of operating constraints to simulate battery management and dispatch in a micro-grid, given a net current profile of incident solar and demand. This includes discussion on the implementation of the rainflow algorithm for counting cycles to approximate battery lifetime (and degradation) as well. This is followed by an extension of the KiBaM to incorporate voltage response for a given current profile, taking into account dynamic resistive (IR) losses based

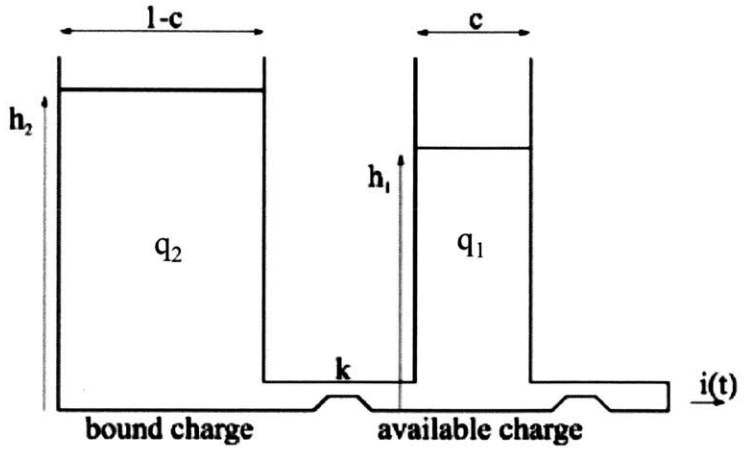


Figure 3-1: Kinetic Battery Model Concept Overview [35]

on the available capacity; this is based on an optimization formulation for selected battery parameters to represent actual voltage data based off of battery cycling data acquired for a lead-acid battery.

3.2 Kinetic Battery Model Implementation & Adaptation

As discussed in Chapter 1, the KiBaM simply and eloquently represents the discrete charge that is both available and that is inaccessible due to concentration gradients that form and impact the mass transport of ions to electrodes where oxidation or reduction reactions are taking place. Visually speaking, the KiBaM can be described in a two-tank model to show that there is only a certain amount of available capacity in the battery at each time step, as seen in 3-1. This value is based on the available capacity in the previous time step and the input/output current desired at each time step (subject to charge/discharge constraints, further discussed in this section) [35].

The key input parameters for the KiBaM model are c (capacity ratio, value between 0 and 1), k (rate constant), and q_{max} (the maximum available capacity in the battery). The parameter c can be viewed as the proportion dictating the real-time available ions near the electrode, while $1 - c$ represents the remaining, inaccessible

proportion of charge; furthermore, k can be viewed as the rate at which charge can be exchanged between these two tanks, representing mass transport across the electrolyte.

Each battery has a unique set of parameters required to utilize the KiBaM model, and can be solved using battery capacities at various C-rates; such values are made available from battery manufacturer data sheets. To solve for c and k, a system of two equations needs to be generated to solve for the two unknowns in Equation 3.3, and that these values are re-computed for different battery capacities as batteries' of even the same chemistry may have different capacities at different charge rates (Equations 3.1 and 3.2). The inputs to these equations are based on solving for a particular capacity ratio and rate constant based on the hourly rates of available capacity (i.e. $t = 1$, $t_1 = 10$, $t_2 = 20$ hours) [35]. In the implementation described in this work, the model developed uses an exponential solver (*fsolve*) in MATLAB in order to come to a solution for a battery's specific c and k values.

$$F_{t_1,t_{20}} = \frac{q_{t=1}}{q_{t=20}} \tag{3.1}$$

$$F_{t_1,t_{10}} = \frac{q_{t=1}}{q_{t=10}} \tag{3.2}$$

$$c = \frac{F_t(1-e^{-kt_1})t_2 - (1-e^{-kt_2})t_1}{F_t(1-e^{-kt_1})t_2 - (1-e^{-kt_2})t_1 - kF_t t_1 t_2 + kt_1 t_2} \tag{3.3}$$

$$q_{max} = \frac{q_{t=20}(1-e^{-20k}(1-c)+20ck)}{20ck} \tag{3.4}$$

The capacity ratio splits the battery into two tanks, essentially separating the readily available charge and chemically bound charge, while the rate constant acts as a current regulator, restricting the conductance and flow of ions between the two tanks [35]. As originally conceived in [35], the change in the volume of each tank (dq_1/dt and dq_2/dt) can be described at each time step as (with the current, I, only appearing in the same equation as q_1, Equation 3.5):

$$\frac{dq_1}{dt} = -I - k(1-c)q_1 + kcq_2 \tag{3.5}$$

$$\frac{dq_2}{dt} = k(1-c)q_1 - kcq_2 \tag{3.6}$$

In [35], the aforementioned equations are solved using Laplace Transforms, transforming these differential equations from the time domain into the frequency domain. To use the KiBaM to simulate the real-time operation of a battery, two main equations need to be solved to obtain values for available capacity, q_1, and bound capacity, q_2, at each time step by feeding in a current profile. In this case, the current profile is a vector of 8760 elements, which is equal to the net power profile (in total load minus available solar), divided by the nominal battery voltage (12V). Note that the net incident solar power is module size and irradiance dependent, and the load profile construction is dependent on a number of factors such as appliances, expected hourly usage, etc.; detailed assumptions and models for both of these are described in further detail in Chapter 4. These equations represent the capacity in the two tanks at the *end* of each time step, i, as calculated in Equations 3.7 and 3.8. Note that sign convention is that negative values of current represent charging while positive values of current represent discharging.

$$q_{1,i} = q_{1,i-1}e^{(-k\Delta t)} + \frac{(q_{total,i-1}kc - I_i)(1-e^{-k\Delta t}) - I_i c(k\Delta t - 1 + e^{-k\Delta t})}{k} \tag{3.7}$$

$$q_{2,i} = q_{2,i-1}e^{(-k\Delta t)} + q_{total,i-1}(1-c)(1-e^{-k\Delta t}) - \frac{I_i c(k\Delta t - 1 + e^{-k\Delta t})}{k} \tag{3.8}$$

$$q_{total,i} = q_{1,i} + q_{2,i} \tag{3.9}$$

$$SOC_i = q_{total,i}/q_{max} \tag{3.10}$$

The original KiBaM also includes input and output current constraints, calculated separately for charging and discharging, that set maximum limits on how much

current the battery can input or output at each time step [35]. And in order to represent the ability for accurate state-of-charge estimation and real-time battery management, minimum and maximum constraints on battery state-of-charge are also included as an adapted implementation of the KiBaM described in this work. Thus, during charging and discharging, there are two constraints: the original KiBaM input (or output) current constraint ($I_{c,max}$ and $I_{d,max}$, Equations 3.11 and 3.14) as taken from [35], and the addition of the battery management constraint based on minimum and maximum state-of-charge limits ($I_{c,SOC}$ and $I_{d,SOC}$, Equations 3.12 and 3.15). Equations 3.13 and 3.16 simply represent the dispatch decision, forcing the model to choose whether the value of the net current profile (in the incident solar power, W, minus the total demand profile, TD, divided by the nominal battery voltage, $V = 12$) can be served directly, or if the battery is constrained by either the KiBaM or state-of-charge constraints — at each time step ($i = 1...8760$, hours over a year). Note that the nomenclature used here is consistent with the nomenclature used in Chapter 4.

The set of charging constraints (denoted by subscript c), including the battery management constraint based on the maximum level of charge ($MLOC$, default value of 100%) are implemented in Equations 3.11—3.13.

$$I_{c,max,i} = \frac{-kcq_{max} + kq_{1,i-1}e^{-k} + q_{total}kc(1 - e^{-k\Delta t})}{1 - e^{k\Delta t} + c(kt - 1 + e^{-k\Delta t})} \tag{3.11}$$

$$I_{c,SOC,i} = -(MLOC - SOC_i) * q_{max} \tag{3.12}$$

$$I_{c,i} = -min(\frac{W_i - TD_i}{V}, I_{c,max,i}, I_{c,SOC,i}) * \eta_c \tag{3.13}$$

Conversely, the set of discharging constraints (denoted by subscript d), including the battery management constraint based on the maximum depth of discharge ($MDOD$, default value of 60%) are implemented in Equations 3.14—3.16.

$$I_{d,max,i} = \frac{kq_{1,i-1}e^{-k\Delta t} + q_{total,i-1}kc(1-e^{-k\Delta t})}{1 - e^{k\Delta t} + c(kt - 1 + e^{-k\Delta t})} \tag{3.14}$$

$$I_{d,SOC,i} = (SOC_i - (1 - MDOD)) * q_{max} \tag{3.15}$$

$$I_{d,i} = min(\frac{W_i - TD_i}{V}, I_{d,max,i}, I_{d,SOC,i}) * \eta_d \tag{3.16}$$

As is discussed further in the subsequent sections, the KiBaM is not a complete representation of battery dynamics — leaving out aspects such as voltage response and variable resistances of the battery as a function of the state-of-charge. To simply address charging and discharging efficiencies in simulation, the η_c and η_d are added in this model — with a round-trip efficiency of a lead-acid battery assumed to be 90%. This is included because the KiBaM doesn't take into account voltage effects, and thus resistive losses, that take place in a battery; in reality, the resistance of the battery changes with both the state-of-charge and whether the battery is charging or discharging [36]. Losses are more explicitly taken into account in subsequent sections when considering voltage effects, but for the purposes of simulation, η is included to approximate these charging/discharging efficiency losses.

For illustrative purposes, an example of the solar and load profiles and the KiBaM variable outputs (q_1, q_2, and q_{total}) are shown in Figure 3-2; these outputs are based on the net current profile from a 120W solar panel, a 75Ah battery, and a residential load profile across 5 households for illustrative purposes; note that the assumptions in determining the solar power output and load profile construction models that populate these vectors are discussed in detail in Chapter 4 [16]. During roughly the hours 2,000-4,000 (essentially March-June), the load profile increases due to the increase in fan usage — induced by the ambient temperature — which affects the available charge in the battery. There is also a period after hour 4,000 where the available solar decreases due to the monsoon season, but the presence of evening lighting loads is not a large enough load, in this example, to keep the battery capacity low during this period of low irradiance. This is further supported by the outputs in Figure 3-3, which

Constraint	Charge	Discharge
Net Load	1159 (77%)	567 (12.6%)
KiBaM Constraint	0 (0%)	2993 (66.6%)
SOC Constraint	2428 (67.7%)	935 (20.8%)
Total Hours	3587 (40.9%)	4495 (51.3%)

Table 3.1: Example of Number of Hours KiBaM Charge and Discharge Constraints Reached

indicates the calculated values of each discharging (top plot) and charging (bottom plot) constraint during each time step over a simulated year.

For both charging and discharging, the model selects the minimum of the three values at each hour — which includes the net current profile and the two constraints at each time step. Again, the first constraint comes from the KiBaM itself, which is the maximum allowable charge or discharge rate at that particular time step. The second constraint comes from the battery management system, which is assumed to have an accurate state-of-charge estimator in order to assess whether or not to over-charge or over-discharge the battery, subject to a maximum level of charge (MLOC) or maximum depth of discharge (MDOD) constraint. In the model, one can change the MLOC and MDOD values (default are 100% and 60% respectively) to simulate the effects of state-of-charge estimation accuracy and the effects it has on final battery selection; as is discussed in the next section, managing the depth of discharge of the battery has a direct effect on degradation and thus cycle life. And lastly, the third value is the actual desired current input (from solar) or output (from load) desired at a particular time step.

Table 3.1 shows the count (in hours) of the number of times each constraint is reached — for both charging and discharging. Again, for illustrative purposes, this particular instantiation of the model is with a 120W panel and a 75Ah battery, serving 5 residential households; the 'Net Load' is either the net solar during charge, or the net load during discharge. It's interesting to note that the KiBaM charge constraint is never reached during the hours that the battery is charging. This is likely due to the fact that the rate of solar energy charging the battery is never high enough to force

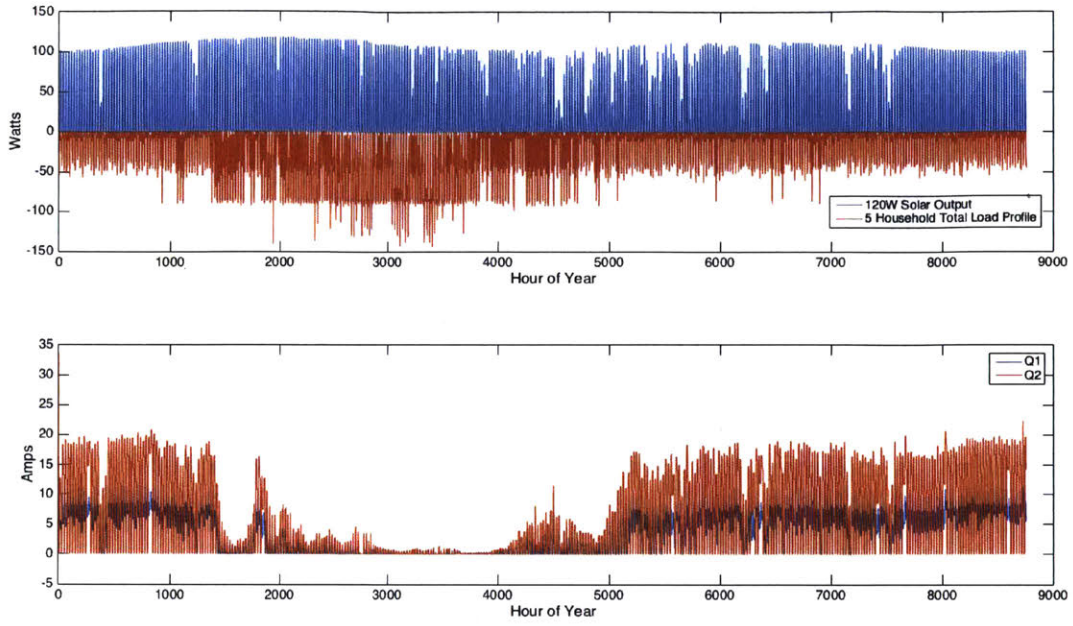


Figure 3-2: Example of Net Load Profile and KiBaM Variable Outputs

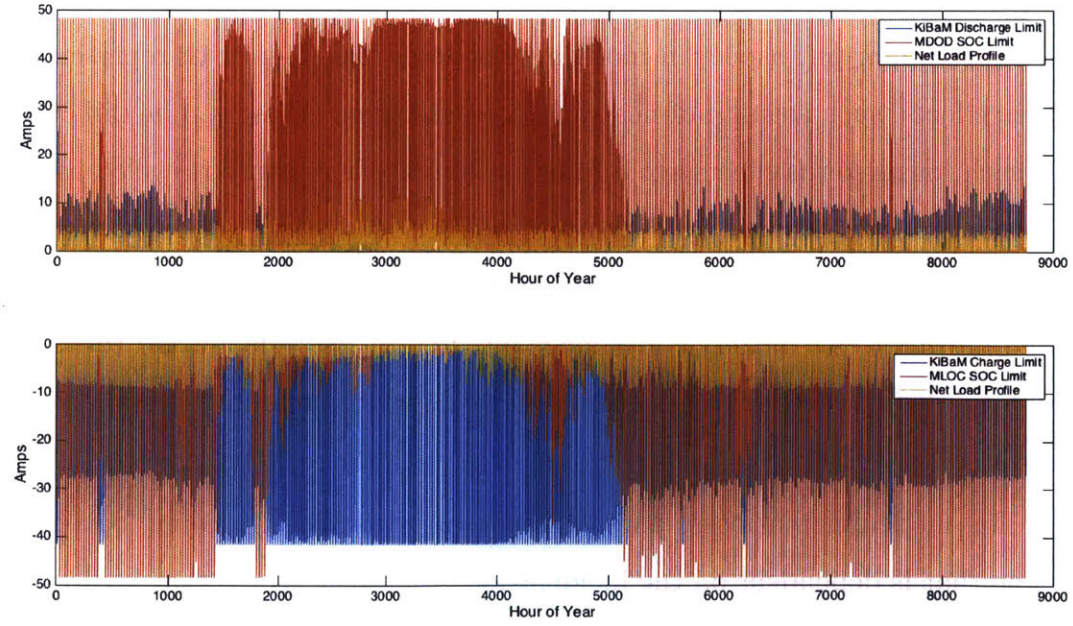


Figure 3-3: Example of Charging and Discharging KiBaM Constraints

the KiBaM charge constraint to be reached — but there are clearly a number of hours where the addition of the SOC constraint is reached (2,428), indicating the presence of spillage. However, during discharge, the KiBaM discharge constraint is the most frequent constraint reached, indicating that the battery was clearly not able to serve the rate of discharge required by the load for 2,993 hours; furthermore, the net load was only served in its entirety 567 of the 4,495 hours the battery was discharging over the year. This is supported by the fact that for this configuration, the reliability is calculated to be only 56.3% (defined to be the average reliability over the year, i.e. the integral of the amount of energy served divided by the integral of the expected energy demanded in load profile for the network; further discussion on reliability and the effect of changing the SOC constraints takes place in Chapter 4).

3.3 Rainflow Algorithm Implementation for Counting Battery Cycles

Another important aspect in modeling batteries has to do with representing longer-term effects, such as state-of-health and degradation. These can be difficult to model as such longer-term effects are a function of how the battery is cycled and operated; furthermore, without actual data over long-periods of time, modeling such effects are also an approximation at best. However, modeling such effects to some approximation are important as a battery's lifetime is dictated by its cycle life and residual capacity after taking into account degradation effects — which undoubtedly impacts micro-grid costs.

For modeling purposes, part of the goal is to actually count battery cycles, a value that is dependent on the incident load and solar profile that is discharging and charging the battery. Being able to count cycles can allow for a model to estimate when a battery has reached its end-of-life based on the rated cycle life, which impacts the replacement costs (outlined in more detail in Chapter 4). To implement such a method, the rainflow counting algorithm is used to track the number of cycles based

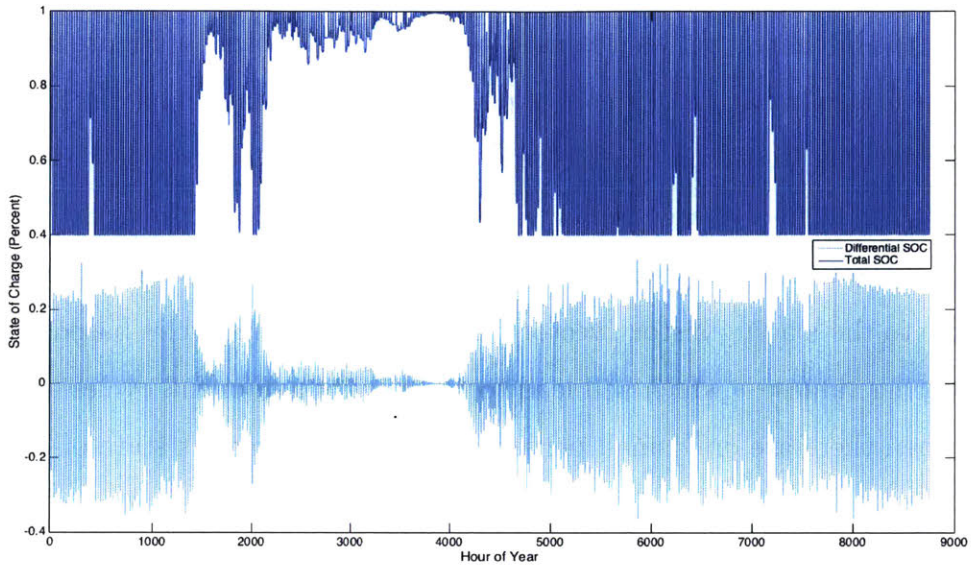


Figure 3-4: Simulated Actual and Differential Battery State-of-Charge

on using the battery's historical SOC over one year.

The rainflow counting algorithm originated for the purposes of fatigue analysis, with a primary application assessing stress and strain responses for materials under loading conditions. Through a determination of 'peaks' and 'valleys' of a loading history, the rainflow algorithm quantifies the stress on a material by counting half or full cycles [39]. This approach is useful as it can be used to understand fatigue and predict failures, but one challenge with relying on this approach is that the basic rainflow algorithm requires a full loading history in order to quantify cycle loading.

For the utilization in the model constructed, the rainflow algorithm determines how and whether to count periods when the battery is charging or discharging as a cycle between time steps — referencing the state-of-charge vector as a reasonable proxy for the battery's loading history over a year. The implementation herein relies on the input of the battery's state-of-charge vector as determined by the KiBaM, with the outputs being the cycle amplitude, the average value of each cycle, and whether to count; the model relies on the MATLAB toolbox for the rainflow algorithm developed in [40].

Consistent with the aforementioned, illustrative configuration, an example of a

battery's hourly state-of-charge vector (values between 0 and 1) and a battery's differential state-of-charge between consecutive hours is shown in Figure 3-4. Given the expected diurnal nature of a charge period during the day and a discharge period during the evening (based on the selected residential solar and load profile), inputting the raw 8760x1 state-of-charge vector yields an overestimate on the cycle count using the rainflow algorithm. This is because, as expected, the rainflow algorithm's outputs is sensitive to the loading history vector imported and counts cycles based on a range of neighboring values — which will lead to counting of half or full cycles even during periods when there are only small perturbations in the battery's state-of-charge.

Thus, the approach taken herein is to transform the 8760x1 vector into a 730x12 matrix — giving 730 12 hour periods (2 per day), and taking the *average* number of cycles of each of the 12 hour periods. The remaining vector consists of the average state-of-charge of the battery during each of the 12 hour periods, a reasonable approximation to make. This is the final vector imported into the rainflow algorithm, which for the purpose of this illustrative example, calculated 364.5 cycles — a logical and expected value for battery cycles over one simulated year. Figure 3-5 validates this notion of the battery seeing roughly 1 charge and 1 discharge period per day, as it depicts the evolution of the daily state-of-charge (24 hour period) over the year (365 lines).

The most important value to extract from the rainflow algorithm implementation is the sum of the total number of cycles per year; this value dictates when the battery should ideally be replaced given the cycle lifetime (discussed in the subsequent section and Chapter 4). An example of the rainflow algorithm's outputs is visually represented in Figure 3-6. The figure shows that most of the cycles are counted around low amplitudes of state-of-charge (i.e. small changes of state-of-charge per cycle) and when the average state-of-charge value per cycle is near the 100% (MLOC) or more towards 40% (MDOD) — which makes sense given the previous analysis of the battery's state-of-charge for the illustrative loading condition shared herein.

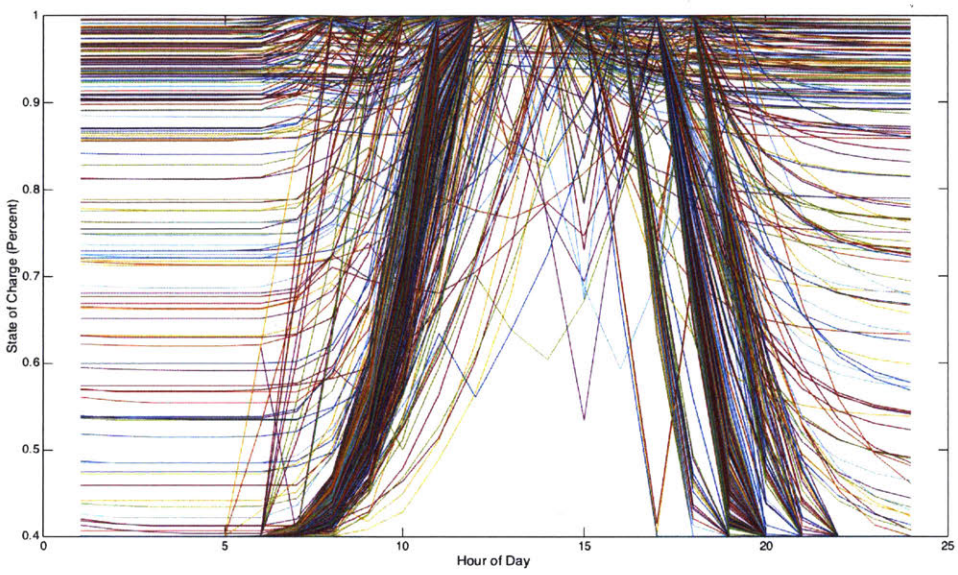


Figure 3-5: Example of Daily State-of-Charge Over Entire Year

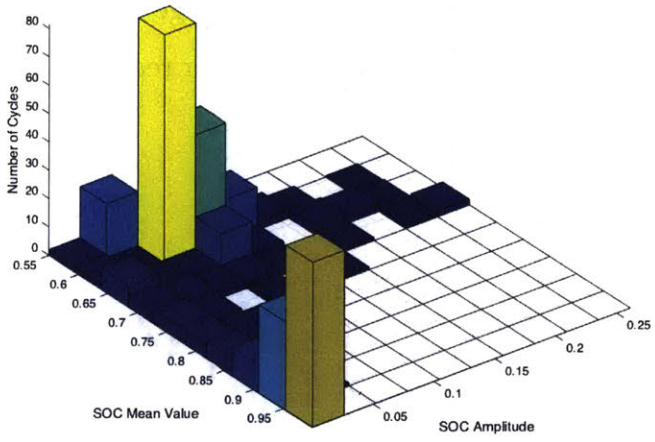


Figure 3-6: Example of Rainflow Algorithm Output [40]

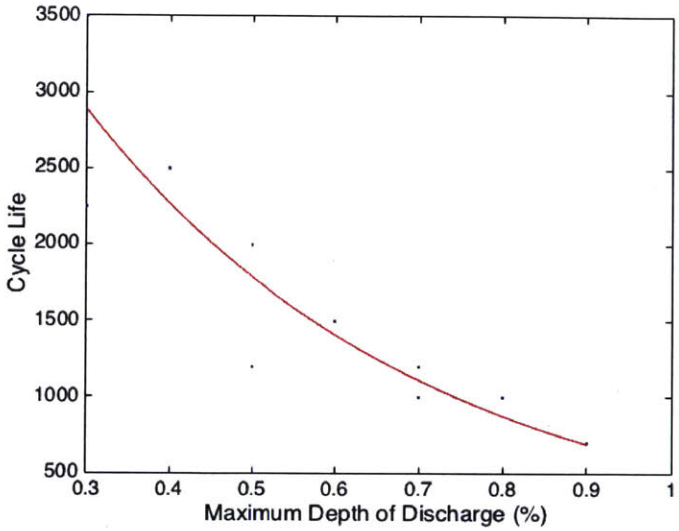


Figure 3-7: Exponential Fit of MDOD versus Cycle Life for Select Lead-Acid Batteries

3.3.1 Effect of Depth of Discharge on Available Cycles

Regardless of the rated cycle life of a battery, how it is operated in the field can have a significant effect on its lifetime. Some battery manufacturers provide data relating the cycle life to the depth of discharge; the depth of allowable discharge directly relates to the number of cycles that a lead-acid battery can realistically withstand over the lifetime of its usage. In 12V lead-acid batteries, a rule of thumb is to not over discharge beyond 50% to 60%; excessive discharge can increase sulphation of the electrodes, decreasing the available electrode area for reactions to take place and thus the effective capacity.

$$CL = 5,891 * e^{(-2.382 * MDOD)} \tag{3.17}$$

Examples of lead-acid batteries' cycle life (CL) as a function of its depth of discharge ($MDOD$), based on a handful of data points gathered from lead-acid battery manufacturers in India, is seen in Figure 3-7. The MDOD factor is a key input to the model, with the cycle life of a battery dictated by the choice of MDOD; the sensitivity to this input parameter is discussed in more detail in Chapter 4, but the

default value for the purposes of the use-case shared herein assumes an MDOD of 60%, corresponding to roughly 1,400 cycles per Equation 3.17.

3.4 Extension of Model and Methodology for Incorporating Voltage Response for Real-Time State-of-Charge Estimation Purposes

A more detailed implementation of a battery model where voltage effects are taken into account requires data on a battery's voltage response as a function of the current. To generate a model that accurately represents voltage dependence on current and various losses is a challenge dependent on parameter selection and optimization in reference to experimental data. Real-time SOC estimation methods have been pursued by both academia and industry for real-time monitoring and managing battery systems in the field; a common approach for measuring real-time SOC is by integrating a 'fuel gauge' chip directly with the battery. Equipped with current sensors, voltage sensors, memory, and embedded algorithms in a micro-controller that rely on interpolation techniques, these chips are made by large electronics companies, such as Texas Instruments (TI) [87]. Once calibrated for the exact chemistry and make, fuel gauge chips can calculate and convey real-time SOC estimation values for batteries operating in the field.

As discussed in Chapter 1, other options for battery models include reliance on mathematical approximations, subject to appropriate parameter selection and extraction, that accurately describe the battery's voltage and SOC as a function of the current loading (charging, discharging, or open circuit). In order to generate and test the model formulation, a reference data set describing a full charging and discharging cycle (measuring current and voltage) is required. The optimization of the functional fit of parameters is assessed by minimizing the difference (in the form of the root mean squared error, RMSE) between the measured voltage and the predicted voltage output. And the novelty of the approach shared herein is an extension of the

Kinetic Battery Model to include optimized parameters that represent underlying electrochemical phenomena — such as conductivity and concentration gradients — that represent the voltage response of a lead-acid battery as a function of a current profile.

3.4.1 Battery Cycle Data Acquisition and Calibration Process

In order to develop a battery model that takes into account voltage effects, an actual data set of a battery's voltage response as a function of a current profile is necessary. The battery cycling protocol used was referenced from Texas Instruments [87]; the battery used for this analysis is a 100Ah Universal lead-acid battery. Starting from a completely discharged state, the protocol called for constant charge rate until the maximum rated battery voltage is reached ($\sim$ 14.5 volts), followed by trickle charge until a C/100 rate is reached; this task was completed using a power supply. After a rest period for at least 3 hours, allowing for concentration gradients across species to settle and for the battery to reach an open-circuit state, the next step was to conduct a discharge cycle. Using an electronic load, a constant current discharge at C/10 (10 Amperes, for this particular battery) was applied until the minimum cut-off voltage of 10.5 volts was reached. With the battery in a fully discharged state, the last step was to similarly let the battery rest for $\sim$ 4 hours.

The data logger referenced in Chapter 2 (16-bit voltage analog-to-digital VersaLog DCV-2 data logger, with a +/-20V range from *CAS Data Loggers*) was also used for data acquisition here as well [80]. In this effort, current on the order of +30/-10A needed to be measured at high resolution, and thus a current amplifier integrated with a sense resistor ($2m\Omega$, in order to mitigate voltage drop) was used [88]. In contrast to a Hall effect sensor, the amplification of the measured voltage drop is proportional to the sensed voltage drop. A depiction of the data logger data acquisition circuit used is shown in Figure 3-8. For the entirety of the charge and discharge cycle, samples were stored at 5 second increments for over 22 hours, yielding a data set of length 16,417

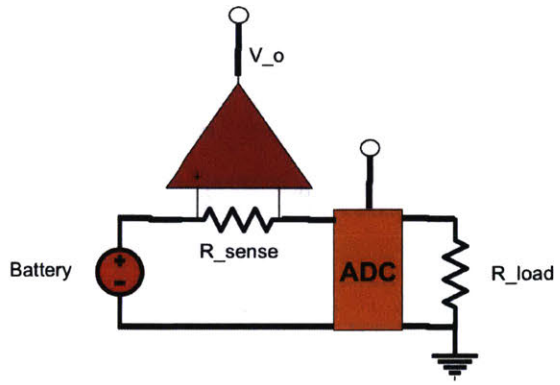


Figure 3-8: Data Acquisition Circuit for Battery Cycle Data

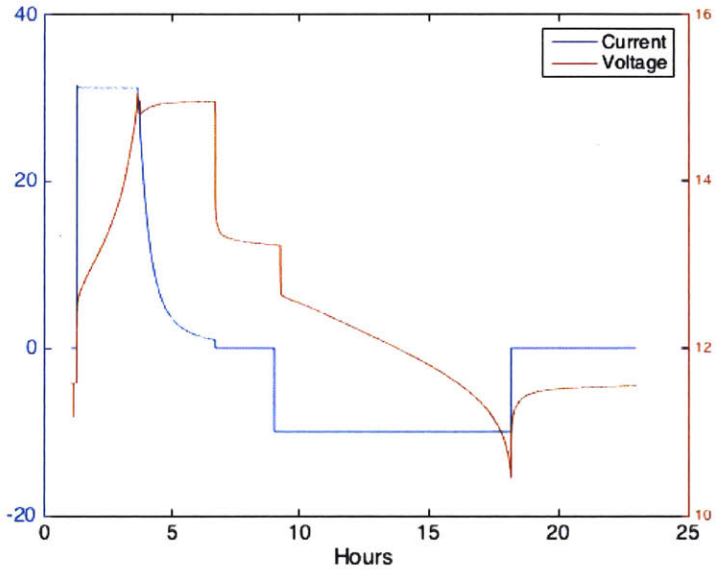


Figure 3-9: Charge & Discharge Cycle: Universal 100Ah Pb-Acid Battery

samples. The round-trip efficiency, based on the integral of the power discharged divided by the integral of the power charged, is calculated to be 85.28%. MATLAB code for importing, calibrating, and visualizing the data set is made available online via accessing [62].

With this data set, the subsequent section discusses the methodology, which can be extended to other batteries and data sets, for developing a more detailed battery model that incorporates voltage responses, various resistive losses, and optimization of battery parameters; the raw current and voltage data acquired for the Universal 100Ah battery is shown in Figure 3-9.

3.4.2 Lead Acid Battery Chemistry Overview

As discussed at the beginning of the chapter, it is important to keep the underlying physical and electrochemical phenomena taking place within a battery in order to relate to the model selection and approach, as having this understanding informs reasonable approaches in constructing representative equivalent circuit, electrochemical, and/or mathematical battery models. Modeling a battery's voltage is chemistry-specific; the half and overall chemical reactions taking place at the electrodes in a lead-acid battery cell during oxidation and reduction oscillate between the formation of lead-oxide at the anode and lead-sulfate at the cathode. The specific chemical reactions and the Gibbs free energy of the half-cell reactions, in reference to a normal hydrogen electrode (NHE), are described by Equations 3.18—3.20 [89] [28].

$$PbO_2 + {SO_4}^{2-} + 4\,H^+ + 2\,e^- \rightleftarrows 2\,H_2O + PbSO_4\ (1.685V) \tag{3.18}$$

$$Pb + {SO_4}^{2-} \rightleftarrows PbSO_4 + 2\,e^-\ (-0.356V) \tag{3.19}$$

$$Pb + PbO_2 + 2\,H_2SO_4 \rightleftarrows 2\,H_2O + 2\,PbSO_4\ (2.041V) \tag{3.20}$$

The difference between the voltages of the half-cell reduction and oxidation reactions is the overall voltage of a lead-acid battery cell ($1.685 - (-0.356) = 2.041$) at standard state. And with 6 cells connected in series, typical for a lead-acid battery, the standard potential ($E°$) is $6 \times 2.041 = 12.246$.

3.4.3 Representative Equations and Selection of Diffusion and Resistance Battery Parameters

With the reference battery data set in hand, a process for optimizing appropriate battery parameters that accurately relates the battery voltage behavior as a function of a current profile is described herein. Of interest is to develop a mathematical model that yields an accurate voltage response based on a current profile. Any battery model construction depends on a selection of parameters, and the approach taken

C-Rate (Hour)	Capacity (Ah)	Amps
20	100	5
10	93	9.3
5	85	17
1	60	60

Table 3.2: Universal 100Ah Battery Capacity & C-Rate

herein builds upon the aforementioned KiBaM parameters: the capacity ratio c, the rate constant k, and the maximum battery capacity q_{max} as described above. These parameters are battery specific, and can be solved with the following capacity/C-rate information taken from the Universal 100Ah battery, as shown in Table 3.2.

The Nernst Equation, as shown in Equation 3.21, approximately describes the relationship between the open-circuit voltage (E) of an electrochemical cell to the standard reference voltage ($E°$), taking into account the temperature, activity of the species, and reaction quotient [89]. A logical interpretation of the reaction quotient is replace the activity coefficients with a proxy for species' concentration (α_{ox}, α_{rx}) — with the oxidized species at the positive electrode and the reduced species at the negative electrode. Thus, the concentration of the reduced species in the numerator can be considered available chemical charge, while the activity of the oxidized species in the denominator can be considered as the unavailable charge — as shown in Equation 3.22. And as the KiBaM aims to illustrate, at any given point in time, the real-time available charge is kinetically constrained and calculated as the ratio of available $q1$ to q_{1max} (equal to $c \times q_{max}$), shown as q_{1SOC} in Equation 3.23.

$$E = E^{\circ} - \frac{RT}{nF} log(\frac{\alpha_{rx}}{\alpha_{ox}}) \tag{3.21}$$

$$E = E^{\circ} - \frac{RT}{nF} log(\frac{SOC}{1 - SOC}) \tag{3.22}$$

$$E = E^{\circ} - \frac{RT}{nF} log(\frac{q_{1SOC}}{1 - q_{1SOC}}) \tag{3.23}$$

$$E = E^{\circ} - \alpha\frac{RT}{nF} log(\frac{q_{1SOC}}{1 - q_{1SOC}}) + \beta(q_{1SOC})^2 + \gamma(q_{1SOC}) \tag{3.24}$$

$$V_{pr} = E - IR_{c,d} \tag{3.25}$$

$$\Delta V_c = IR_c = IR_{cond} + IR_{kin,c}(\frac{1}{1 - q_{1SOC}}) \tag{3.26}$$

$$\Delta V_d = IR_d = IR_{cond} + IR_{kin,d}(\frac{1}{q_{1SOC}}) \tag{3.27}$$

Note that R is the ideal gas constant ($8.314 JK^{-1}mol^{-1}$), T is the ambient temperature (assumed to be $298K$), n is defined as the number of electrons transferred in the overall reaction (2 in this case), and F is Faraday's constant ($9.648 \times 10^4 Cmol^{-1}$). The units of RT/nF come out to be $0.0296 JC^{-1}$, or $0.0296V$ (which includes converting from natural logarithm to base 10 logarithm). However, as argued in [90], the slope of the Nernst equation (in RT/nF) does not sufficiently represent the change in the open circuit voltage as a function of the concentration of chemical species (state-of-charge). Thus, additional fitting parameters — α, β , and γ — are introduced in a modified realization of the Nernst Equation in Equation 3.24 [90].

Lastly, IR losses (voltage drops) are also included in the model construction. Specifically, a term for general electrical resistance of the cell is represented as R_{cond} — which is assumed to be constant. Additional resistances vary as a function of the state-of-charge, and whether the battery is charging or discharging, and this is aimed to be taken into account by mass transport resistance terms, represented by $R_{kin,c}$ and $R_{kin,d}$ in Equations 3.26 and 3.27. A depiction of the charging and discharging resistance following the functional form are show in in Figure 3-10. As the plot

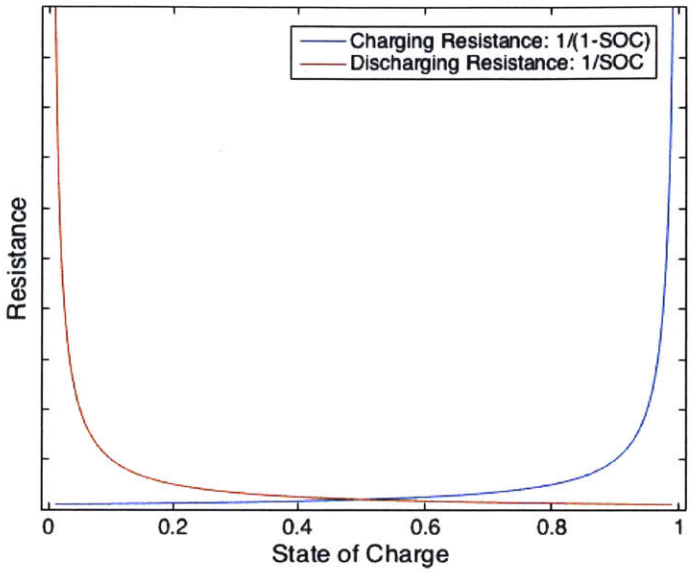


Figure 3-10: Notional Depiction of Functional Charging and Discharging Resistances

shows, the charging resistance increases with state-of-charge and vice versa for the discharging resistance. Note that this model is undefined at the boundary conditions for the state-of-charge, i.e. if the state-of-charge is zero or one; thus, the model implementation restricts values for the state-of-charge to be between 1% and 99%.

Thus, the actual battery voltage (V_{pr}) in Equation 3.25 is calculated from the open circuit voltage determined from the modified Nernst Equations (with the addition of fitting parameters and a reliance on the available charge as dictated by KiBaM) less the voltage drops from the resistances. The next section described the optimization approach for the parameters across the entirety of the acquired data set.

3.4.4 Battery Parameter Constraint Selection & Optimization Formulation

In this formulation, the number of parameters in this model, including the three KiBaM parameters, account to a total of nine. These parameters need to be initialized and simultaneously optimized that minimizes the predicted and actual voltage response curve based on the battery cycle training data set acquired. The optimization relies on bounded constraints, which need to be set and determined logically.

From KiBaM, the capacity ratio c can only vary between 0 and 1, while the rate constant k needs to be a positive value; the upper bound for the latter is chosen to be 10. The maximum available battery capacity, q_{max}, can also be viewed as not an entirely fixed value — so the optimization allows this value to vary between 15% of the nominal q_{max} value. Note that the three initial KiBaM parameters' values, as described in Table 3.3, are calculated based on the values given in Table 3.2.

The additional parameters introduced in the modified Nernst equation described above, in α, β, and γ, can vary between positive and negative dimensionless values — and a range of -100 to 100 is chosen. And lastly, for the three resistance parameters, the range is chosen to be 0Ω and 10Ω to not allow for negative resistance values.

With a battery model and constraints formulated, the next step is to optimize the parameters such that the predicted voltage response is as close to the actual voltage response as possible based on the actual voltage data acquired. The objective of the optimization was to minimize the root mean squared error (RMSE) between the predicted ($V_{pr,d}$) and actual voltage vectors ($V_{act,d}$), subject to optimizing the aforementioned parameters; note that the initial values for KiBaM are also subject to being further optimized subject to reasonable bounded constraints, specifically c, k, and q_{max}. The optimization formulation is as follows across all data points ($N = 16,417$), and includes the upper and lower bound constraints on parameter values:

$$\min_{RMSE} \quad RMSE = \sqrt{\frac{\sum_{d=1}^{N}(V_{pr,d} - V_{act,d})^2}{N}}$$

$$s.t.$$

$$1 \leq k \leq 10$$

$$0.001 \leq c \leq 1$$

$$-100 \leq \alpha \leq 100$$

$$-100 \leq \beta \leq 100$$

$$-100 \leq \gamma \leq 100$$

$$0.85 \times q_{max} \leq q_{max} \leq 1.15 \times q_{max}$$

$$0\Omega \leq R_{cond} \leq 10\Omega$$

$$0\Omega \leq R_{kin,c} \leq 10\Omega$$

$$0\Omega \leq R_{kin,d} \leq 10\Omega$$

3.4.5 Optimization Results and Discussion

Using the interior-point algorithm with the *fmincon* optimization solver in MATLAB, an optimized set of parameters was found. The final RMSE determined is 0.1100 volts, which can be interpreted as the average deviation between the predicted and actual voltages (again, across the 16,417 sample data points). The optimization required 125 iterations to converge, and the entirety of the program, which also includes importing data and initializing the parameters/constraints, took 243.39 seconds (roughly 4 minutes) to complete.

In terms of the final parameter values, as shown in Table 3.3, the resistance parameters are on the order of milli-ohms, a logical order of magnitude for a battery. Note that none of the parameters reach either the lower or upper bound constraints — however, the rate constant from KiBaM (k) reaches its lower bound constraint and

Parameter	Lower Bound	Initial Value	Final Value	Upper Bound
k	1	7.58	1.000	10
c	0.001	0.591	0.9027	0.999
α	-100	1	-29.7234	100
β	-100	1	-1.3704	100
γ	-100	1	0..7637	100
q_{max}	85	101.112	102.6195	115
R_{cond}	-10	0	0.0123	10
$R_{kin,c}$	-10	0	0.0083	10
$R_{kin,d}$	-10	0	0.0114	10

Table 3.3: Output of Optimized Battery Parameters for 100Ah Universal Battery

differs fairly significantly from its initial value; furthermore, the KiBaM capacity ratio (c) does increase from its initial value, and nearly reaches its upper bound constraint. Based on this model formulation, it is interesting to note the deviation of the k and c parameters as originally calculated from the available values off of the Universal 100Ah data sheet, and in this case, the optimization has increased the proportion of the available charge while decreasing the rate at which charge can transfer between the available and bounded charge tanks.

The two plots in Figure 3-11 show the IR drops in relation to the current profile and the q_1 state-of-charge. Note that the shapes of the q_1 state-of-charge in the top plot and the various IR losses in the bottom plot are dictated by the current profile. This is because that though both the charge (+30A) and discharge (-10A) exhibit periods of constant current, the constant charge period is followed by a period of constant voltage when the maximum charging voltage is reached — which eventually leads to a trickle charge in somewhat of the functional form of an exponential decay. The electrical resistance is a scalar value, with the associated IR drop proportionally following the shape of the current profile. And for both charging and discharging, the resistive losses respectively increase exponentially in relation to the q_1 state-of-charge.

The upper plot in Figure 3-12 shows the final predicted voltage output based on the optimized parameters, in comparison to the actual measured voltage. This shows good agreement with the original voltage values, again with an RMSE less than one-tenth of a volt. In the bottom plot, the output of the modified Nernst equation (from

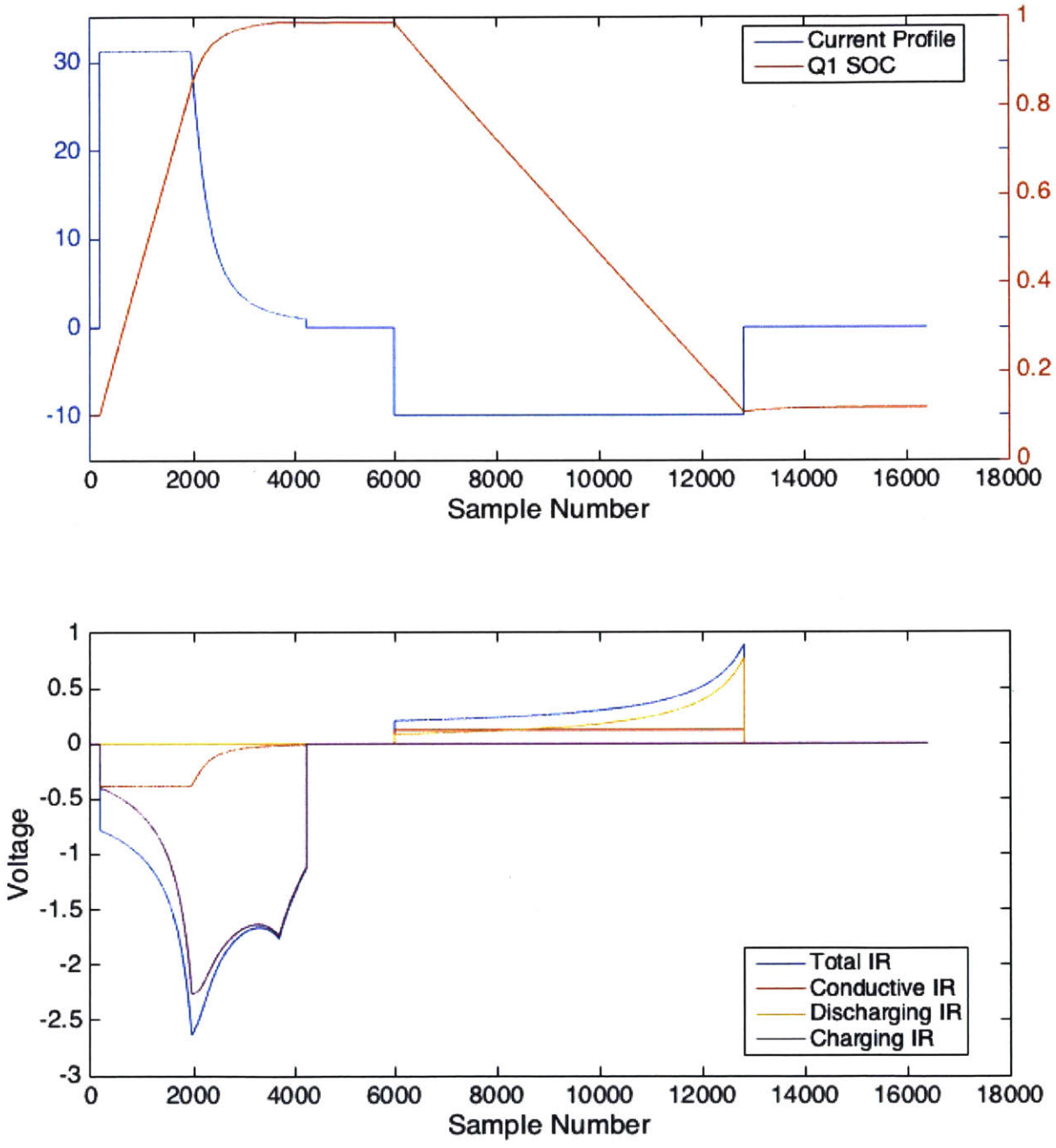


Figure 3-11: Output of IR Losses vs. Current Profile and Q1 SOC

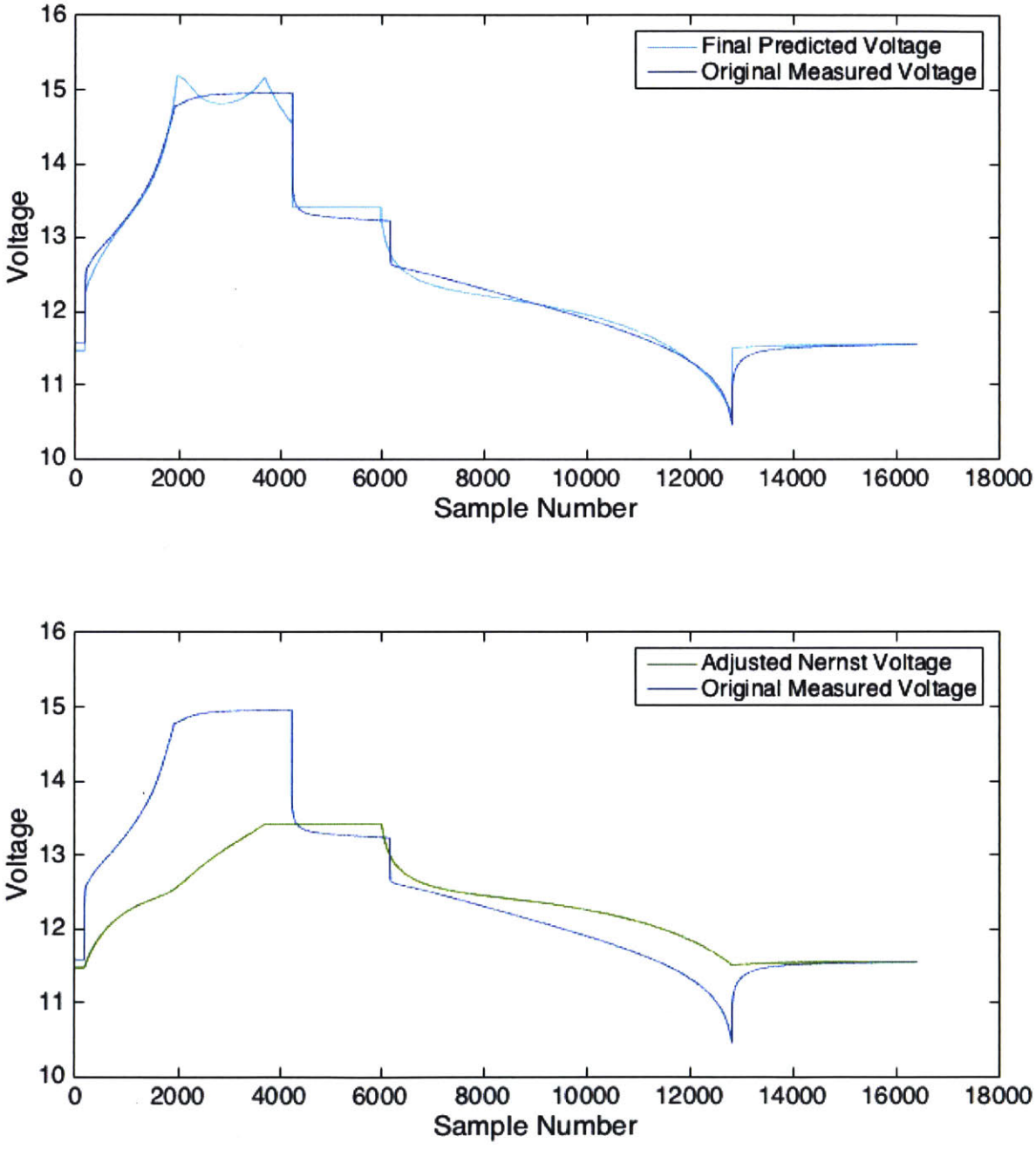


Figure 3-12: Output of Predicted Final and Nernst Voltages vs. Measured Voltage

Equation 3.24) is shown in comparison with the actual measured voltage to illustrate the importance and difference of fit when incorporating such IR losses in the battery model (albeit the optimization was designed to minimize the difference between V_{pr}, versus E).

3.5 Conclusion

With the advent of distributed renewables, having realistic models and simulations of key components are essential. Batteries in particular are important to model, yet the complex underlying electrochemical phenomena make them challenging to represent. The work presented in this chapter has first shown the results from an adapted implementation of the kinetic battery model (KiBaM) — originally conceived to mathematically express internal battery dynamics associated with ionic species diffusion and concentration gradients near electrodes during charge and discharge. Results show that the incorporation of battery management constraints in simulation effects how the battery is dispatched — with the associated economic effects discussed in Chapter 4. Though the KiBaM is not well-suited for real-time applications, this chapter also presents an extension of the model to incorporate voltage effects. Specifically, this chapter has shown a novel construction of a battery model, through a parameter selection and optimization methodology, that provides accurate voltage predictions based on expected current loading.

Chapter 4

Technical and Economic Modeling Analysis for Optimizing Generation Asset Sizes

4.1 Introduction

Micro-grids and solar home systems have been looked to as key enablers of electrification, receiving attention in the form of grant programs, capital subsidies, and NGO efforts in recent years. Yet, both of these approaches are still challenging to implement due to issues such as revenue collection and community buy-in for micro-grids, while the high upfront costs of solar home systems can make for prohibitive individual investments [4]. In both cases, generation assets in solar panels and battery capacities tend to be over-sized to ensure regular and reliable evening electricity service to residential customers, especially for periods of low solar insolance. As discussed further in Chapter 4, these conventional approaches inherently increases costs, leading to long payback periods and financially unattractive rates of returns.

As discussed in Chapter 1, the advent of low-cost computation, power electronics, and sensors — encompassed into power management devices — can enable the next generation of micro-grids for rural electrification. These capabilities can allow for a

variety of power management strategies and can be integrated in a distributed, 'prosumer' network architecture, as described in [91] for example. While typical micro-grids provide fixed hours of evening electricity services, effective real-time demand-side management based on load disaggregation can differentiate critical and non-critical loads, and thus regulate the amount of power consumed during operation to maintain network reliability thresholds.

More specifically, power management strategies in resource-constrained, isolated solar micro-grids impact both the real-time availability of electricity supply and expectation of electricity demand. Of interest in this work is to illustrate that micro-grids with demand-side management can alleviate some cost challenges with conventional electrification approaches by more optimally sizing generation assets for given expected levels of demand and solar irradiance — defined and considered at sub-village scales in comparison to centrally planned micro-grids. As eluded to in Chapter 1, there are a few reasons for analyzing decentralized micro-grids in particular. First, decentralized micro-grids that rely on solar panels and batteries can still take advantage of economies of scale by drawing from the same solar panel and battery. However, having a micro-grid that isn't focused on village-wide electrification can alleviate traditional hurdles in acquiring customers at once and placement of solar arrays and battery banks. Lastly, enabling small-scale micro-grids of sizes from 5-10 households can potentially catalyze individuals residing in off-grid areas to invest in and earn from their own electricity infrastructure that can be autonomously managed with minimal human intervention for operation.

This chapter presents a framework, both technical and economic, to illustrate the value of having power management devices with demand-side management capabilities in decentralized micro-grids designed for electricity access. The model presented operates in a series of sequential, computational steps —- all of which is implemented in MATLAB with a basic version of the micro-grid model is available online in [62]. Details and governing mathematical equations, models utilized, and relevant results are the subject of this chapter, with the key contribution and rationale for conducting this technical analysis is to identify the optimal (least-cost) combination of solar and

battery assets that meet reliability constraints. In order to come up with values for reliability, and assess the performance of various solar and battery combinations, key components of the network such as wiring losses, DC/DC converter efficiencies, solar module production, and battery operating constraints need to be appropriately modeled. Thus, a key focus of this chapter is the technical construction and mathematical model to show generation asset design and basic micro-grid operation.

The goal of this chapter is to present the value creation opportunity for micro-grids with demand-side management, relying on the technical formulation and simulation discussed in the previous chapter. In the actual model implementation, the technical model described in Chapter 3 feeds directly into the economic analysis and financial model discussed here. The main argument illustrated is that micro-grids with embedded demand-side management capabilities enabled through power management devices as previously described can decrease costs in comparison to conventional micro-grids and individual solar home systems. Specifically, the cost-benefit comes from more optimally sizing the key cost components in a micro-grid — in the solar modules and the batteries — subject to meeting average yearly reliability constraints. The economic analysis focuses on a greenfield use-case, meaning building a micro-grid from scratch (as opposed to retrofitting or extending existing installations). Key cost inputs, financial assumptions are discussed, along with results and further analysis.

4.2 Description of Load/Appliance Choice Scenarios for Demand Representation

As explained in Chapter 2, understanding the nuances of demand profiles as a function of appliances and other variables, such as time of day and temperature, is of critical importance. In any power system, the choice of generation assets and assurance of resource adequacy is a function of the expected demand profile — whether aggregated at a feeder level, household-by-household, or appliance-by-appliance.

The model described here relies on the methods included in the Reference Electri-

fication Model (REM), which generates a randomized demand profile at each household given the number of consumers in the network based on appliance-level input assumptions. As referenced in Chapter 1, REM takes inputs in from survey results on expected electricity consumption needs, and creates typical household energy consumption vectors of desired length in hours (typically 8760, the number of hours in a year). The REM model randomly permutes start/end times of appliance activities within certain time ranges and introduces day-to-day variability of electricity usage. REM also allows for exogenous variables, such ambient temperature and sunlight levels, to induce fan and light usage, respectively [16]. The input variables are based on historical average irradiance and temperature data over a year timeframe — which can be provided for a particular longitude and latitude from the National Renewable Energy Laboratory's (NREL) PVWatts database and calculator [83].

As part of this effort, a binary encoding of critical (1) and non-critical (0) loads are additional inputs into the demand profile construction, representing the ability to disaggregate individual loads. Each household's demand profile is separated into two 8760x1 vectors, for critical and total load profiles, and is then integrated across the number of consumers in the network. An example of one household's demand profile in the 'residential load scenario' can be seen in Figure 4-2 — again, created individually for each of the 5 households in the instantiation of the model shared herein [16].

To keep somewhat consistent with the loads and appliances installed in the solar home system in Jharkhand as discussed in Chapter 2, the first instantiation of this model and the demand profiles will also be based on those appliances, called the 'residential load scenario' with an assumption of 5 households connected to the network; the description of these loads (in LED lights, fans, and mobile charger) per household are shown in Table 4.1 — along with assumptions on hourly usage and exogenous variables that would induce the appliance's usage (i.e. ambient temperature, amount of sunlight). Note that the generic nature of this model can allow for a larger number and higher diversity of loads in alternate use-cases.

Figure 4-1 shows the effect that the 'enabled when' criteria have on the generation

Table 4.1: Demand Load Profile Inputs: Residential Load Scenario

	Appliance		
Parameters	Light (LED)	Fan	Cell Phone Charger
Number	2	1	1
Hours per Day	4	4	4
Watts	5	14	2.5
Critical (Y/N)	Y	N	N
Enabled	Irradiance $\leq 0.05W/m^2$	Temp $\geq 31°C$	N/A

of load profiles over simulated hours. The top plot shows the influence of the ambient temperature on the fan usage — when above 31 degrees C, while the lower plot shows how the sunlight induces the light usage — when below 5 watts per meter squared. Again, each of the demand profiles are generated one user at a time for each hour of the year ($i = 1...8760$), and then a cumulative load profile for the whole network is generated by recursively adding each load profile together ($j = 1...h$). Examples of an individual household's demand profile ($TP_{i,j}$) and the cumulative total load profile (TP_i) across the network for an entire year are shown in Figures 4-2 and 4-3; note that the equations that follow also hold for the critical demand profile (CP).

4.3 Description of Selected Network Architecture & Devices

The direct current (DC) network architecture was chosen to be modeled in this effort due to its potential for scalability, design for safety, and explicit reliance on integrating low-cost components for this application. Each modular, decentralized micro-grid would consist of generation (in solar panels), storage (in lead-acid batteries), wiring, and power management devices at the network and household levels. Specifically, there are two types of power management devices considered here. The generator (also referred to as 'source') device would consist of an MPPT (maximum power point tracking) charge controller, a boost converter to a 24V DC network — with multiple outputs to connect either a bus or individual households. The generator

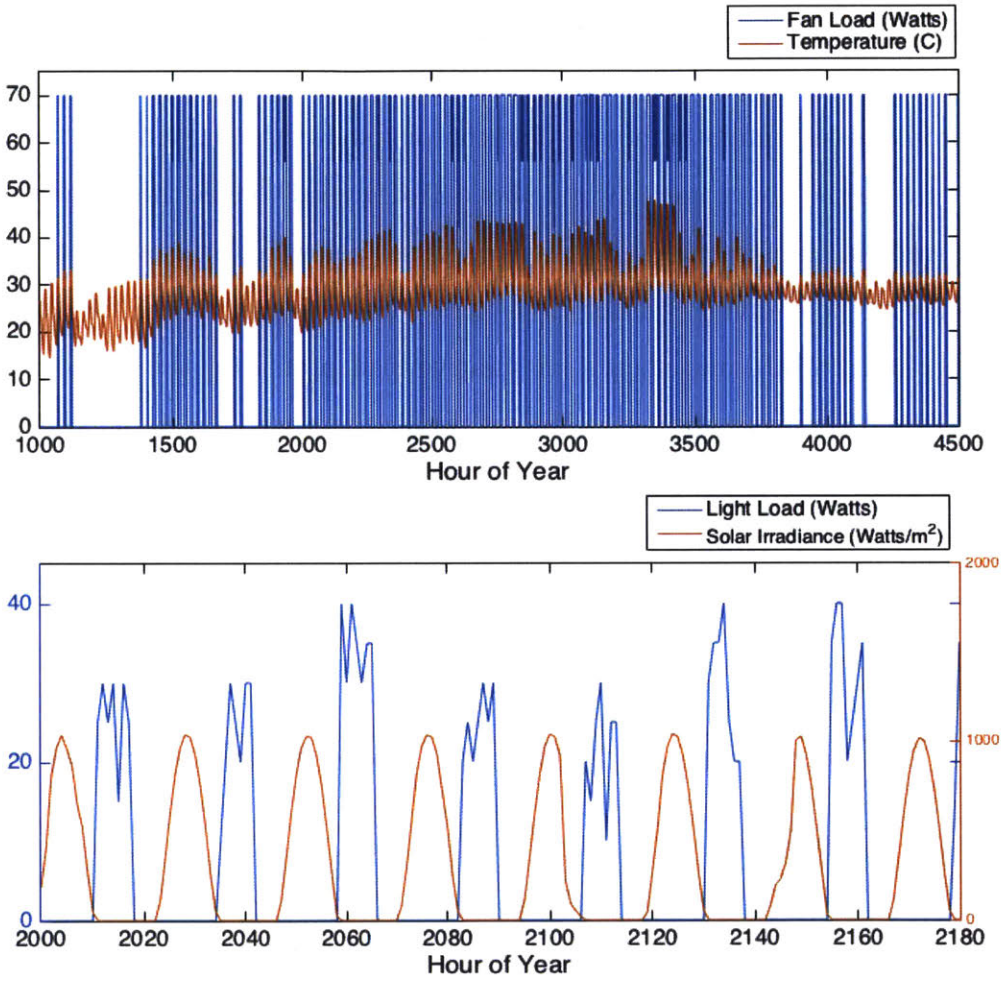


Figure 4-1: Example Total Fan and Lighting Load Conditioned on Ambient Temperature and Sunlight

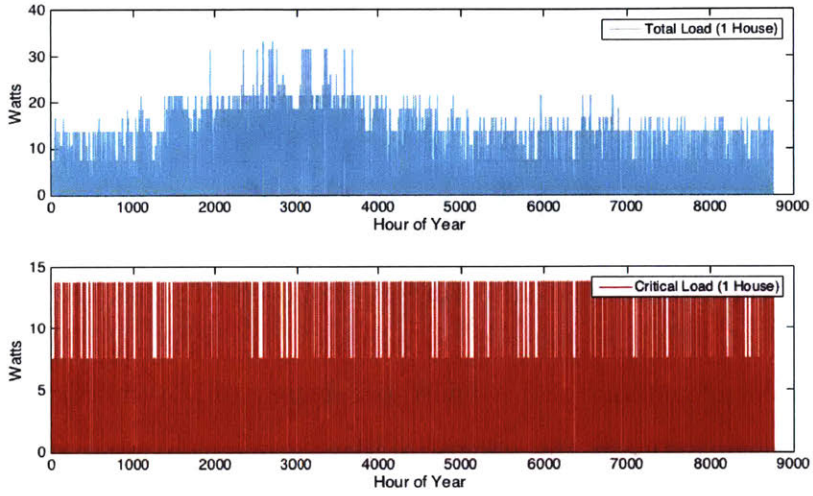


Figure 4-2: Example of Total and Critical Yearly Load Profile for One Household

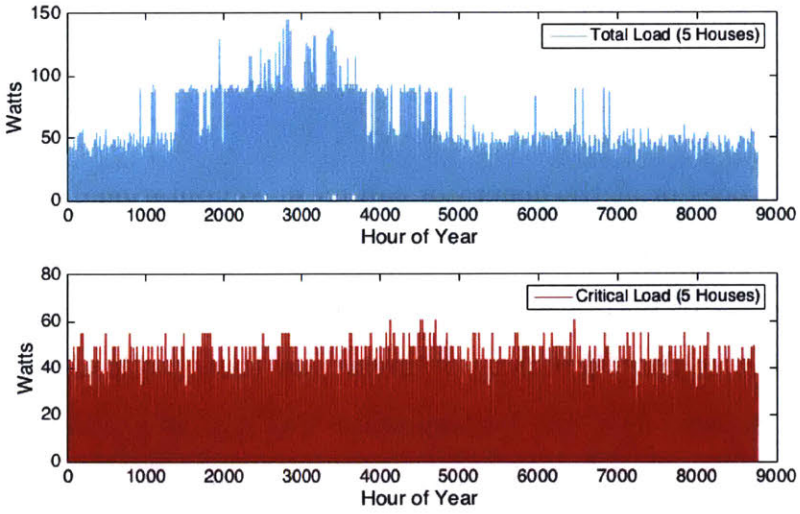


Figure 4-3: Example of Total and Critical Yearly Load Profile for Five Households

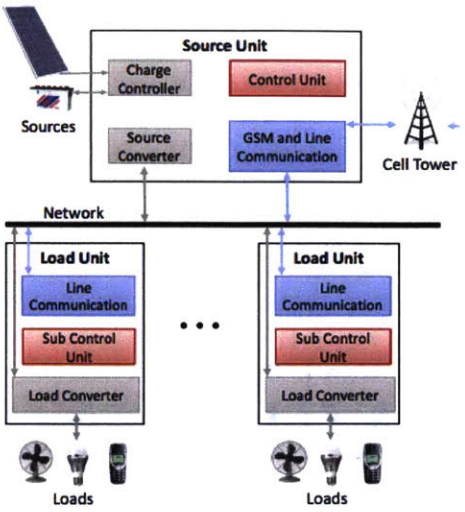


Figure 4-4: Modeled Architecture & Proposed Network Layout [91]

device includes local memory and a micro-processor, and bi-directional communication can take place between the generator device and consumer devices. At each household, the consumer device (also referred to as the 'load' device) consists of a single-input, multi-output buck converter with current-control capabilities, switches, and sensors at each outlet. The relevant aspects included in the model shared in this work, specifically in regards to converter efficiencies and network layout, are discussed in the remainder of this section.

The central processor at the generator can make computational decisions for load dispatch, prioritization, curtailment; depending on algorithm selection, the ability to conduct forecasts of both available electricity and demand is possible but is not explicitly modeled herein. This type of device can allow for load flexibility or prioritization, and conveying of the battery state-of-charge as a proxy for a real-time 'price' to the end user. This conveyance of the real-time state of the system is a key aspect in next generation micro-grids for rural electrification, as users can receive signals/information on resource scarcity, available balance, etc. that can enable 'pay-as-you-go' strategies. This type of engagement with users will undoubtedly require future work to understand in detail, from a social science perspective, the most effective signals and behavioral responses in such contexts and is part of the discussion in Chapter 5.

4.3.1 DC-DC Converters Model

The role of DC/DC converters is to regulate the voltage output (in this case, rated DC voltage of the loads or the regulated DC voltage of a bus) that can handle a range of input voltages. The overall network topology is depicted in Figure 4-4, showing the layout of the source and load units relative to the solar panel, battery, network, and the end-user appliances. Yet the selection of the specific converter circuit topology, individual components (i.e. capacitors, transistors, inductors, thermal management, etc.) and logic embedded within (i.e. duty cycle, switching frequency, mode of operation) is driven by the cost, efficiencies, voltage range, and power levels desired. The subject of providing safe, reliable, and low-cost power electronics in the context of small-scale, ad-hoc micro-grids for electricity access is part of the detailed analysis conducted in [81], with the proposed overall architecture presented in more detail in [91].

DC/DC converters can lose efficiency due to switching, parasitic, and conductive losses — which relate to the desired output power in relation to the rated power of the converter. The boost converter referenced herein was specifically designed to rely on low-cost components and operate at high efficiencies. Furthermore, the boost converter in the generator devices is able to integrate with a 12V battery, a 250W panel (via an off-the-shelf charge controller in Linear Technology's LT8490 [82]) and regulate the output voltage into the network to be 24V as envisioned in [81]. For the purposes of this work, the efficiencies of the boost converter is included based on experimental data of conversion efficiency of the boost converters as a function of power (up to 250W), with the raw data measurements taken as part of the converters' design in the work conducted in [81].

Similarly, each load device includes a buck converter to step down the network voltage for usage in appliances — designed for high efficiency, low-cost, and safety via isolation topologies. The buck converter was designed to handle up to 25W of load, consistent with the assumptions modeled in the 'residential load' scenario shared in this work. As with the boost converter, the efficiencies of the household-level buck

converters are included based on the measured data of the buck converter efficiency as a function of the power (up to 25W), again with the raw data measurements referenced from [81].

In the model construction presented here, the expected efficiency losses through the DC/DC converters are obtained through a polynomial fitting method based on the measured data points. For illustration, network boost converter losses are shown in Figure 4-5, separating losses when serving critical and total loads to the entire network; this is based on the efficiency of the source module stepping the voltage from 12V to 24V across varying power levels. Separately, buck converter losses are modeled at each household and shown in Figure 4-6, again separating both critical and non-critical load profiles; the losses associated with the buck converter are due to stepping down the input bus voltage from 24V to the 12V load outputs. Again, the measured data of example of DC/DC converters, both buck and boost with single input / multi-output topologies designed for power levels expected in residential households in a decentralized micro-grid application with computational abilities for conducting demand-side management, were originally developed as part of the work on low-cost power converters designed, tested, and characterized in [81].

The equations below mathematically represent how these losses are computed. At each hour of the year (i), Equation 4.1 described the network losses (NL), aggregating the total demand (TD) over all the households in the network (h), and multiplying this by the functional form for the efficiency of the network boost converter (f_{NL}). Similarly, Equation 4.2 describes the household losses (HL) based on the functional form for the efficiency of the household-level buck converter (f_{HL}) — with the outputs of both equations in watts.

$$NL_i = \sum_{j=1}^{h} TD_{i,j} \times (1 - f_{NL}(TD_i)) \tag{4.1}$$

$$HL_{i,j} = TD_{i,j} \times (1 - f_{HL}(TD_{i,j})) \tag{4.2}$$

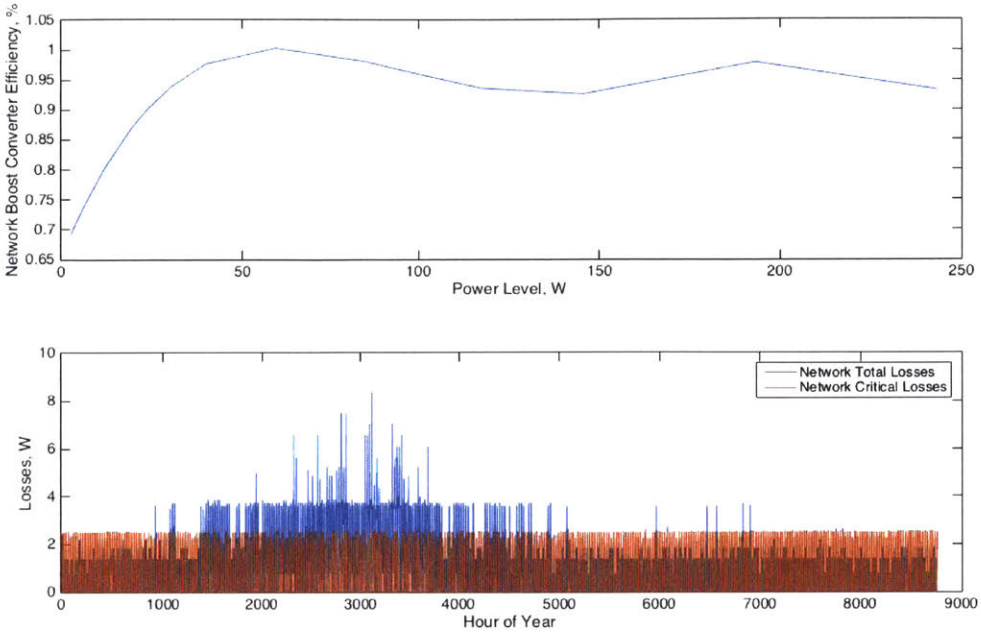


Figure 4-5: Measured Boost Converter Efficiencies and Simulated Network Losses [81]

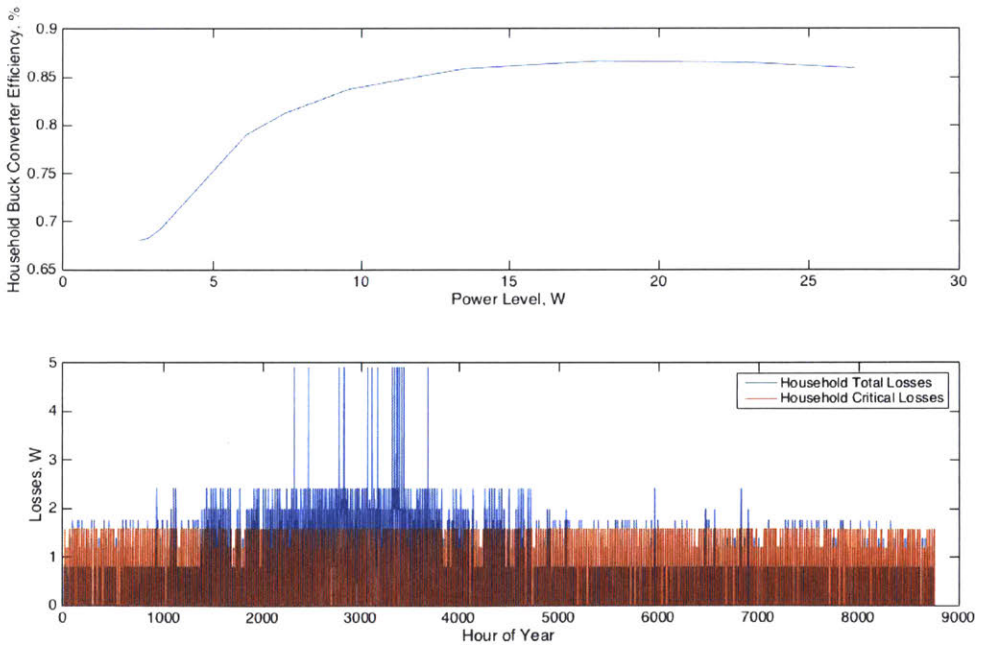


Figure 4-6: Measured Buck Converter Efficiencies and Simulated Losses at Household [81]

4.3.2 Micro-Controller Power Consumption

The micro-controller on-board in the power management device is required for communication between the generator and consumer devices. More specifically, a micro-controller is required in order to read-in sensor information across the network, conduct real-time estimates of the state of the network, make decisions on prioritizing, serving, or curtailing appliance consumption — and sending signals.

The selected micro-controller for the power management device under discussion is a 16-bit dsPIC33 from Microchip Technology Inc. [81]. The selected micro-controller was chosen for its combination of computational speed (40 MIPS), memory (64 KB), RAM (16,384 bytes), and cost ($4.61 at 5,000 units). More specifically, the dsPIC 33 is required for reading and processing sensor data (current and voltage across sources and loads), conducting basic computation, and sending control and communication signals. In regards to power consumption, the input voltage supply range for a 16-bit micro-controller is between 3.0—3.6 volts, and the source/sink current draw is on the order of 10-20 mA (milli-amps), equating to roughly 0.05 watts in power consumption [92].

In applications such as medical devices or wearable technologies, relying on batteries in the order of mAh capacity, understanding the power consumption of micro-controllers under various modes of operation is or critical importance. However, given the orders of magnitude difference from having a noticeable impact on energy requirements of a micro-grid system, the baseload power consumption of the micro-controller is neglected in this analysis.

4.3.3 Wiring Losses

For micro-grids employed within a particular village (or hamlets within), the wiring losses included in low-voltage DC networks may not present a significant issue. Nonetheless, line losses are an important aspect to be included in the modeling effort.

Based on the architecture presented in [91], the wiring gauge selected in this model is 14 AWG, with a resistivity of 0.008286 Ω/l. The wiring losses are modeled

by first taking wire resistivity, and multiplying that by the length of the wiring in the network. The wiring configuration is not specified in this model, but the total wiring requirement is calculated assuming roughly 40 meters required per household, connected via a daisy-chain topology from the placement of the solar panels and the battery (assumed to be near one of the households); the choice of this value is based on the average wiring distance between households required for conducting a field trial near the peri-urban area of Patamda, Jharkhand in June 2015. In cross-referencing with a local micro-grid company in Jharkhand, the exact wiring of any particular micro-grid is inextricably related to the layout of the particular village, households, etc., but assuming 40 meters per household is a reasonable approximation, erring on the side of over-estimating wiring requirements. This is supported by the value of roughly 10 meters of wiring assumed to be required per household (using 16 AWG) in the analysis conducted in [44]. Based on the maximum value of the load profile presented in the earlier section ($\sim 150W$), with a network voltage of 24V, the maximum current required would be 6.25A at the network — which is well within the constraints of 14 AWG wiring (15A ampacity at 60°C).

As shown in Equation 4.3, in the case of 5 households connected to a network (h), the total amount of wiring distance is assumed to be 160 meters (w). The resistivity of the wire (Ω) is then multiplied by the aggregated current demanded in the network (I) squared, which is obtained by dividing the expected aggregated load profile by the network voltage ($V = 24$) in Equation 4.5; this is used to calculate wiring losses (WL, in watts). An example of losses are shown in such a network in Figure 4-7.

$$w = (h-1) \times 40 \tag{4.3}$$

$$I_{i,j} = TD_{i,j}/V \tag{4.4}$$

$$WL_i = \sum_{j=1}^{h} I_{i,j}^2 \times \frac{\Omega}{w} \times w \tag{4.5}$$

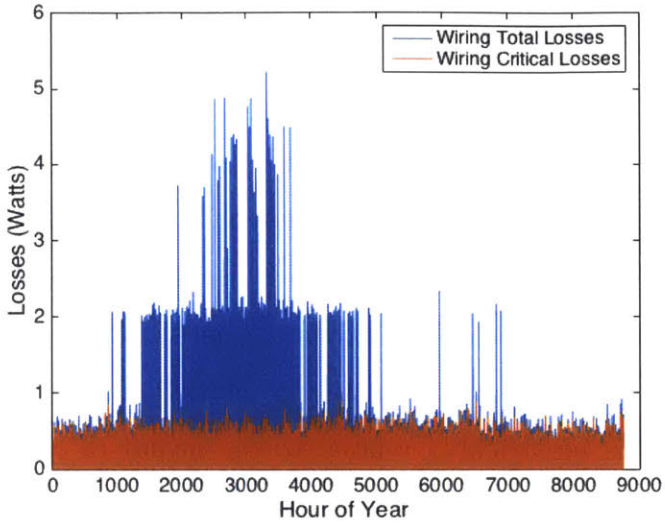


Figure 4-7: Example of Wiring Losses in Network

4.3.4 Aggregated Load Profile

The main reason for including both the wiring and power conversion losses in this modeling effort is that such efficiency losses need to be included to represent the entirety of a load profile that needs to be served. Even though the power lost in transmission and conversion is not delivered or used by the load, these losses are included in the aggregated demand profile — as this is a more realistic representation of the entirety of the load profile that needs to be served. And in turn, including these losses as part of the overall power profile in the network can affect the selection of the solar and battery combination required.

To summarize mathematically, the Equation 4.6 below describes the total load profile (TD), including the network losses; again, this equation holds for the aggregated critical load profile as well (CD):

$$TD_i \quad = TP_i + WL_i + NL_i + \sum_{j=1}^{h} HL_{i,j} \tag{4.6}$$

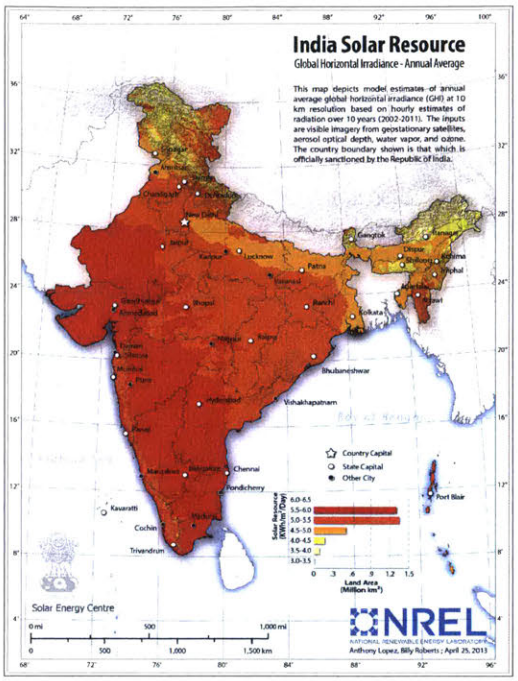


Figure 4-8: Annual Average Global Horizontal Irradiance: India

4.4 Solar Module Model

4.4.1 Solar Irradiance Resource Data

For the purposes of the use-case of this model presented herein, the geographical location and coordinate choice is the peri-urban area of Patamda, in the state of Jharkhand, India; this is mainly due to the on-the-ground collaboration the Tata Steel Rural Development Society (TSRDS), located in Jamshedpur, Jharkhand. As shown in Figure 4-8, the areas surrounding Ranchi, the state capital of Jharkhand, has a favorable solar resource — on the order of $\sim 5.0 - 5.5$ kWh/m^2 per day; these estimated, historically averaged values are measured in Global Horizontal Irradiance (GHI), which includes both the Direct Normal Irradiance (DNI) and the Diffuse Horizontal Irradiance (DHI) [83].

The National Renewable Energy Laboratory (NREL) PV Watts database makes available data sets on average, historical irradiance values constructed on an hourly

basis for a year (8760 values). An example of the output of the values — at the geographical coordinates chosen for this analysis (22.95°N, 86.35°E) — are depicted in Figure 4-9; note that there is a clear drop in available solar resource during the monsoon season. The daily and seasonal variation in available solar resource is important to keep in mind, as it effects the available energy the battery has to store in order to serve evening loads.

4.4.2 Solar Power Output

Based on the available solar insolance (IR) per unit area (m^2), the following equations were used in order to determine the power output (W) from the peak power generating capacity of a solar panel (Wp, rated at $1{,}000W/m^2$) at each hourly time step (i). Note that the parameter α that is a temperature-adjusted module efficiency parameter ($PV_{eff,ref}$ versus $PV_{eff,temp}$); higher temperatures can decrease lifetimes of solar panels in comparison to the reference temperature ($T_{ref} = 25°C$), but in the short-term, can increase power output due to the higher generation of charge carriers in more easily allowing electron-hole pairs to be excited into the material's conduction band.

$$W_i = \frac{IR_i}{m^2} \times m^2_{panel} \times PV_{eff} \tag{4.7}$$

$$m^2_{panel} = Wp/(1000W/m^2) \times 1/PV_{eff,ref} \tag{4.8}$$

$$. \; PV_{eff,temp} = PV_{eff,ref} \times (1 - (\alpha \times (T_{ambient} - T_{ref}))) \tag{4.9}$$

$$\tag{4.10}$$

Again, it is clear from Figure 4-9, the monsoon season takes an impact on the available solar energy in the locale chosen, shown by the dip in available energy just after the middle of the year (roughly July-August). As discussed in the previous chapter, isolated micro-grids (without a centralized grid interconnection) based on solar power may "spill" excess electricity that is unused during the day and when the

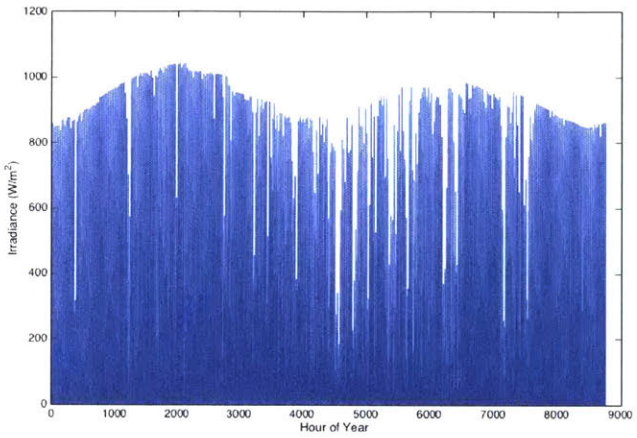


Figure 4-9: Historical Average Solar Irradiance near Patamda in Jharkhand, India

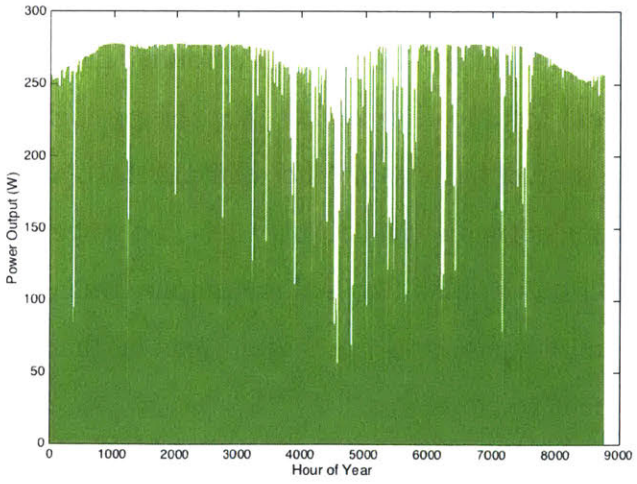


Figure 4-10: Hourly Output of 300W Panel Based on Irradiance in Jharkhand, India

battery is full — while also not being able to serve demand during periods of low solar irradiance. These parameters are a function of the module size, the size of the battery, and even the amount of day-time loads present in the network.

4.5 Matrix Population and Search Method for Generation Asset Selection Subject to Reliability Constraints

The previous sections in this chapter have discussed the technical representation of the key components included to model micro-grids of interest. Specifically, the chapter thus far has outlined in detail the representation of demand, network architecture, and solar power generation — with the lead-acid battery operation included in Chapter 3. Before the cost and financial analysis, the final step of the model is to select the least cost combination of solar module and battery capacity in order to meet a predetermined reliability threshold. The model computes the reliability over the entire year for both critical and total load profiles — populating each cell in the matrix for every available combination of battery (k) and solar panel (l), as depicted in Table 4.2. The discrete combinations of individual solar panels and battery capacities are based on a particular distributor's availability in Jamshedpur, India in order to constraint realistic solutions for implementation in off-grid areas in Jharkhand as an example, and further in subsequent sections.

Table 4.2: State-Space Matrix: Available Solar/Battery Combinations

		l^{th} solar panel (W)									
		50	75	80	100	120	125	150	200	250	300
k^{th} battery (Ah)	60										
	75										
	100										
	120										
	150										
	165										
	180										
	200										

In this model, reliability is defined as the sum of the total load served divided by the total expected load over the entire year; again, in this modeling context, the load profile is assumed to be entirely known a priori but dispatch decisions are made every time step as discussed in Chapter 3. Furthermore, the definition of reliability ($R_{k,l}$, in %) is the total amount of electricity served ($EST_{i,k,l}$, $ESC_{i,k,l}$) divided by the total amount of expected electricity demand (TD_i, CD_i), integrated over the entire year (8760 hours) and calculated for both serving critical and total load profiles. Though the high priority and low priority load profiles are separated, this approach does not enforce a reliability threshold at sub-yearly scales (i.e. monthly, weekly, daily, or hourly); again, this concept relates to the selection of a dispatch heuristic discussed in Chapter 3.

$$TR_{k,l} = \sum_{i=1}^{8760} \frac{EST_{i,k,l}}{TD_i} \tag{4.11}$$

$$CR_{k,l} = \sum_{i=1}^{8760} \frac{ESC_{i,k,l}}{CD_i} \tag{4.12}$$

In order to find potential solutions, the model requires an input of desired reliability thresholds for both critical and total (critical plus non-critical) load profiles. This is the key capability represented in power management devices described to enable micro-grids with demand-side management: that electricity demand can first be disaggregated and prioritized — followed by the decision whether to serve or curtail this demand (at each hour in simulation). As defined by the consumer, critical loads are high priority loads that would be served first in any resource-constrained scenario; remaining, non-critical loads can be considered to have lower priority. Further discussion on user preferences and load prioritization takes place in Chapter 5.

Given that it is unlikely that there exists one particular solution would meet an exact reliability threshold, the model accepts reliabilities that are at least the inputted values. The default values for the critical reliability is 99%, and the default value for the total reliability is 90%; again, these are all user inputs that can be changed. Using

a two-dimensional search methodology, the algorithm then identifies the k^{th} and l^{th} indices of each of the matrix where a combination of the solar panel and battery falls within the range of accepted reliability thresholds for both serving the critical and total load profiles; an example of the outputs of the reliability across available solar and battery capacities in the 'residential load' scenario are shown in Figures 4-11 and 4-12.

The next step is that the algorithm compares where the sets of identified indices intersect, meaning which combination of solar panel and battery capacity meets *both* total (TR) and critical (CR) reliability thresholds. In order to find the optimal solution, the last step for the algorithm is to pick the index which has the least cost combination of the solar and battery assets ($c_{k,l}$), taking into account the economies of scale for both solar modules ($\$/W$) and batteries ($\$/kWh$); further discussion on the calculations associated with the leveraging economies of scale along with the overall micro-grid's system economics and financial viability is included in Chapter 4.

The optimization heuristic employed is based described in the following equations; note that $c_l = \$/W$, and $c_k = \$/kWh$ for respective solar and battery per unit costs, with the indicies k and l corresponding to combinations of available solar module size (PV) and battery capacity (B), with a nominal battery voltage of $V = 12$:

$$\begin{aligned} \min_{c_{k,l}} \quad c_{k,l} = \frac{B \times c_k \times V}{1000} + PV \times c_l \\ s.t. \quad TR_{k,l} \geq 90\% \\ CR_{k,l} \geq 99\% \\ k \in \{1...n\} \\ l \in \{1...m\} \end{aligned}$$

The feasible solution set can be interpreted first by the values of each matrix that are greater than or equal to the reliability thresholds, and second by the overlap of those indices. Again, the optimal solution is found by using a two-dimensional search

methodology to come up with overlapping indices — with results on the optimal selection and system costs based on the model described in this chapter is discussed in detail in the following sections.

Figures 4-11 and 4-12 illustrate how reliability varies as a function of the selection of lead-acid battery and solar panel and constitute the available search space. The z-axis represents the average yearly reliability in both graphs, with the x-y coordinate plane representing discrete values of available solar panels (in watts) and batteries (in amp-hours). In Figure 4-11, the trends towards increasing reliability seems to be continuous in comparison to to Figure 4-12; the presence of discontinuities in the latter figure is because in this version of the model inputs, the critical load profile is not serving any daytime loads, and is solely based on serving evening loads (in lights). Thus, for serving critical loads, the reliabilities are essentially near zero for smaller batteries — a logical result from the model.

4.5.1 Further Analysis of Defined Level of Reliability

For the final selected generation asset combination, in a 250W solar panel and 100Ah battery, the calculated reliabilities are 99.45% and 94.26% serving the critical and total load profiles, respectively; in this instantiation of the model, the reliability thresholds are set to be 99% for the critical load profile, and 90% for the total profile. In this version of the model, reliability is essentially defined to be the average reliability served over the entirety of the year. Figures 4-13 and 4-14 illustrate the calculated hourly reliability and compare the amount of non-served energy at each hour to the demand profiles (again, for both total and critical load profiles).

The top plots in both figures show the hourly values for reliability, and the bottom plots show the comparisons between the non-served energy and expected demand profiles. For the critical reliability, the requisite threshold is higher, shown by the fact that nearly all of the hourly reliability values are near 1 (i.e. 100%) for serving the evening lighting loads. For the total reliability, the main hours of the year where reliability is lower is during the simulated peak periods of higher amounts of fan usage (again, induced in the demand profile construction by ambient temperatures

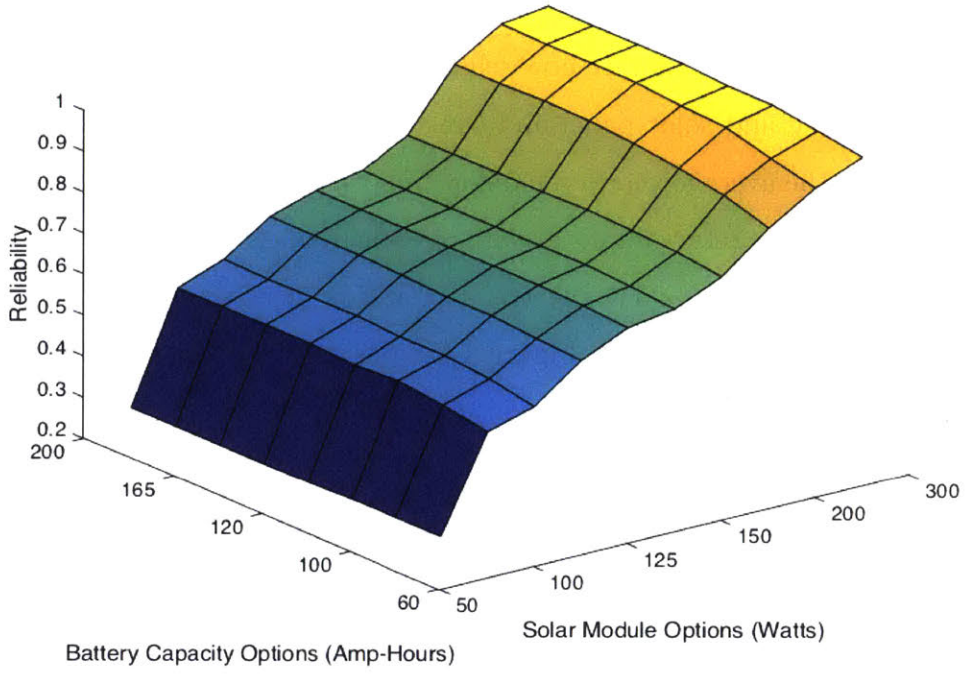


Figure 4-11: Total Reliability vs. PV and Battery Capacities

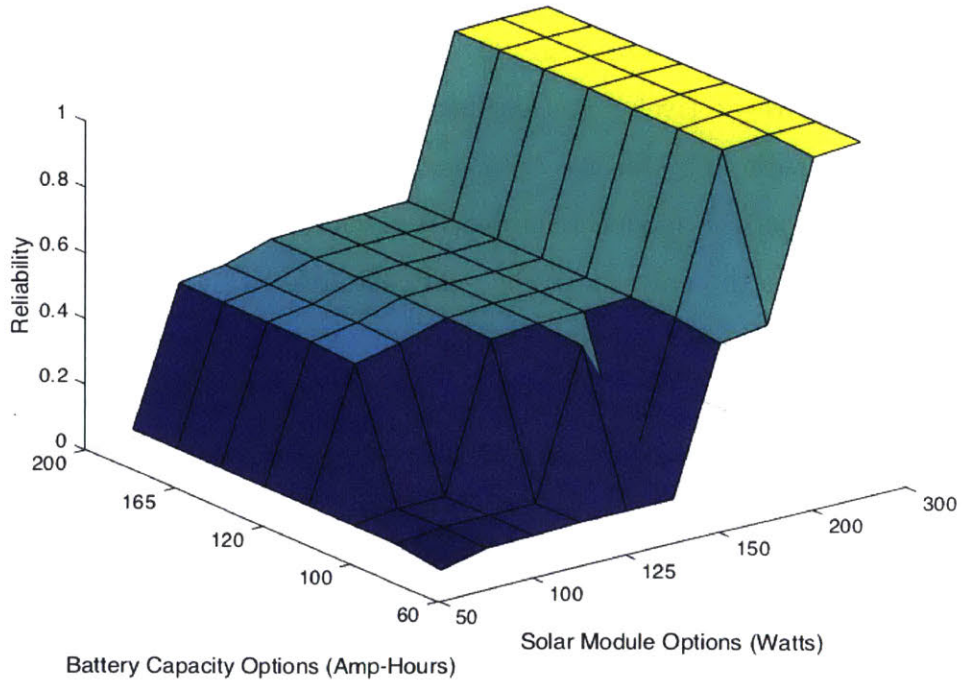


Figure 4-12: Critical Reliability vs. PV and Battery Capacities

and unable to be served by the available solar power). Though there are hundreds of hours where the reliability is significantly below the reliability threshold of 90%, in aggregate, the amount of energy served versus the amount of energy demanded meets the reliability threshold when considering the entirety of the year. Furthermore, though there may be many hours of the year when reliability is low, the magnitude of those values (in terms of watts) may be small — and thus not have a significant effect. Given that behavioral and real-time peak shifting effects are not taken into account in simulation, one way to view this metric is as a lower bound for the reliability provision; discussion on implementing varied demand-side strategies in the field is the subject of discussion in Chapters 5 and 6.

Regardless, it is worth acknowledging that the definition of the reliability undertaken may be imperfect. As discussed both in Chapter 1 and later in this chapter, equipment provider's rationale for over-sizing systems is to minimize the probability of the event that a load (and thus, an activity) is not served in its entirety. Similar to demand response efforts in the developed world, the goal of this effort is to separate an acceptable level of service for critical loads from the remaining loads. But again, understanding these thresholds for what is acceptable from the user's perspective needs to be understood in advance of any implementation and is discussed in Chapters 5 and 6.

4.6 Choice of Battery and Solar Combinations Based on Distributor Availability & Economies of Scale

Part of the economic rationale for building decentralized micro-grids as opposed to individual solar home systems is due leverage economies of scale. Academic modeling approaches tend to focus on the exact optimal generation assets to be sized for a given power system. The modeling approach conducted for this analysis is focused on finding a least cost combination of solar panels and batteries to meet a certain level of demand — and in the context of electricity access, this assumption should

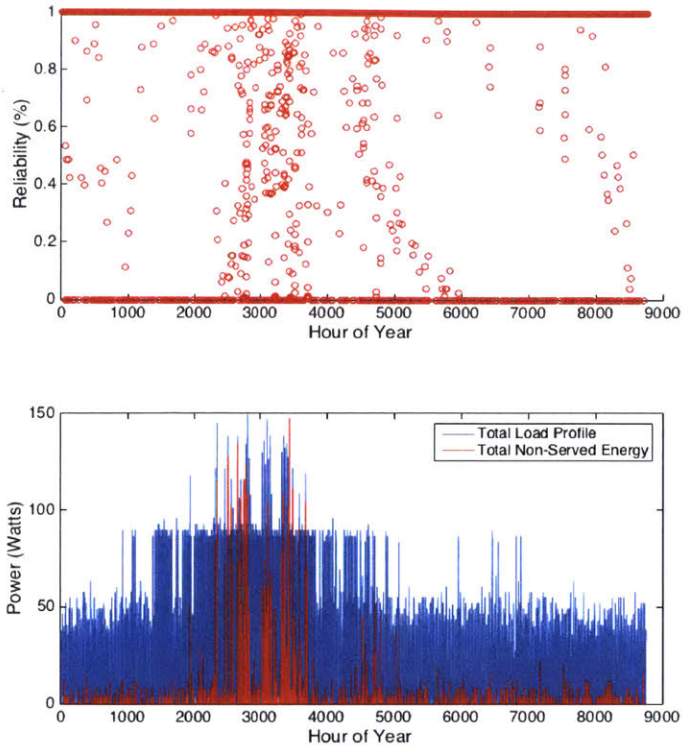


Figure 4-13: Simulated Hourly Reliability: Total Load Profile (94.26%)

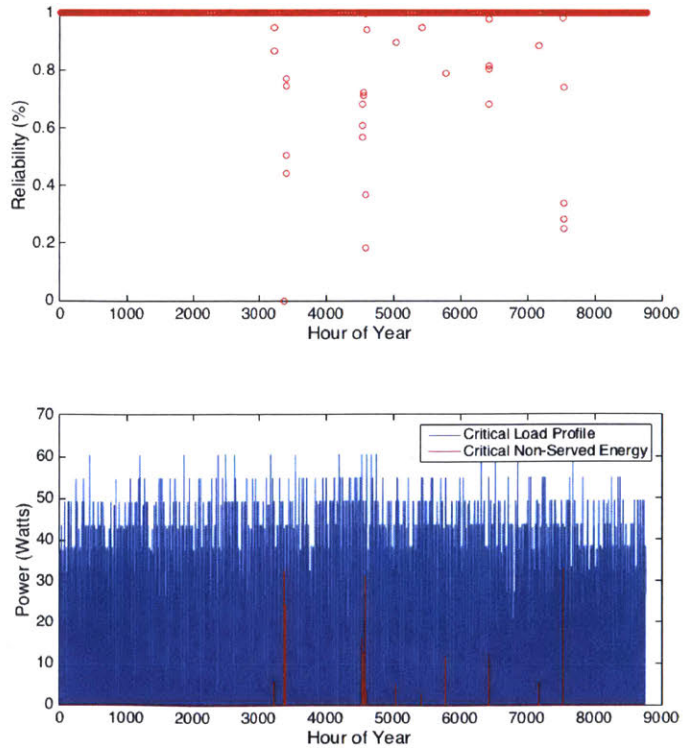


Figure 4-14: Simulated Hourly Reliability: Critical Load Profile (99.45%)

be dependent on available solar panels and batteries from equipment manufacturers ideally available at local distributors. Though there are many different sizes of solar panels, especially when looking across many manufacturers, not all of those increments (i.e. 10W or 20Ah) or combinations may be available in remote, rural areas. Thus, as an illustrative example, this modeling approach initializes the available state-space (again, depicted in Table 4.2) based on available Su-Kam solar panels and Amara Raja battery capacities from a local distributor in the city of Jamshedpur, India. This distributor sources and sells Su-Kam and Amara Raja solar photovoltaic modules along with Amara Raja, Exide, and Su-Kam lead-acid batteries of various capacities. In considering a realistic operation of a micro-grid business, a company would likely source generating equipment from a select few verified suppliers — and the model presented herein aims to reflect that reality.

Another reason for this choice is because models that are based on strict optimization of battery and solar panel selection might identify a more optimal yet less realistic solution in terms of implementation. Having such a representation of costs and discrete values of solar panels and battery capacities actually available in the nearest urban area for a micro-grid installation provides a realistic context and use-case. Furthermore, due to economies of scale, both solar panels and batteries have a lower unit cost ($\$/W$ and $\$/kWh$ respectively) with increasing capacities. This model takes into account these aspects, as gathered from local distributors and shown in Figures 4-15 and 4-16. Again, including these aspects formulates the state space for available solar and battery combinations subject to reliability constraints, which is the key decision-making step in the model.

For clarity, the two-term exponential fit equations describing the economies of scale for both solar panels ($\$/W$) and batteries ($\$/kWh$) are shown in the equations below:

$$\$/kWh = 288.8 * e^{-0.08682*Ah} + 125.3 * e^{-0.001121*Ah} \tag{4.13}$$

$$\$/W = 0.5689 * e^{-0.04871*W} + 0.8098 * e^{-0.0001196*W} \tag{4.14}$$

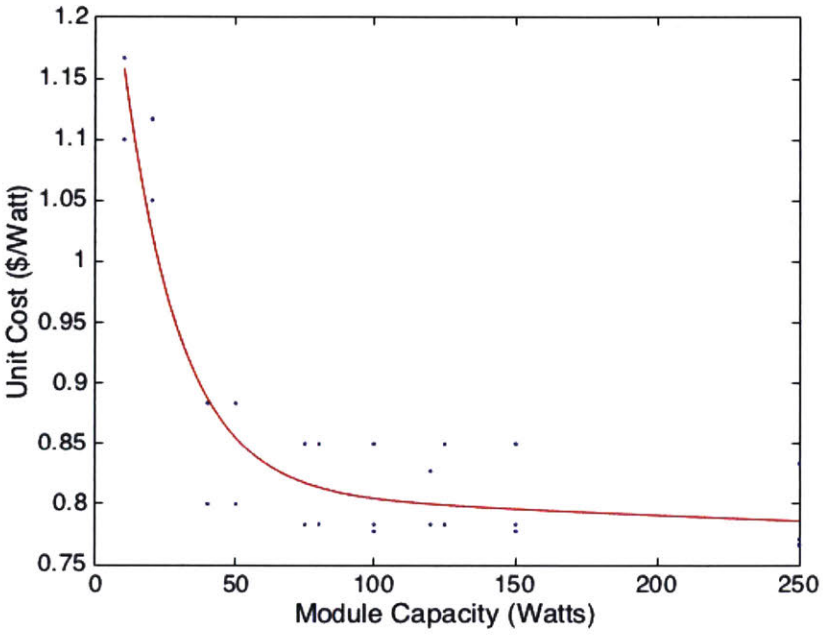


Figure 4-15: Exponential Fit for Unit Cost vs. Available PV Module Sizes

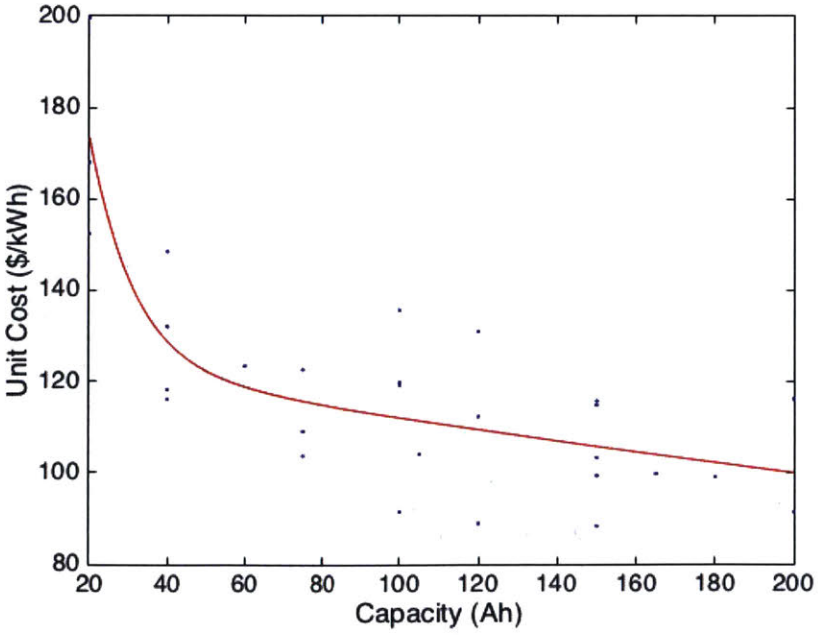


Figure 4-16: Exponential Fit for Unit Cost vs. Available Battery Capacities

The final matrix output, in terms of all of the cost combinations of solar and batteries, is shown in Figure 4-17. Again, the feasible set is determined by the set of i and j indices that meet both critical and total load profile reliability thresholds, and the final step of the algorithm chooses the least cost combination of the solar panel and battery asset. This figure clearly doesn't show a linear increase in costs, as each of values in each of the cells is calculated based on the objective function that relies on an exponential relationship of the per unit costs of batteries and solar panels.

For the instantiation of the model, with 5 residential household demand profiles (including network losses), the availability of solar and battery combinations, and the set reliability thresholds of 99% for critical loads and 90% for total loads, the least cost selection of solar and battery assets comes out to be **250W** and **100Ah** — a combined cost of **\$196.49 + \$134.47 = \$330.96**. The selection of high levels of reliability for micro-grids with real-time demand-side management show that reliability is not being sacrificed in order to be cost-competitive with conventional micro-grid approaches, as further discussed in the subsequent sections. This asset selection also corroborates the modeling choice for 5 households (with these particular loads), especially in the solar module selection, as the realized economies of scale benefit does taper off around these selected values.

4.7 Greenfield Costs of Modeled Micro-Grid and Financial Analysis

The contribution shared herein explores the cost advantage that a micro-grid with demand-side management capabilities has in the context of a use-case for rural electrification. In order to conduct a full analysis, the bill-of-materials needs to be tabulated; Table 4.3 includes the cost input assumptions, again based on prices gathered in Jamshedpur, India, for requisite equipment/components for a micro-grid.

The requisite power management network devices are split into 'generator' (source) and 'consumer' (load) devices. This nomenclature simply means that the generator

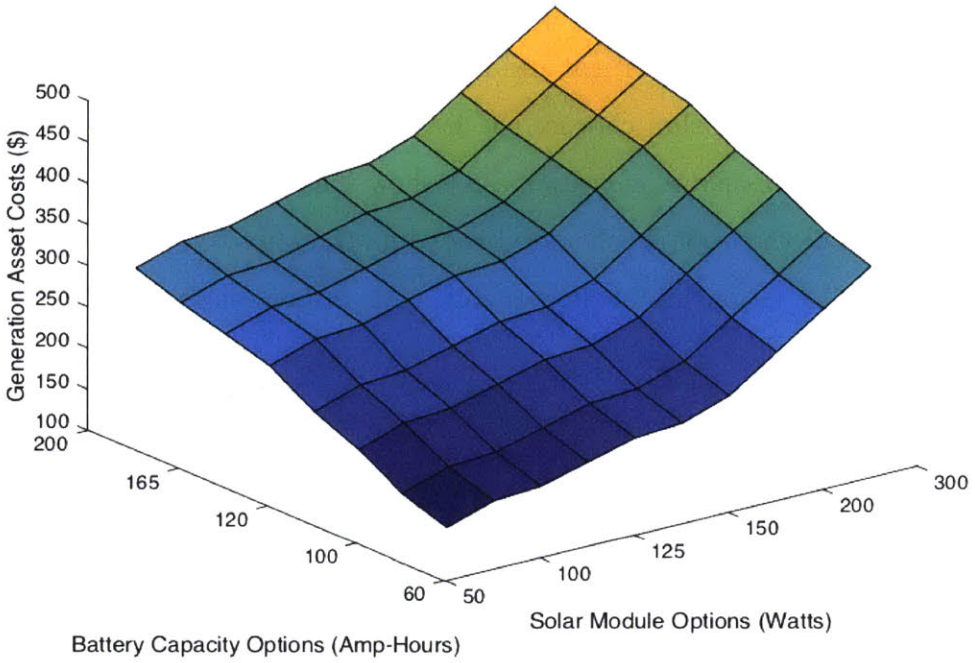


Figure 4-17: Costs of Solar and Battery Asset Combinations

device resides near the solar panel and the battery, and includes a charge controller along with the computational ability to manage the network. Furthermore, the 14 AWG wire selection is sufficient for carrying 24V DC, again with the description of the expected power dissipation discussed earlier in this chapter.

4.7.1 Key Micro-Grid Cost Inputs

Consistent with the costs of the generation assets, the costs for the other aspects required in building a micro-grid are based off of available prices from local appliance and electrical shops in the city of Jamshedpur, India — gathered during the summer of 2016. As Table 4.3 shows, the additional cost inputs per household include wiring, power management devices, and appliances.

4.7.2 Costs of Power Management Devices

For the generator device and consumer devices, the bill of materials is based on the analysis conducted in [81] for designing safe, reliable, and low-cost power electronic

Item	Cost (Rs.)	Cost ($)	Value
Electrical Wiring	Rs. 3.6/m	$0.06/m	40m/household
Communication Wiring	Rs. 1.8/m	$0.03/m	40m/household
LED Cost	Rs. 100/unit	$1.67/unit	4 units/household
Fan Cost	Rs. 600/unit	$10/unit	1 unit/household
Mobile Charger	Rs. 100/unit	$1.67/unit	1 unit/household
Generator Device	Rs. 2400/unit	$40/unit	1 unit/network
Consumer Device	Rs. 900/unit	$15/unit	1 unit/household
Pole	Rs. 200/unit	$3.33/unit	1 unit/household

Table 4.3: Key Cost Inputs

devices in the context of off-grid electricity access. Specifically for the generator device, the key components assumed as part of the network architecture described in the previous chapter include the main costs such as the components required for the power stage, micro-controller, sensors, printed circuit board, etc.; furthermore, the cost of the MPPT charge controller needs to be included — and the cost for the generator device at supplier scale (10,000 units) is estimated to be $40. For the consumer device, the key components similarly include the components required for the power stage (and isolation/protection for safety), sensors, etc. The cost for the consumer device at supplier scale (10,000 units) is estimated to be $15.

4.7.3 Initial Capital Costs

As discussed previously, the state-space matrices, which represent the available solar and battery combinations, are populated with average yearly reliabilities serving critical and total load profiles. Figure 4-17 show combined costs of the solar and the battery combinations; after a search is conducted across both reliability matrices, the overlapping pair of indices are selected, and the output of the algorithm chooses the least cost and feasible k^{th} battery and l^{th} solar panel solution. The combination of the solar and battery, plus the costs included in Table 4.3 consist of the capital costs for the system.

Figure 4-18 shows the distribution of capital costs in the micro-grid described. Total initial capital costs, comes out to be $542.06 — coming to a $\$2.17/W$ installed

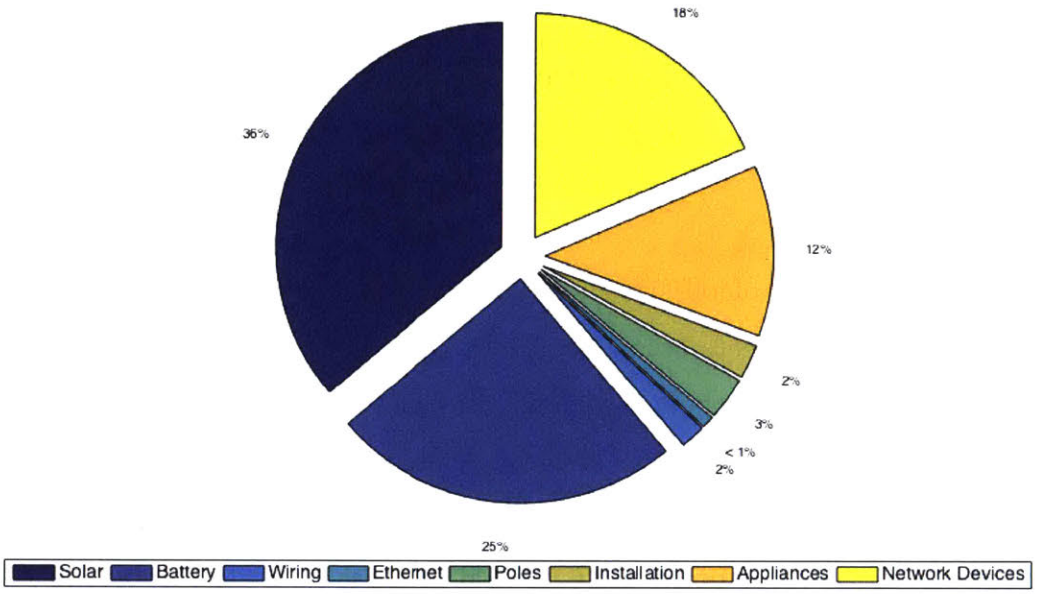


Figure 4-18: Distribution of Capital Costs of Optimized Generation Asset Micro-Grid Network

Asset	**Lifetime**
Solar Module	15 years
Battery [60% MDOD]	1,400 cycles [Figure 3-7]
Poles	5 years
Appliances	2 years
Network Devices	5 years

Table 4.4: Lifetime of Equipment Assets

and a $108.41 per household (again, for a five household installation).

4.7.4 Replacement Costs Based on Equipment Lifetime

In addition to the initial capital investment, the economic model takes into account replacement costs of the key assets in the network based on the lifetime of each asset (as shown in Table 4.4. In this case, the battery replacements are taken into account by taking the expected number of cycles in a particular year (based on the rainflow counting algorithm discussed in Chapter 3) and dividing that by the cycle lifetime; this gives the expected number of years that the battery will last given how it is cycled in the particular year simulated.

For a given system lifetime the number of times (and associated costs) for replacing each asset is calculated by the following heuristic:

- **while** y <= system lifetime
    1. **if** mod(y, poles lifetime) = 0
        (a) replace poles in year y
    2. **if** mod(y, solar panel lifetime) = 0
        (a) replace solar panel in year y
    3. **if** mod(y, appliance lifetime) = 0
        (a) replace appliance in year y
    4. **if** mod(y, network devices lifetime) = 0
        (a) replace network devices in year y
    5. **if** mod(y, battery cycle life) = 0
        (a) replace battery in year y
- y=y+1;
- **end**

4.7.5 Financial Model Overview & Results

The key financial inputs as shown in Table 4.5 are used in net present value (NPV) and levelized cost of electricity (LCOE) calculations. Over the lifetime of the system, the LCOE calculates all the recurring annual costs (such as maintenance, replacement, and initial capital costs) and is divided by the total amount of energy (in kWh) that the network served. This denominator is assumed to be the same amount taken from the yearly simulation described in the previous chapter, a shortcoming of this approach as it does not take into account demand growth and incrementing generation assets to meet that demand.

As discussed, the model takes into account the capital costs, the replacement costs, and the maintenance costs for a micro-grid. Furthermore, there is assumed to be no capital (or operational) subsidy taken into account, though there are a number of ongoing capital incentives for distributed solar installations in India at the central and state government levels; additional discussion on subsidies takes place in Chapter 5. In this use-case of the model, again for the residential load profile scenario with respective total and critical load profile reliability thresholds at 90% and 99% serving five households, the levelized cost of electricity ($LCOE$) is calculated to be $\$0.32/kWh$ (see Equation 4.16). The numerator is based on the presented value (NPV) of the cash outflows or costs (C), and the denominator is the sum of the entirety of the energy served (EST) in the micro-grid in each year, y (and not energy generated, which is typical for stand-alone photovoltaic systems); one of the shortcomings of the model is the assumption that the demand and the amount of energy served remains constant each year. Note that the yearly discount rate used is 12% which is a considered to be reasonable value for renewable energy projects in India as evaluated in [93].

$$NPV = \sum_{y=1}^{Y} \frac{C_y}{(1+d)^y} \tag{4.15}$$

$$LCOE = \frac{NPV}{\sum_{y=1}^{Y} \sum_{i=1}^{8760} EST_{i,y}} \tag{4.16}$$

Parameter	Value
Yearly Discount Rate (d)	12 % [93]
Monthly Discount Rate (d')	0.95 %
Payback Period (P)	5 years
System Lifetime (Y)	20 years
Maintenance Rate	2.5 % / year of C_0
Exchange Rate	Rs. 66/ $

Table 4.5: Key Financial Inputs

4.7.6 Business Model Viability

The technical capabilities of the power management device described herein are only a piece of the puzzle; generating a financially sustainable business model enabled by such a device is also necessary. Typically, micro-grid companies and service providers charge a monthly charge to users for electricity service, and in India, this value is typically pegged to the amount consumers are paying for kerosene fuel for lighting. This value tends to be around $2/month based on many accounts [4] [44] — largely due to the presence and reliance on kerosene subsidies in rural areas. With this in mind, the analysis conducted in the model elucidates the minimum revenue required, in terms of a monthly payment per household connected to the network (MP), in order to reach a positive net present value in 5 years, taking into account the net present value of the system's costs over the 20 year system lifetime.

In extending this analysis to the business model, the required monthly fee to break even, based on a monthly periodic payment per customer to cover the NPV of the micro-grid costs in a time frame of a payback period of 5 years (P), is $5.44 (using the effective monthly discount rate, d', in Table 4.5), which includes a $5 connection fee. This is undoubtedly a high cost and above typical willingness-to-pay in basic residential electricity service in off-grid, rural areas in India.

Figure 4-19 shows the cash inflow and outflows for such an investment. In terms of costs, the blue line shows the capital cost outlay (C_0) and the recurring costs of maintenance and replacement based on equipment lifetimes (C_y); the red line shows the revenue accrued from the connection fee (R_0), and the yearly revenue (R_y) across

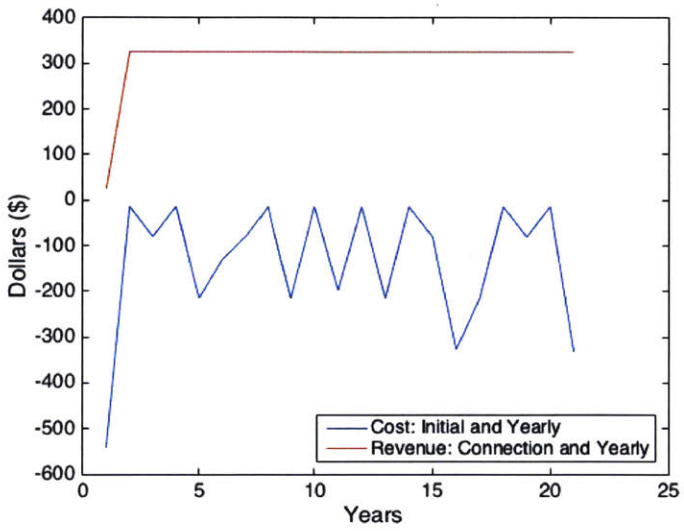


Figure 4-19: Yearly Cash Inflows and Outflow

the households (h) based on the monthly payment required for an NPV positive investment as described in Equations 4.17 and 4.18. For this use-case, the yearly internal rate of return (IRR) calculated to be 26.07%.

As discussed further in this chapter, this number illustrates the challenge that conventional micro-grid companies regularly face in terms of financial viability in general. There are a number of approaches to alleviate this challenge, such as relying on grants to cover cost and revenue differentials or subsidies made available from the government (on the order of 30%, further discussed in Chapter 5), or lowering per unit costs of appliances/wiring through purchasing in bulk. It is worth mentioning that though the results discussed here include the expected costs of maintenance, it does not include the cost of operations (from a company's perspective) nor the cost of collections. The inclusion of mobile payments is another potential advanced capability for next generation micro-grids, which can help mitigate revenue loss due to lower levels of payment and the costs of door-to-door collections.

$$NPV = (R_0 - C_0) + \sum_{y=1}^{Y} \frac{R_y - C_y}{(1+d)^y} \tag{4.17}$$

$$MP = \left(\frac{d' \times NPV}{1 - (1+d')^{(-P \times 12)}}\right) \times \frac{1}{h} \tag{4.18}$$

4.8 Sensitivity Analysis to Key Model Inputs

The past two chapters have described the series of computational steps and initial results for a particular use-case in assessing the design selection of generation assets in micro-grids with demand-side management capabilities. However, as is clear from the previous discussion, this model is based on a number of inputs — the selection of which have underlying inter-dependencies that impact results of the model. The purpose of this section is to illustrate some of the complex underlying factors and relationships between variables to get a better sense of what inputs — and why — impact both the technical and economic outputs.

To recall, the use-case of the model thus far has assumed the following main inputs:

- **Demand Inputs:** Five customers/households' aggregated residential load profiles taken for a representative year (see Table 4.1);
- **Solar Resource:** Historical solar irradiance in Jharkhand, India (see Figure 4-8);
- **Solar/Battery Choices:** Available solar panels and lead-acid batteries per distributor availability, and associated costs (see Table 4.2);
- **Battery Operation:** Default value for maximum depth of discharge (MDOD) for lead-acid battery of 60%, corresponding to 1,400 cycles (see Figure 3-7);
- **Reliability Thresholds:** Baseline average yearly reliability thresholds for serving total (90%) and critical (99%) load profiles (see Figures 4-11 and 4-12);

- **Cost Inputs:** Values for appliances, power management devices, network, etc. based on prices gathered from local shops in Jamshedpur, India (see Table 4.3);
- **Equipment Lifetime:** Lifetime of equipment assets, in years, that dictates replacement costs (see Table 4.4);
- **Financial Inputs:** Discount rate, payback period, and system lifetime which impact business model viability (see Table 4.5).

4.8.1 Effect of Payback Period, Discount Rate, and Connection Fee on Monthly Payment and Internal Rate of Return

However, the required monthly payment and the internal rate of return for an NPV positive investment is sensitive to the choice of the connection fee, discount rate, and payback period in terms of financial inputs. The inclusion of charging a connection fee can help cover the capital and installation costs — lowering the break even monthly payment requirement, while the discount rate affects the time-value of money. Figures 4-20, 4-21, and 4-22 provides insight to understand the effects of these three inputs.

Holding the other inputs constant, Figure 4-20 gives a sense of the effect of increasing connection fees and the discount rate subsequently have on decreasing the monthly payment requirement. With no connection, future cash flows need to be higher to compensate for the capital (and recurring) cash outflows, and a lower discount rate makes cash flow in the near term is worth more. Figure 4-21 shows how the monthly payment is affected by the discount rate and the payback period. A shorter payback period combined with a lower discount rate forces monthly payments to be significantly higher, both decreasing as these parameters are relaxes. Lastly, Figure 4-22 shows the sensitivity of the internal rate of return to the choice of discount rate and payback period. The payback period has a strong effect for values less than 5 years, with the highest rates of return shown for higher discount rates and lower payback periods. These contour plots show that regardless of technical capabilities

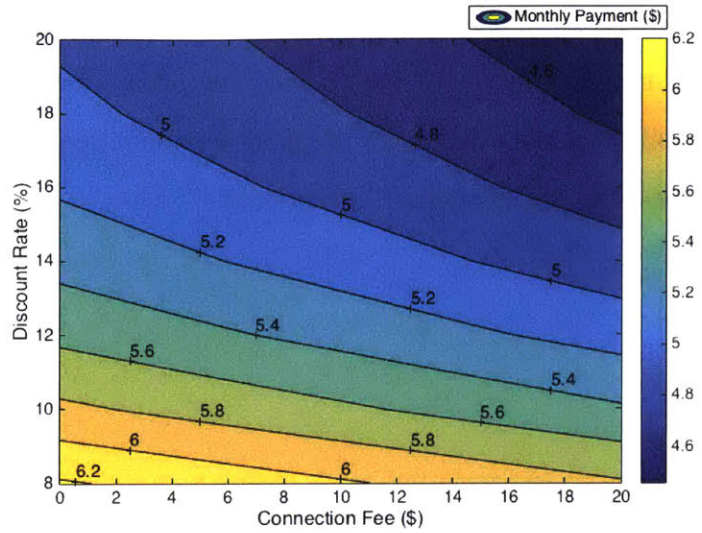


Figure 4-20: Monthly Payment Based on Discount Rate and Connection Fee

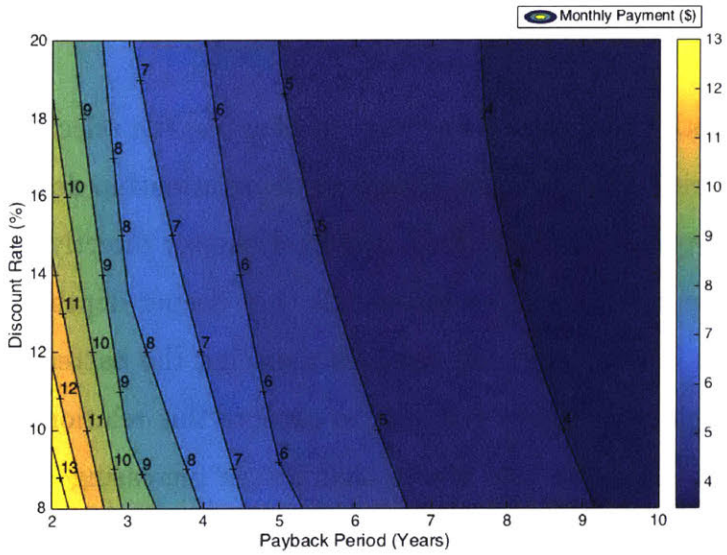


Figure 4-21: Monthly Payment Based on Discount Rate and Payback Period

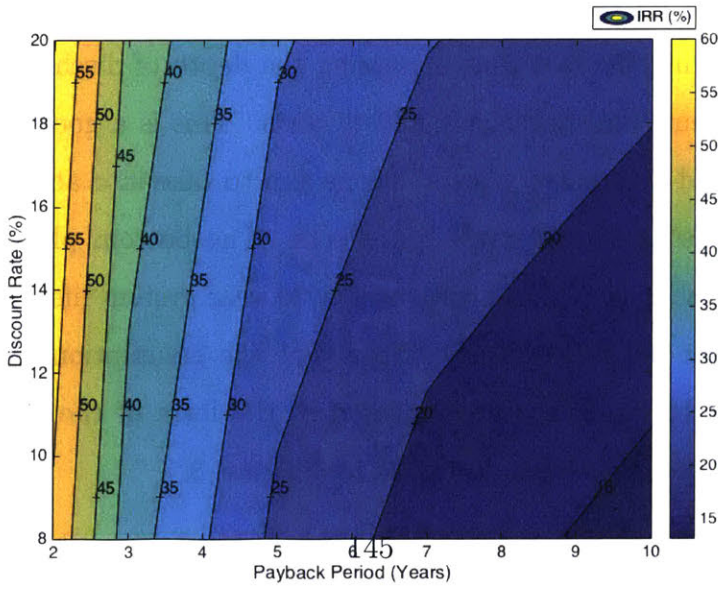


Figure 4-22: IRR Based on Discount Rate and Payback Period

embedded in next generation micro-grids, the business model assumptions on inputs such as the discount rate, connection fee, and payback period have significant effects on the financial viability in regards to the monthly payment required per household and the internal rate of return of such an investment.

4.8.2 Effect of Maximum Depth of Discharge and Cycle Life on Levelized Cost of Electricity

As discussed in both the previous and current chapter, the selection and operation of a battery is of critical importance. Based on the relationship described in Chapter 3, the allowable depth of discharge for a lead-acid battery directly impacts the cycle life. Therefore, the key tradeoff to consider is that deeper depths of discharge can allow for a smaller battery size, but requires replacing the battery more frequently in turn. The two plots in Figure 4-26 aim to capture this relationship based on the model constructed. The top plot shows that for an increasing depth of discharge (corresponding to a decrease cycle life), the choice of battery capacity decreases. However, the levelized cost of electricity forms a parabolic-like shape (given that only discrete values for battery capacities are made available in the construction of the model), capturing the fact that increasing the depth of discharge requires more frequent replacements and negatively affects costs. This is a good indicator on the fact that many lead-acid battery installations aim to take into account some notion of the depth of discharge and cycle life effects. The bottom plot shows precisely the increasing number of replacements over a 20 year system lifetime based on the decreasing calendar life of a battery. Note that the assumptions on the choice of MDOD and cycle counting are implemented in the form of the MDOD-constraint and rainflow counting algorithm described in Chapter 3.

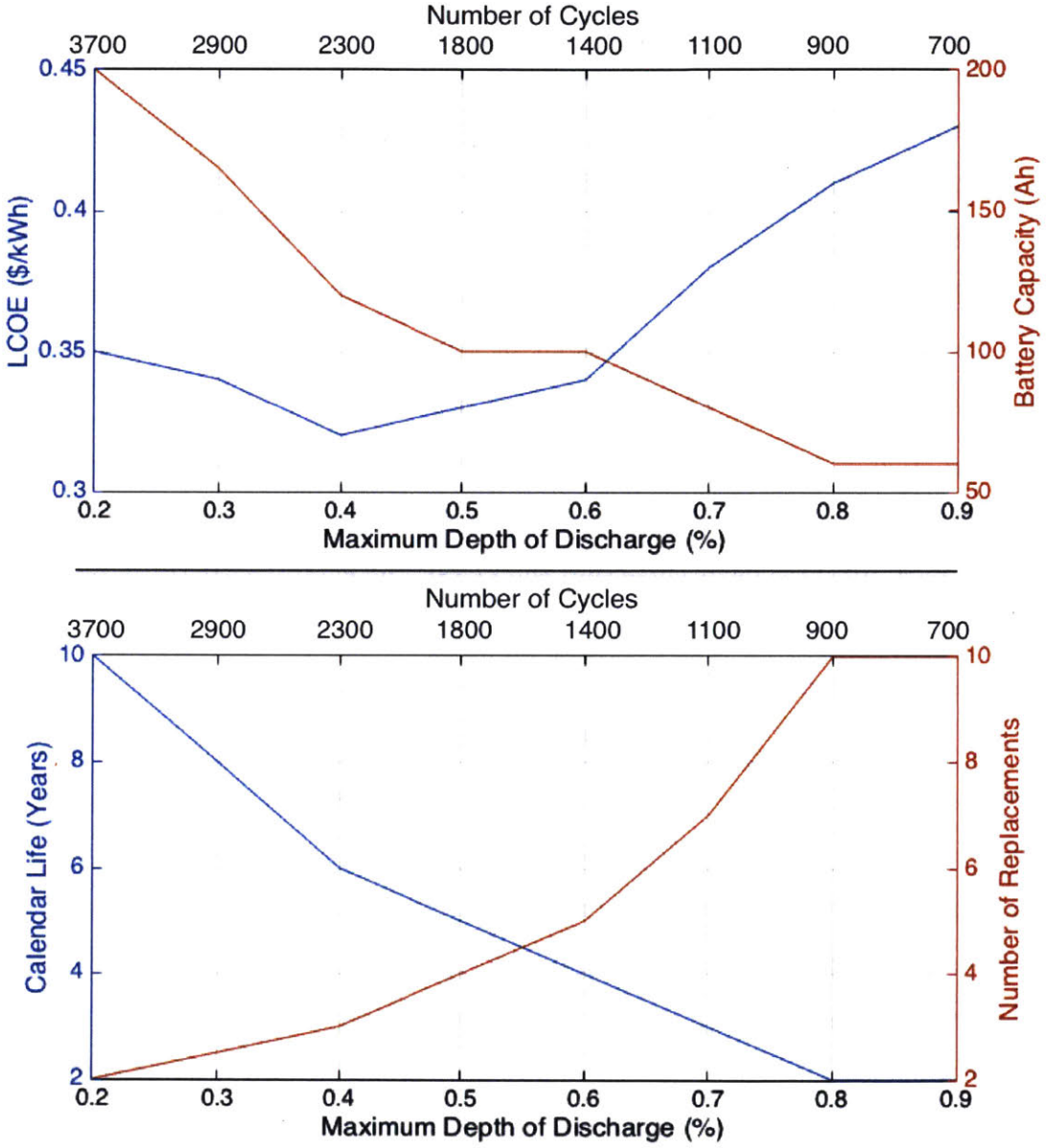


Figure 4-23: Tradeoff Between MDOD and Cycle Life with Battery Selection and Replacement Costs

4.8.3 Effect of Reliability Thresholds on Costs and Generation Asset Selection

In any power system design, the choice of reliability provision for demand directly dictates the types and sizes of generation assets. In isolated micro-grids with demand-side management capabilities under consideration in this analysis, the choice of solar and battery assets can be optimized assuming that yearly reliability thresholds can be met for disaggregated load profiles. Thus far, the use-case presented herein has shown that for meeting total and critical reliability thresholds of 90% and 99% for five households' residential load profiles, a least-cost combination of a 250W panel and 100Ah battery can meet those requirements.

Figure 4-26 shows three contour plots assessing the relevant cost parameters as a function of varying the total and critical reliability thresholds from 80% to 99%. For the most part, all three parts show that the LCOE and capital costs (both per unit and combined total of generation assets) do increase with increasing reliabilities. The first interesting point is that the critical reliability only starts to affect the costs towards the end of the reliability spectrum; recall that the definition of critical loads are evening lights, showing that there is a minimum battery requirement for even unacceptably low levels of reliability. Second, the top and middle plots show that the costs are not monotonically increasing as the reliability thresholds increase. Again, the model is optimizing for the least cost combination of **both** the solar panel and the battery subject to meeting reliability thresholds — and there may be many combinations that are feasible solutions. Thus, the 'lumpiness' of having only discrete combinations (and thus costs) of available solar panels and batteries as reliability thresholds are incrementally increased is the most likely explanation for this. Figure 4-25 aims to illustrate this argument, showing that for the 80 available pairs of solar panels and lead-acid batteries based on the initialized state-space, the varying proportion of the solar costs in relation to the combined solar module and battery capacity costs.

Furthermore, the middle plot is showing the per unit ($/W) costs based on the rated power of the solar panel, and does not take into account the battery in the

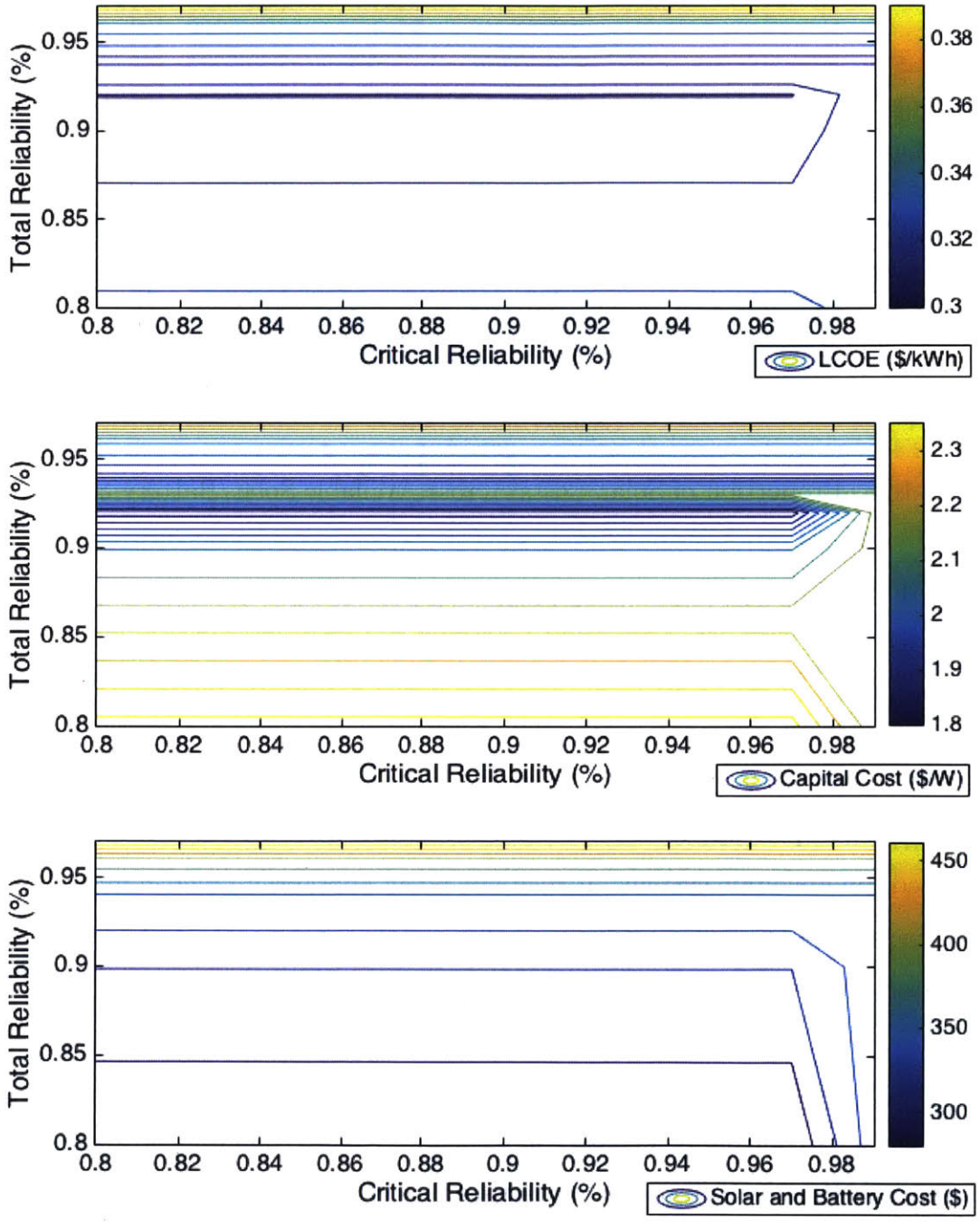


Figure 4-24: Effects of Reliability Thresholds on Cost Metrics

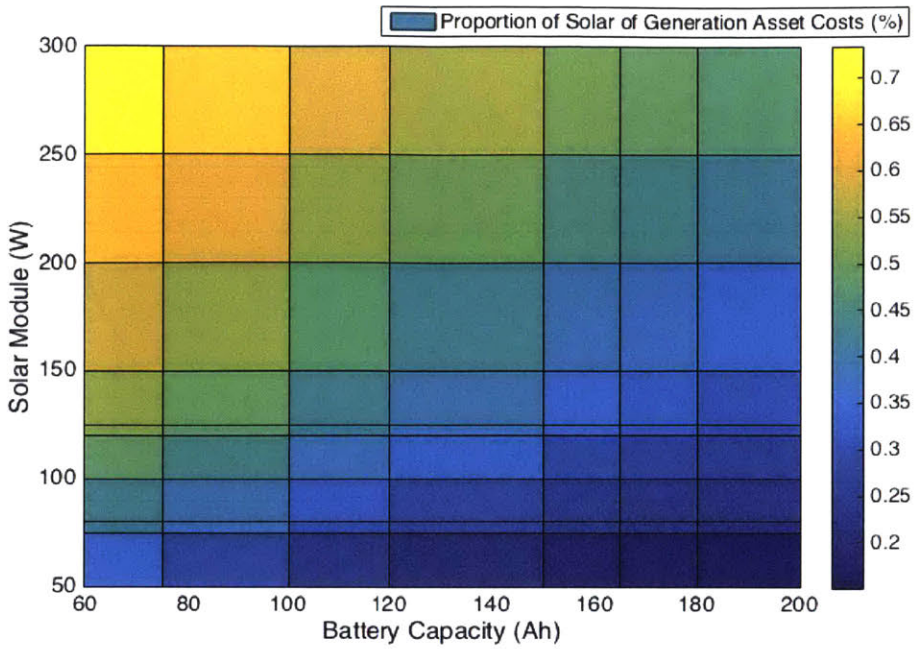


Figure 4-25: Proportion of Solar Costs Across Available Solar/Battery State-Space

denominator. Thus, as reliability increases, there clearly are combinations present that may increase the solar panel while decreasing (or keeping the same) battery capacity — which may have a net effect of decreasing the \$/W. One conclusion is that though the per unit metric is commonly used when assessing standalone, grid-connected, photovoltaic systems, it may not be an appropriate metric in micro-grids where the storage requirements represent a significant amount of the costs in the numerator.

Figure 4-26 explicitly points out the selection of the the solar panel (top plot) and battery capacity (bottom plot) based on total and critical reliability thresholds. These plots support the previous arguments in that though there may be multiple solutions, in some instances the model selects a larger solar panel and a smaller battery as total reliability (which includes the key daytime load of the fan) increases. However, to get to the high levels of critical reliability, both the battery and solar panel have to be increased.

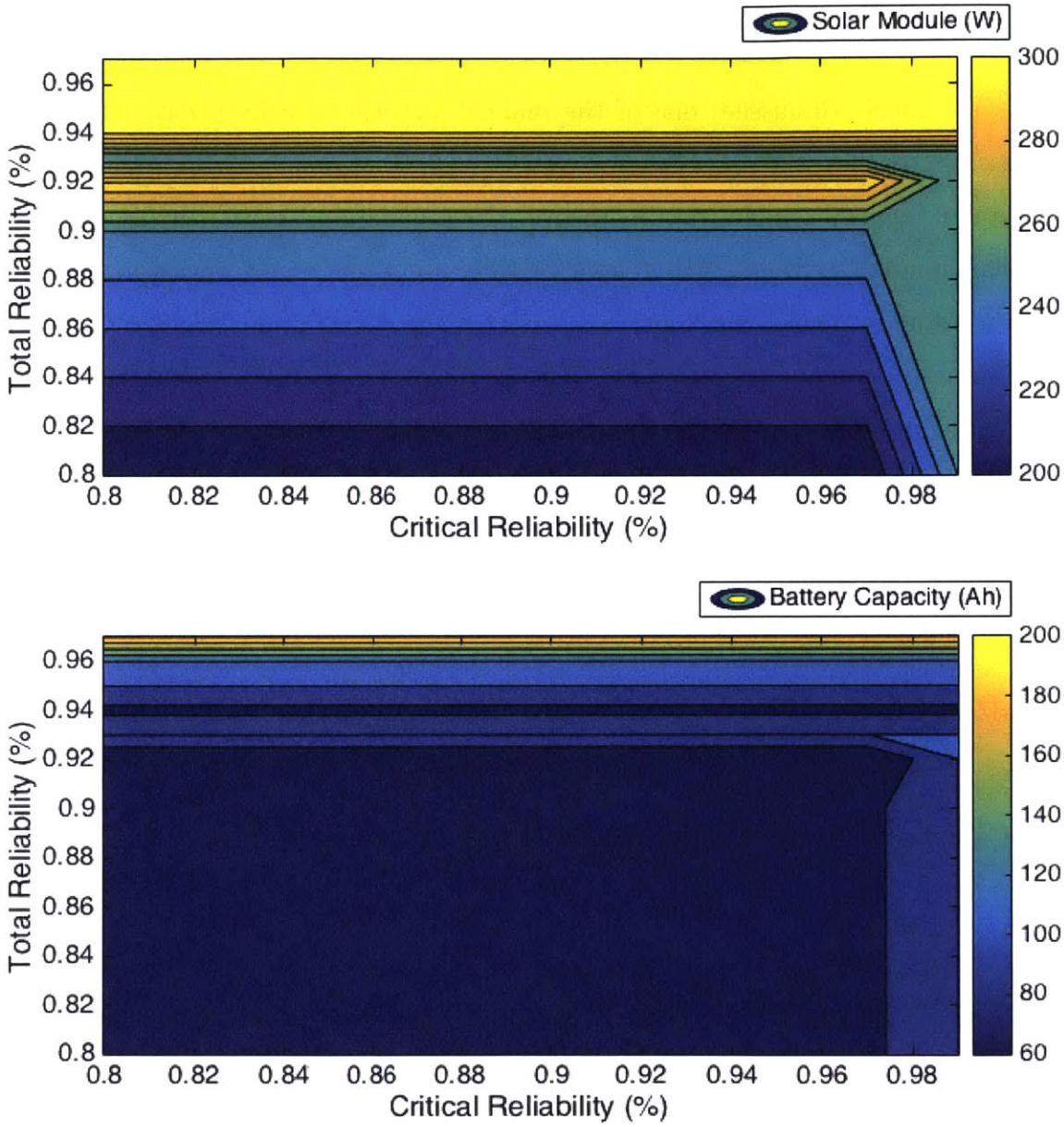


Figure 4-26: Solar Module and Battery Capacity Choice Based on Reliability

4.9 Model Benchmarking & Cost Comparisons: Examples of Conventional Solar Home Systems & Micro-Grids

As previously discussed, one of the main drawbacks of conventional electricity access approaches is the tendency — due to a lack of demand-side management and network control capabilities — to over-size generation assets. In discussions with solar home system equipment manufacturers and micro-grid operators, reasons for over-sizing systems (which drives costs) include to maintain brand reputation and ensure autonomous operation of a micro-grid during periods of low solar irradiance by providing high levels of system reliability throughout worst case scenarios. The following sections will highlight examples of conventional generation asset sizing seen today, with a benchmark and comparison of the optimized generation asset sizing method used in this model with existing solar home systems.

4.9.1 Tata Power Solar and SELCO Home Systems: Benchmarking Model with Generation Asset Size and Differences in Geographical Irradiance

In the Tata Power Solar (TPS) home system models, the solar panel and battery are designed to meet roughly four hours of evening electricity service. As an example, the Tata Power Solar Venus II model includes a 70W panel, a 75Ah lead-acid battery, a charge controller, 4x9W CFL lights, and 1x14W DC fan (total of 50W in load per household); note that these are the same systems of which electricity consumption data was acquired from and presented in Chapter 2.

SELCO has been a pioneer in solar home system development and energy access business models for the past couple of decades, and have developed a number of solar home system models varying in generation asset sizes and diverse combination of loads. SELCO's smallest system includes a 10W solar panel, a 10Ah battery, and

is designed for 16 watt-hours of daily lighting consumption, while SELCO's largest systems includes a 120W solar panel, a 240Ah battery, and is designed for 336 watt-hours of daily electricity consumption. In considering SELCO's largest system, the Super Bright Home 14 HLS, the specific loads included are 2x5W, 4x7W, and 4x11W CFL lights, and 2x15W fans (total of 112W in load per household).

Similar to the residential load profile scenario presented here, load profiles are generated for each one of these systems and are fed into the model constructed to benchmark the generation asset sizing — with a reliability threshold set to be 99%. To illustrate the importance of the available solar resource, the model is run based on using the historical irradiance both for Karnataka (Tata Power Solar and SELCO's company headquarters are both in Bangalore) as well as Jharkhand. The solar resource based on the geographical coordinates selected is more favorable in Karnataka versus Jharkhand; Figure 4-27 further illustrates the difference between the average solar irradiance in both regions over a year.

In keeping the available solar and battery state-space unchanged, over 20 feasible solar and battery combinations were generated from the model. As shown in Table 4.6, the final outputs of the model seems to significantly over-size the solar panel required in terms of the least cost combination for the TPS system, and the solar panel selection in Karnataka is closer to the actual size of 70W in comparison to Jharkhand — while the battery capacity chosen is the same. However, for the SELCO Super Bright Home 14 HLS, it is interesting to note that the model outputs essentially the opposite solar panel size and battery capacity in comparison to the actual system size.

4.9.2 Tata Power Solar and SELCO Home Systems' Costs

Based on values obtained from a distributor in Jamshedpur, India, the cost for a Tata Power Solar Venus II home system (and thus per household) is Rs. 23,000 ($\sim$ \$350). On a $\$/W$ basis, the costs comes out to be $\sim$ $\$5/W$, an important reference point to keep in mind for cost comparisons in subsequent sections. The costs of SELCO's home systems range from \$6 to \$12 per watt and \$100 to over \$900 per system, based

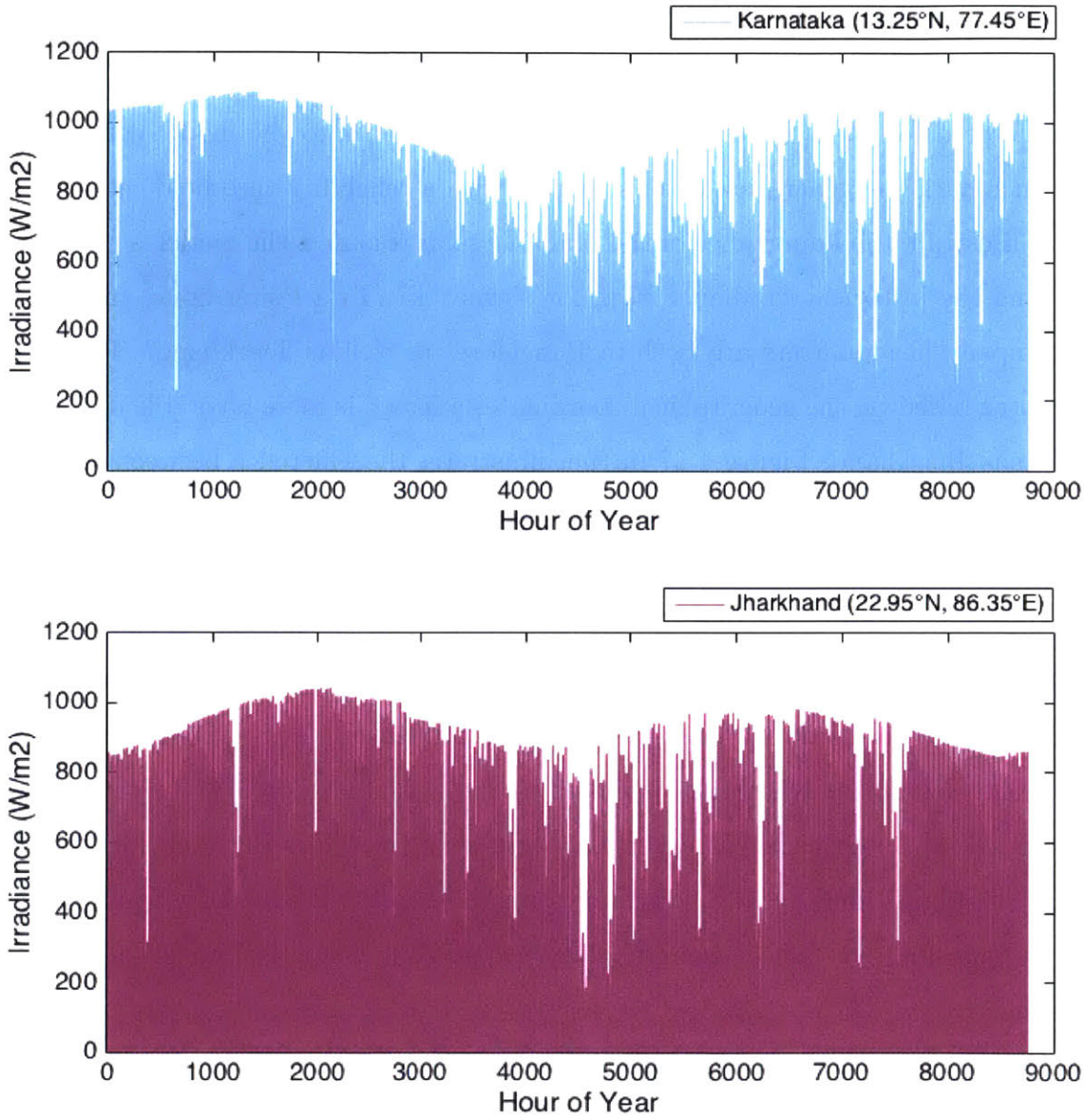


Figure 4-27: Comparison Between Solar Resource in Karnataka and Jharkhand [83]

	Jharkhand	Karnataka
TPS Battery [75Ah]	75Ah	75Ah
TPS Solar Panel [70W]	200W	125W
SELCO Battery [240Ah]	120Ah	120Ah
SELCO Solar Panel [120W]	300W	250W
Avg. Daily Solar Insolance	5.586 $kWh/m^2/day$	6.965 $kWh/m^2/day$
Geographical Coordinates	$(22.95°N, 86.35°E)$	$(13.25°N, 77.45°E)$

Table 4.6: Comparison of Modeled Generation Asset Sizing for Tata Power Solar and SELCO Home Systems in Jharkhand and Karnataka

on various combinations of lights/fans. For the Super Bright Home 14 HLS, the cost of the system is Rs. 61,000 ($\sim$ \$920).

4.9.3 Mera Gao Power Micro-Grid: Generation Asset Sizing Example

Mera Gao Power is a company operating many micro-grids for the past several years in off-grid areas in India, with their primary focus being in Uttar Pradesh. The rule of thumb used by companies like Mera Gao in sizing batteries and solar panels for their micro-grids can be seen in Equations 4.19 and 4.20; it is important to recognize that to-date, Mera Gao's electricity services is only for evening loads in LED's and a cell phone charging point per household. These assert sizing equations are from the work conducted in [44]:

$$BattCap = \frac{TotalPower * Hours}{MDOD * RoundtripEff} * Days \tag{4.19}$$

$$PVSize = \frac{TotalPower * Hours}{ExpHoursofSun} \tag{4.20}$$

If we use assumptions consistent with the residential load profile scenario (26.5W of load), across 5 households for 4 hours per day for evening electricity usage, the expected total daily energy demand is equal to 530Wh per day. Assuming a MDOD of 60%, a round-trip efficiency of 90%, and 3 days of autonomy yields a battery size

~240Ah. Again, this battery size is mainly driven by the number of days of autonomy expected or desired in micro-grids without demand-side management capabilities that can curtail or shift load during periods of low solar irradiance. For the solar panel, assuming 4 hours of expected of *full* sunlight per day (i.e. at the 1000 $W/^2$ that solar panels are rated at), the solar panel size is calculated to be ~130W.

Using the same economies of scale equations discussed earlier in the chapter, the generation assets costs would be $379.52 (equal to $275.74 in battery and $103.78 in solar). Compared to the generation asset size selection modeled herein, this selection is slightly more expensive and is driven by the larger battery size required for autonomous operation. However, keeping the additional capital costs of the appliances and wiring the same — and omitting the ethernet wiring and network / power management device costs — the capital costs for a hypothetical Mera Gao micro-grid would be $485.82, coming out to $3.73/$W$.

4.9.4 Actual Micro-Grid System Costs in Jharkhand, India

As discussed in this work, many micro-grid companies operating in off-grid, rural areas rely on integrating available equipment/components in nearby urban or peri-urban areas. In discussing with a local solar home distributor and micro-grid company in Jamshedpur, India, they were willing to share their strategy for sizing and costing out a micro-grid for 10 households.

Due to the lack of available demand-side management or network coordination devices, the company knew that they had to over-size the battery to provide requisite back-up; the operation of the micro-grid was based on a manual (not timed) switch, for 2 hours in the morning (as residents awoke for a day of farm work in the fields) and 4 hours in the evening. For a 10 household installation, with each household receiving 2x3W LED's, 1x14W DC fan, and 1x2.5W cell phone charger (total of 22.5W in load per household, expected 4-5 hours per day of usage), the company planned on using 3x200W solar panels (600W), and 1x200Ah lead-acid battery.

Based on a quote from the local distributor, the total cost of this particular installation, including the cost of the appliances, wiring, installation, etc. was Rs. 87,500

Equipment Provider	Capital Cost ($/*Household*)	Per Unit ($/$W$)
Tata Power Solar Venus Model	350	5
SELCO Models	100-900	6-12
Mera Gao	97.16	3.73
Jharkhand Distributor	132.50	2.20
Modeled Micro-Grid	**108.41**	**2.17**

Table 4.7: Summary of Capital Cost Comparisons

($1,325); resolution on the line item costs were not made available. Regardless, this comes out to a fairly low per unit cost of $\$2.2/W$, with a capital cost of $132.5 per household.

4.9.5 Summary of Capital Cost Comparisons & Discussion

The aforementioned examples provide an idea, though non-exhaustive, on the capital costs of solar home systems and micro-grids as a reference point. A summary of the costs of the four examples (two solar home system providers, two micro-grid examples) are shown on a per household and per unit basis in Table 4.7. It is clear that the micro-grid modeled herein with demand-side management capabilities enabled through a power management device, is significantly more competitive when looking at solar home systems. This is partially due to the fact that solar home systems rely on smaller solar panels, and thus higher $\$/W$ per unit costs — showing that aggregating demand is a good thing from a cost perspective (at least to a point). However, because of the aforementioned reason that $/W may not be a good metric for comparison, the $/household capital costs are also included. It's also important to note that the business model of solar home system equipment providers are far different, as it mainly relies on one-time sales of systems to individuals versus an energy service provider owning the asset and receiving regular payments in exchange for electricity services.

By looking simply at the numbers in Table 4.7, the modeled micro-grid in this work has a marginal benefit on a $\$/W$ basis, but not on a $\$/Household$ basis when compared to a hypothetical Mera Gao-type micro-grid. This may not be the defini-

tive result expected for a number of reasons. First, the choice of generation assets is a function of the reliability constraints — so relaxing the reliability constraints would undoubtedly change the choice of assets and thus system costs. Relatedly, the modeling approach thus far does not explicitly take into account the potential for reducing operational costs when compared to conventional micro-grids, as an accurate representation of such a benefit would be challenging to model in simulation. Though there is an increased complexity introduced through integrating such power management devices, operational costs could be reduced due by restricting types of loads being connected, maintaining network stability across households and heterogeneous appliances, managing battery state-of-charge, enabling mobile payments instead of door-to-door collections.

Furthermore, the decentralized nature of the micro-grid can alleviate high customer acquisition costs that are common with conventional micro-grids. For example, the micro-grid example by a local equipment distributor in Jamshedpur, numerous village meetings and visits over the course of months to first establish which households were interested in basic electricity service, and then to have the households commit to a monthly tariff. And even after households signed up one by one, many households began not paying for service after only a month — and the conventional micro-grid was not outfitted with capabilities to disconnect households that were not paying for service. Smaller, decentralized micro-grids can help address this challenge by connecting smaller number of customers within a village that have an early adopter mentality and both a commitment and willingness-to-pay for service. Individuals can also be incentivized to invest in their own electricity infrastructure by monetizing transactions amongst neighbors, and over time, decentralized micro-grids can be connected together to effectively utilize excess solar generation and manage demand.

4.10 Comment on Developed Program's Computational Stability & Local Memory

The program developed throughout the course of this effort was not designed for optimal computation efficiency, as the goal was to help drive insight at the individual micro-grid installation level and thus not expected to be extrapolated to design and simulate over hundreds or even thousands of potential customers. Regardless, given the number of variables, operations, and local memory required, a few key points related to computational stability are worth mentioning.

Key drivers for computational complexity in this model are due to the demand profile construction and the kinetic battery model / dispatch heuristic functions. The demand profile function generates a vector, with some randomization, of expected power demanded starting at the appliance level. The outputs are a series of matrices of dimension (number of hours x number of consumers). In order to generate the total load profile for the network, each column vector is recursively added to the previous column vector. The dispatch function, wherein the KiBaM is embedded, takes the available solar power and expected demand profiles and calculates the requisite KiBaM variables over the course of a simulated year. Due to the number of constraints and differences in calculation required during charging and discharging, this part of the program requires not only the most amount of computation but also local memory. Furthermore, the dispatch of serving total and critical load is also computed separately.

With essentially 15 variables being stored to conduct the KiBaM analysis for 8760 hours for each type of load profile, the number of floating-point values of type double (64 bits) using the R2015A version of MATLAB is on the order of $15 \times 8760 \times 2$. If more detailed analysis is desired, such as storing these variables for every additional customer added to the network (for $i = 1...n$) multiplies the amount of double types that need to be stored by n in the form of a matrix of $8760 \times n$ (as opposed to 8760×1) — while also increasing the amount of calculations required but can be

limited by the amount of local memory required versus what is available. Previous implementations of this model in such a format encountered such local memory issues, providing incomplete simulations that yielded values for reliability that did not make sense. Furthermore, the number of times this entire process is conducted is dependent on the state-space of available solar panels and battery capacities. To populate each of the reliability and cost matrices, this means that the program loops through $(m \times n)$ times, with m being the number of battery capacities and n being the number of solar panels for discussion purposes (for a total of 80 combinations in the instantiation of the model described herein, see Table 4.2). For reference, the model as described in Chapters 3 and 4 takes on average between 25 and 30 seconds to run in its entirety.

4.11 Conclusion

As discussed in Chapter 1, there have been numerous efforts focused on techno-economic analyses of micro-grids of various configurations. This differentiated approach shared herein provides a realistic and contextually relevant understanding of the performance and costs of solar and battery-based micro-grids with demand-side management capabilities.

Specifically, this chapter shed insight on the technical design, operation, economic value, and cost competitiveness of relying on decentralized micro-grids with demand-side management. In comparison to both solar home systems and conventional micro-grids, based on the input and operating assumptions shared in this and the previous chapter, micro-grids with demand-side management can reduce the battery size mainly due the fact that autonomous operation can be mitigated by real-time management and control. Furthermore, this analysis includes the incremental costs of the required power management devices to enable such micro-grids, and illustrates the capital cost benefits of doing so. It is worth noting that the costs and analyses shared herein do not take into account company operations, but are rather shared from the perspective of an individual considering investing in local electricity access infrastructure at a small-scale (both in terms of appliances and number of households).

In any model, the results are a function of the inputs. The model construction framework and the simulation results shared herein have aimed to be as contextually relevant as possible, incorporating available generation assets and cost inputs as seen in Jamshedpur, in the Indian state of Jharkhand. Furthermore, the aim of the model is that it can be used in other contexts with changes of the inputs, such as the number of uses, expected wiring distance or gauge, etc. — but is built solely on the basis of integrating solar and lead-acid batteries within a low-voltage, DC network.

The key decision in the model, in the selection of optimized solar and battery assets, is based on the concept of reliability. Thus far, reliability has been considered as the ratio between the electricity served (including losses in the network) versus the expected electricity demand (again, assuming the demand profile is known a priori) — a reasonable approximation for the purposes of simulation. However, in practice, understanding and quantifying the value of reliability is a significant yet important challenge and has been the subject of related work as discussed in Chapter 1. Furthermore, the version of the model presented herein allows for partial serving of loads — whereas in reality, the decision to serve a load should be binary. In closing, Chapter 5 focuses on considerations for load prioritization, appliance-level reliability, and conveyance of real-time information — all of which requires intimate knowledge of users' preferences and willingness-to-pay.

The last two chapters have walked through a series of sequential, computational steps constructed in this model, encompassing the battery model simulations. Again, the goal of the overall algorithm is to find a solution for the least cost solar and battery combination that meets reliability thresholds for an aggregated demand profile in a micro-grid network with demand-side management capabilities. The results from the initial use-case described are further analyzed with detailed sensitivity analysis — showing the impacts of key inputs for battery operation and business model assumptions.

For more clarity, a visual process flow diagram depicting the entirety of the algorithm's approach is shown in Figure 4-28.

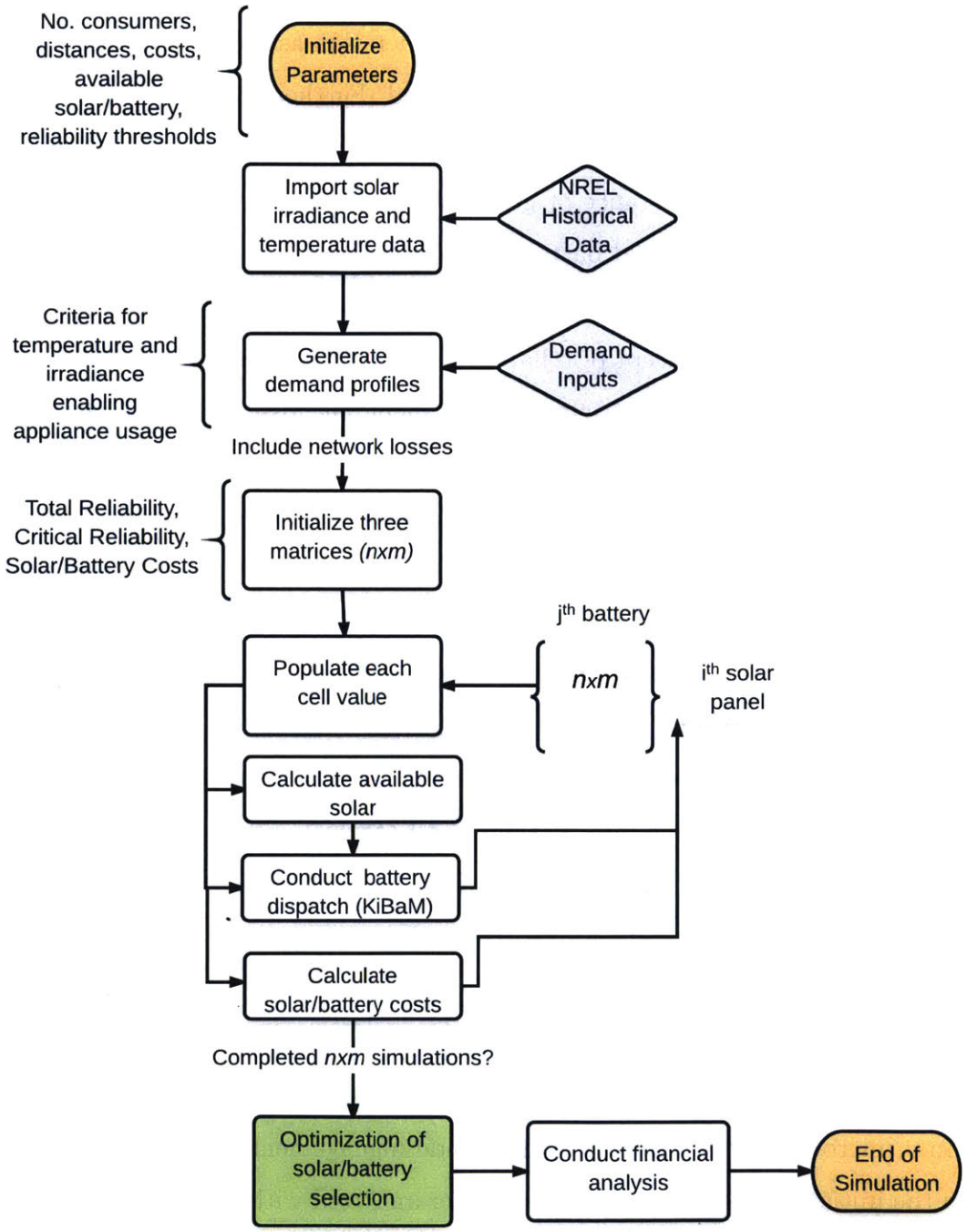


Figure 4-28: Process Flow Diagram for Constructed Model

Chapter 5

Regulatory Recommendations and Social Implications of Dynamic Price Setting in and Interconnection of Micro-Grids with Demand-Side Management

5.1 Introduction

The previous chapters have primarily focused on aspects related to the design, components, and economics of decentralized micro-grids with demand-side management capabilities. Given the assumptions made in the construction of the model, including the expected hourly levels of demand and the availability of solar/battery assets locally, the work presented herein thus far illustrates the potential value for such micro-grids in the more optimal combination of solar/battery assets — which leads to a reduction in costs, taking into account the incremental costs required due to the power management devices for the network and at each household. Given the overview and detailed description of micro-grids with demand-side management in

the previous chapters, the focus in this chapter is to analyze the implications — both policy and social — that need to be understood in order to nurture the next generation of micro-grids to take root in electricity access scenarios.

In micro-grids with demand-side management capabilities, such as the architecture proposed herein, an understanding of users' individual preferences, methods for conveying real-time information on the state of the system to users, and interconnection policy with the central grid need to be considered. Though the ability to provide different service levels and control loads' electricity consumption is a valuable capability, it doesn't come without implications on end-users' expectations and experience. Furthermore, most off-grid electricity service providers charge flat, monthly tariffs for a standardized provision — typically evening utilization of fixed appliances. Yet the potential to set and convey a real-time electricity prices and tiers of service presents itself with a set of regulatory questions in the short term that are discussed herein.

And lastly, crafting logical policy for interconnecting with future centralized grid extensions in currently unelectrified rural areas need to be thought through in the longer term. India should aim to have a symbiotic relationship between grid extension and distributed renewables when it comes to providing electricity access to the hundreds of millions in the country to-date. To put this in context, India's power system today is still predominantly supplied by coal-based thermal power generation. India has also made significant emissions reduction targets and plans for 20GW of installed solar capacity by 2022 — which will require massive levels of investment. Enabling technologies and business models, with clear interconnection policy, will help further catalyze private sector investments in off-grid, distributed solar generation.

Again, in being consistent with the use-case discussed in the previous chapters, this chapter will zero in on the regulatory landscape in the Indian state of Jharkhand by way of example.

5.2 Current Regulatory Landscape & Challenges Faced By Distribution Companies in India

As an overview, it is worth discussing the state of regulatory challenges facing India's distribution companies to give context for off-grid companies and electricity service providers. Today, India's distribution utilities face a number of fiscal and operational challenges. The main issue is that distribution utilities in India are selling electricity services below cost, creating a recurring stream (and now a massive accumulation) of debt. This issue is a well-documented problem of regulatory capture given that many distribution utilities are manipulated and influenced by politician promises to provide 'free' electricity — with that promise acted upon in coordination with the timing of public elections, as demonstrated in [94].

The key reason for why India's public sector distribution companies face massive levels of debt and are financially insolvent is due to the over-regulation of retail prices for electricity at the state level — as static electricity tariffs are set below cost of supply. One of the main goals of India's landmark Electricity Act (EA) of 2003 was to eventually privatize distribution companies to return them to high standings of financial solvency. Furthermore, the EA's goal was to separate physical wires from electricity supply, essentially splitting the natural monopoly of building out the distribution grid from players who could have 'open access' for retailing electricity (using the network) to consumers; this process of unbundling has taken place at various rates across states [2].

As a result, rural residential customers pay over-subsidized rates that are cross-subsidized through higher rates charged to commercial and industrial consumers of electricity. For example, in 2012-2013, residential and commercial/industrial customers consumed 45 % and 32 % of electricity generated respectively, yet in terms of revenue contribution, residential sector paid 26 % versus 49 % paid by commercial/industrial users. The breakdown of revenue and consumption shares in India during 2012-2013 is shown in Figure 5-1.

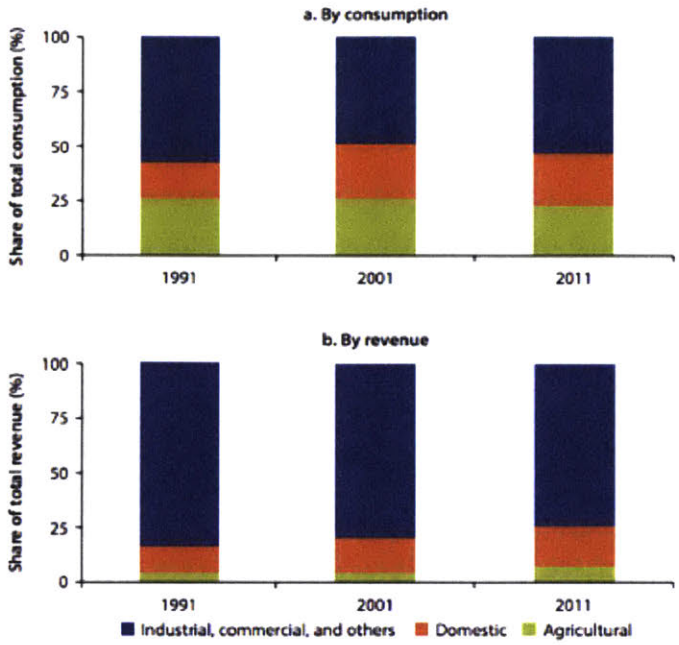


Figure 5-1: Overall Electricity Revenue Share in India [2]

5.3 Interactions and Regulations Between Grid and Off-Grid Public/Private Companies and Services

There is existing regulatory documentation regarding the landscape for companies — private or public — aiming to extend electricity access. The Electricity Act (EA) of 2003 explicitly states that:

> "where a person intends to generate and distribute electricity in a rural area to be notified by the State Government, such person shall not require any license for such generation and distribution of electricity but he shall comply with the measures which may be specified [...]."

In addition, the EA technically does allow for distribution companies to interact with 'revenue franchisees' and 'input-based franchisees'. Revenue franchisees were encouraged to improve quality of service and revenue collection on behalf of distribution companies, while input-based franchisees could purchase electricity from distribution

companies and were responsible for all activities related to extending electricity access [95]. Additional evidence of this lack of clarity can be found in the draft of the Renewable Energy Act, which simply states that "decentralised [renewable energy] projects should be able to connect and interact with utility grid" [96].

Though not without good intention, these provisions are insufficient in creating an environment for the private sector to participate in renewable energy-based off-grid electrification and renewable generation — which will only be further unleashed if the interplay between centralized and decentralized policies are delineated and appropriate financial incentives are put in place. In order to do so, there are a few key aspects that energy legislation in India needs to address.

First, legislation must address concurrent yet competing strategies for centralized and decentralized electrification. This will convey that there is an overarching implementation strategy for electrification – leading to more certainty for investment. As discussed in Chapter 1, India's government has funded two distinct electrification programs — the RGGVY (off-grid electrification) and the RVE (centralized grid extension) programs. India should include legislation that removes bureaucratic hurdles to allow RGGVY and RVE to work in parallel in achieving the same goals, something that is not done to-date [63].

In addition, the central government needs to explicitly delineate rules for interconnection between centralized grid extension and off-grid installations. The lack of clarity on whether off-grid investments get abandoned, get acquired, act as infrequent consumers, or serve as independent power producers will provide private sector entrepreneurs and investors with some sense of clarity [97]. Furthermore, legislation needs to provide legality for off-grid private sector enterprises to legally operate as a provider of electricity services. Though requiring no distribution license is a start (as outlined in the EA), based on conversations with practitioners in India, private entrepreneurs can have trouble accessing financing and obtaining trust from consumers without proof of approval or consent from the government.

Regarding off-grid distribution investments, such as in solar powered community micro-grids, a standardization of power and asset purchase agreements is advised

to provide clarity to the private sector. For example, a "must-take" clause can be included in agreements with the state utility — with oversight from a state agency such as the Jharkhand Renewable Energy Development Agency (JREDA) — to purchase assets or pay private companies to continue managing the micro-grid in order to receive cost recovery and reasonable rates of return; this should appropriately compensate the risk of such a venture instead of dissuading private sector participation [97].

Policy-makers must acknowledge the potential benefits of interconnecting distributed solar in micro-grids to the central grid. Most distribution networks in rural areas are highly unreliable as it is today, so connecting existing distributed solar installations can help mitigate the over-loading of rural feeders and provide back-up during times of peak consumption. If policy-makers can make interconnection policy more explicit, such as locational-specific net metering that incorporates costs inflicted to the network, then technical requirements in hierarchical control architectures, bi-directional grid-tied inverters to interact with micro-grids, and optimal distribution system operation can come into focus.

5.3.1 Enabling Retail Competition in Off-Grid Areas & Roles of Regulators

Given the current financial state of India's distribution companies and the vast number of citizens that still live without a reliable or any electricity connection, India's central government should accelerate private sector participation in off-grid areas. Specifically, India should aim to create a competitive retail market that provides access to electricity services of relevance. Part of the reforms would be for India to allow electricity prices to vary based on cost of supply and time-of-use to create an incentive for private companies to compete — versus being forced to operate at a loss. This shouldn't be done without regulatory oversight; as discussed in Chapter 4, there should be a baseline reliability or quality of service that can be decreed from an entity such as JSERC, and it is up to private companies to determine willingness-

to-pay strata across villages and appliances — and implement requisite technology solutions.

Given low-levels of electrification and initial low abilities to pay, competition in off-grid retail markets should allow for market players to provide varying levels of service with varying costs. This can go hand-in-hand with a diversity of loads or productive uses of electricity; if a farmer needs pumping during each afternoon with high reliability (high priority), this could be priced differently versus if a consumer would prefer to have 3-5 hours of lighting in the evening (lower priority) — or vice versa [63]. Providing enhanced levels of service reliability (again, potentially over a baseline regulated tariff corresponding to a minimum service provision, amount of electricity, or reliability threshold) through a retail market can bring buyers and sellers together with different preferences and ability to provide varying levels of reliability. From a cost perspective, as Chapters 3 and 4 showed for a particular micro-grid architecture, micro-grids have increasing capital costs as a function of increasing reliabilities. Private sector micro-grid operators can alter cost structures based on the ratio of solar panels to battery, and even include (or exclude) diesel generators as backup depending on preferences of consumers — which will undoubtedly differ based on local economies, income streams, electrical appliances desired, etc.

For example, the Huatacondo micro-grid in Peru includes five categories of electricity service; each category has a certain number of allowable interruptions to supply without a regulatory penalty [11]. In India, regulators must make clear the various reliability categories and monitor both the tariffs charged and the quality of service to hold electricity providers accountable [97]. Allowing existence of reliability categories can give consumers options while allowing suppliers to consider varying cost structures and technology solutions, such as the architecture described herein, in micro-grid settings.

Centralized power systems in the developed world have a reputation for providing exceptionally high levels of reliability and quality of service across customer archetypes. In general, electricity is considered to be a "basic service" and a "basic human right" [98]. But as generally known, and further supported by the example

of a micro-grid with demand side management presented in this work, the costs of any power system is a direct function of the reliability desired. Demand-side management capabilities can mitigate these increases in costs at the expense of periodically curtailing loads during periods of low solar resource when considering isolated, renewable-based micro-grids.

Another recommendation is for regulation to allow logical management of demand in rural areas (versus random, intermittent interruptions); more specifically, in isolated micro-grids solely based on renewable energy resources, demand can be considered as the inputs into dispatch of an energy resource. Given low initial willingness-to-pay in relation to cost recovery, as briefly discussed in Chapter 4, consumers should no longer be viewed as passive customers but as active participants in the provision and consumption of electricity. Thus, measures should be instituted from a regulatory standpoint to enable individual consumers to provide preferences on energy consumption activities, appliances, and priorities. Furthermore, and regardless of the context, consumers must be able to react (actively or autonomously) to dynamic electricity prices based on the state of the system, which varies with time based on a variety of factors previously discussed in this work.

The concept of demand scheduling for a constrained resource (typically solar energy stored in a battery, or a finite amount of fuel for a diesel generator) should take root at the distribution retail level in off-grid areas — a process that will involve local regulators, electricity service providers, and end-consumers. The encouragement of adopting such demand-based control architectures is far different than the way in which the central grid conducts optimal unit commitment (given the vast number of generators in a given power system). Instead of viewing the grid as a series of decisions of supply unit commitments to meet demand loads, scheduling demand to meet a finite amount of supply provides a way to rethink how to manage demand — again, subject to baseline and reasonable quality of service and reliability constraints to help mitigate high capital costs of off-grid systems.

Implementation of such a strategy would undoubtedly not be facile. Determining household level reliability preferences, load priorities, and dynamic profiles would be

a challenging data collection exercise, with decisions undoubtedly to be met with various uncertainties (i.e. behavioral, weather, etc.) in real-time dispatch. However, during the connection processes to rural households, the electricity service provider can convey such concepts to the user — in that electricity provided might not be provided 24/7 and that certain loads will be given priorities. It is up to the regulator to encourage such relationships between off-grid retailers and end-users, along with utilization of distributed hierarchical control architectures that incorporate such scheduling, to better manage demand.

5.4 Solar Subsidies & Load Coincidence Factor

As discussed in Chapter 2, each appliance has a different load profile that may be related to exogenous variables, may be correlated with usage of other appliances, and may correspond to a particular user's activity. In the REM demand profile construction method, the usage of the relevant appliance is triggered by the temperature and time of day. With additional, more productive loads, other variables (such as seasonality) may be taken into account. In considering real-time dispatch — and appliances that drive the cost of the system — it is worth understanding which appliances are daytime loads that could be served directly by solar power to better tailor capital subsidies from the government.

To understand what proportion of an appliance's load profile would be served by the solar panel versus the battery, a solar-load coincidence factor (SLCF) is defined by:

$$SLCF_{appliance} = \frac{\sum_{i=1}^{8760} Wh_{i,demand}}{\sum_{i=1}^{8760} Wh_{i,solar}} \tag{5.1}$$

Note that the denominator is dependent on the module size. Based on the residential load profile scenario for five households described in Chapters 4, the SLCF's for the fan over a simulated year are shown in table 5.1, and the SLCF can be viewed as a useful proxy for determining the presence of daytime loads in a network. Loads

Module Size	Fan SLCF
50W	45.25%
75W	68.52%
80W	71.5%
100W	79.17%
120W	83.54%
125W	84.32%
150W	87.44%
200W	90.98%
250W	93.06%
300W	94.36%

Table 5.1: Solar Load Coincidence Factors (SLCF) for Fan Usage

with a higher SLCF could utilize the available solar energy directly — reducing losses in efficiency during battery charging and discharging and potentially costs by requiring a smaller battery; the results of the fan were chosen to be presented here because the fan is induced by higher temperatures, which typically corresponds which higher levels of irradiance during the daytime. (The cell phone charger is induced randomly throughout the day, while the lights have an SLCF of 0 regardless of the panel size). This is reflected back in Figure 4-12, showing essentially levels of zero reliability with small batteries serving evening, lighting loads.

Today, India's MNRE has enacted solar subsidies at the central government level, but not including details on the integration with batteries or the types of appliances/loads to be served. As of 2014, there exists a flat 30% capital subsidy for decentralized solar installations less than 1kW, and a 40% subsidy for installations between 1kW and 3kW [3]; these subsidies are likely helpful to companies operating in this space, but the argument here is that these subsidies can be further tailored based on the application. An alternative approach may be to specify the types of loads to be served by distributed solar and extend the subsidy to other key capital costs in micro-grids (i.e. batteries, network devices, etc.).

Allocated funds should also be considered to be made available for operational subsidies. As discussed at length in Chapter 4, the financial sustainability of profitable micro-grids today can be very challenging and is exacerbated by the low willingness-

to-pay associated with kerosene subsidies. Thus, having phased and recurring operational subsidies for electricity service providers in micro-grids can better ensure the longevity of maintenance and quality of service.

5.5 Current Regulatory Approach for Tariff Setting & Relation to Micro-Grids

In Jharkhand, the Jharkhand Bijli Vitran Nigam Limited (JBVNL) is the state-owned distribution company (DISCOM) — recently unbundled from the generation and transmission entities. In the state today, the only competition to JBVNL in the distribution sector is JUSCO (Jamshedpur Utilities Service Company), a private yet fully owned subsidiary of Tata Steel — one of the dominant industries and employers in the Jamshedpur area. The Jharkhand State Electricity Regulatory Commission (JSERC) regulates the distribution activity and awards distribution licenses, and each licensee has to abide by a tariff framework put forth by the JSERC (along with revenue requirements, capital investment plans, targets for distribution losses, etc.) [99].

The JSERC must also approve a capital investment plan for each distribution company, and sets targets for aspects such as distribution losses and customer revenue; the term ARR (Annual Revenue Requirement) is used to set revenue targets. JSERC lists all the cost elements that would be needed for an ARR to meet, and denotes whether they are "controllable" (i.e. predictable), or "uncontrollable" (i.e. may or may not need to be passed along to consumers in terms of cost). For a publicly owned state generation company, JSERC approves a FPPPA (fuel price and power purchase agreement) for each one that dictates the arrangement between state generation and distribution companies.

In theory, any distribution company needs to recover their costs based in tariffs charged to consumers. As Figure 5-2 depicts, JBVNL has a number of categories of distribution consumers along with both a fixed monthly and per kWh of consumption

charge. However, the tariffs for electricity consumption are clearly flat and do not vary based on supply/demand variations; across the customer categories, the tariffs range from Rs. 1.20 — Rs. 3.95 per kWh (roughly $0.02 — $0.06 per kWh). By any standard, this is an incredibly low price of electricity, and a tariff that is not representative of the cost of any generator.

With that in mind, the JSERC and JBVNL are aware of the effects of the low levels recovery. The justification for operating in this manner is explicitly mentioned in their most recent ARR tariff proposal document:

> "JSEB serves a large rural consumer base, amongst which a significant number of consumers fall in the Below Poverty Line (BPL) category. This set of consumers is extremely poor and cannot afford electricity at the rates which are being levied on the domestic consumers in urban areas. However, in today's time, electricity has become an essential commodity for every common man and its role in improving the social and economic upliftment of the underprivileged cannot be gainsaid. Denying electricity to any citizen is tantamount to limiting the growth prospects of the entire family. JSEB completely understands this and hence in order to ensure the availability of electricity even to people falling in the lowest economical strata, JSEB has ensured connectivity of many remote villages on its network." [99]

Again, most tariffs in India are set versus being appropriately computed or responding to cost of electricity fluctuations; note that there are generally accepted practices in developed world power systems to regulate natural monopolies that aim to balance fairly structured tariffs and appropriate rates of return [98]. This current approach to tariff setting reveals itself based on the incurred debt seen by publicly-owned distribution companies that are influenced to sell electricity below cost of generation or purchased electricity. As mentioned previously, a major reason for that is the interplay of rural voters' influence from politicians promising cheap to free electricity during times of elections. However, there seems to be growing consensus to

Consumer Category	Fixed Charge	Energy Charge	
	Rate	Unit	Rate
DS-I (a), Kutir Jyoti Connections, metered	Rs. 25 per connection per month	Rs./ kWh (0-50 units)	1.20
		Rs/kWh (Above 50 units)	1.20
DS-I (a), Kutir Jyoti Connections, unmetered	Rs.50 Per Connection Per Month	Rs./kWh	NA
DS – I (b)- other rural domestic consumers, metered	Rs.40 Per Connection Per Month	Rs./ kWh (0-200 units)	1.50
		Rs/kWh (Above 200 units)	1.50
DS - I (b)- other rural domestic consumers, unmetered	Rs.200 Per Connection Per Month	N/A	N/A
DS-II	Rs.70 Per Connection Per Month	Rs./kWh (0-200 Units)	2.95
	Rs.120 Per Connection Per Month	Rs./kWh (200 Units and above)	3.95
DS – III	Rs.200 Per Connection Per Month	Rs./kWh	3.95
DS HT	Rs.100 Per kVA Per Month	Rs./kWh	3.75

Figure 5-2: Tariffs for Distribution Consumers by JBVNL [99]

move towards cost-reflective tariff frameworks, with one government proposal advocating for tariffs to be within 50% of the cost of service for below poverty line (BPL) consumers — and gradually progressing towards 80% [100].

Another reason for these issues is due to the lack of functioning electricity markets that extend to the state level in India, which don't allow fluctuations in the cost of supply to be mitigated by any sort of price elasticity in demand. This is further compounded by the lack of effective regulation in India's electricity sector — evidenced by the lack of capacity markets and enforcement of reliability and quality of service standards. Figure 5-3 shows the interplay of the various institutional actors in India's power sector — from the central generation and transmission utilities, to the state-level entities. As a point of comparison, it is worth nothing that JUSCO, as a private distribution company, has highly reliable service ($\leq$ 99%, primarily serving urban customers in Jamshedpur area); while JBVNL has less reliable service ($\sim$ 60%, primarily serving customers located more in rural areas) [99].

Today, it is convention that micro-grid companies are able to charge fees that differ from the regulated tariff as long as it is viewed as a service (i.e. evening lights and mo-

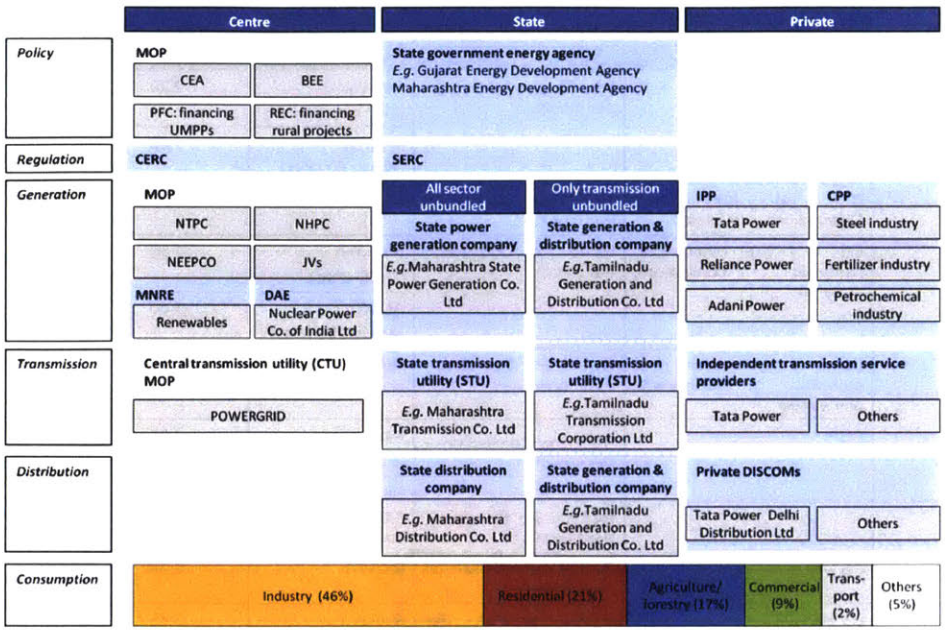


Figure 5-3: Institutional Structure of India's Power Sector [2]

bile phone charging). As previously discussed, most micro-grid operators set monthly fees (on the order of $2/month), which is pegged to the typical willingness-to-pay for off-grid consumers for basic electricity service — such as provided by companies like Mera Gao. Based on the results shared for generation asset sizing and minimum monthly payments required, it is undoubtedly tough to receive adequate cost recovery in a reasonable time frame based on this average willingness-to-pay constraint.

The average willingness-to-pay for basic electricity service in India is well-regarded to be lower than in most of Africa, the major reason attributed to the widespread kerosene fuel subsidies present in India. Kerosene is commonly used as a lighting fuel in rural areas, and for many without access to electricity, the rational household economic calculation when considering a basic electricity service is to compare current expenditures on a substitute. And the amount spent on kerosene is suppressed by the subsidies present from the government; based on survey data gathered in Jharkhand, the Public Distribution Service (PDS) provides a subsidized price of Rs. 17 per liter of kerosene, up to three liters. This dictates the starting point that many off-grid electricity service providers have to consider monthly charges — and also sets a baseline when considering to implement a micro-grid that can convey notion of a

House	1	2	3	4	5
Occupation	Teaching	Farming	Farming	Farming	Farming
Daily Schedule	Mostly home in summer; errands in town.	5am-11am: field/farming; 11am-4pm: home/lunch/rest ; 4pm-6pm: leisure/rest/dinner. ~10pm: sleep	5am-11am: field/farming; 11am-4pm: home/lunch/rest ; 4pm-6pm: leisure/rest/dinner. ~10pm: sleep	5am-11am: field/farming; 11am-4pm: home/lunch/rest ; 4pm-6pm: leisure/rest/dinner. ~10pm: sleep	5am-11am: field/farming; 11am-4pm: home/lunch/rest ; 4pm-6pm: leisure/rest/dinner. ~10pm: sleep
Load Prioritization					
Lights (LED)	1	1	1	1	1
Cell Phone Charger	2	3	3	3	2
Fan	3	2	2	2	3

Estimated Time Range of Usage					
House	1	2	3	4	5
Fan	10am-8pm	11am-4pm	11am-4pm	11am-4pm	11am-4pm
Lights	12pm-10pm	6pm-10pm	6pm-10pm	6pm-10pm	6pm-10pm
Cell Phone Charger	n/a	n/a	n/a	n/a	n/a

Figure 5-4: Qualitative Survey Results from Five Households

real-time 'price' to end-users.

5.6 Incorporating Individual Users' Preferences & Determining Tiers of Electricity Service

5.6.1 Preference Differentiation Based on Survey Results near Patamda, Jharkhand

As mentioned in Chapter 2, in addition to work with installing data loggers for quantitatively measuring electricity consumption with solar home systems in a village outside of the peri-urban area of Patamda, Jharkhand, a handful of household-level surveys were conducted in coordination with Tata Steel's Rural Development Society. These qualitative surveys were conducted in order to gain insight on household's basic schedule of activities, prioritization of basic appliances, and estimation time range of load usage. As shown in Figure 5-4, questions were asked on prioritization of lights, cell phone chargers, and fans; and consistent with the residential load profile scenario used in Chapters 3 and 4, for the five households survey herein in this particular village, lights were ranked as the highest priority load.

These types of insights are useful in incorporating household-level preferences

on different appliances. However, additional effort would be required in determining responses to real-time price signals to obtain some proxy for appliance-level reliability and willingness-to-pay.

5.6.2 Conceptualization of Real-Time Pricing Based on Battery State-of-Charge Thresholds

As discussed in the previous chapters, one of the explicit and unique capabilities of an advanced micro-grid with demand-side management is to differentiate and prioritize loads. As explained in Chapters 3 and 4, in the model formulation shared herein, this was shown through the delineation between the expected critical and total load profiles — again, aggregated across households over the network at hourly time steps over the course of an example year. Yet the realization of that capability means discretely curtailing users' loads, in the form of a binary decision on whether a load can or cannot be served based on available energy — a decision that requires both a priori information on user reliability preferences and appliance-level willingness-to-pay. And in real-time, one can envision a primitive form of demand-response such that user's can decide whether or not to continue using an appliance during periods when the system is strained.

With that capability comes a responsibility and a requirement to understand and incorporate end-users' preferences. At the extreme, for optimal real-time operation and dispatch, getting to these answers requires a complete understanding of aspects such as user-specific electricity demand elasticities to changes in 'price'. The method used in determining Ramsey Prices is a relevant reference point, used in electricity tariff design, and is based on adjusting tariffs to consumers in relation to their individualized elasticity. Though useful, power systems today don't discriminate across consumers; this is partially due to the fact that consumers' demand is typically inelastic and that information on real-time electricity prices are inaccessible to consumers today [98].

Realistically, obtaining this level of information is not only likely to be onerous,

SOC Threshold	Household Balance (Watt-seconds)	ROBD
Green (100%-75%)	216,000	1
Yellow (75%-55%)	172,800	2
Red (55%-40%)	86,400	10

Table 5.2: Example of Daily Electricity Balance Allotment

but also not entirely relevant for such settings given that for the purposes of micro-grids thus far, the use-case is in areas for initial access to electricity. Thus, such end-users may not have a reference point on reliable versus unreliable service or the need to have a real-time 'price' — though the former is likely different for rural areas with grid connection and extremely poor quality of service from local distribution companies.

In the absence of such information in the short-term, another approach is to consider thresholds of the battery state-of-charge and a method for conveying a real-time 'balance' to the end-user. This approach can be supported by users' appliance preferences in terms of the order of curtailment if and when the battery state-of-charge crosses a certain, predetermined threshold. As an example, for a 100 Ah battery (the optimal size found in the previous chapter — paired with a 250W solar panel for a 5 household network), the three key state-of-charge thresholds are shown in Table 5.2. Additionally, given a nominal voltage of 12V, the type of information that could be displayed on a simple LCD screen is the *maximum* available watt-seconds available per household per SOC threshold. Given an expected diurnal operating charge/discharge cycle, this balance allotment can be considered on a daily basis.

As previously discussed, the main reason for having a micro-grid with demand-side management is so as not to oversize the generation assets. Given a smaller battery, it's expected that the battery will consistently oscillate between the MLOC and MDOD (as described in Chapter 3). In the example state-of-charge thresholds in Table 5.2, the rate-of-balance decrease wouldn't change when the battery is near full; however, for the subsequent thresholds, the rate of balance of should decrease at a faster rate. Thus, based on Table 5.2 and back-calculating based on the rate of balance decrease for each threshold, the overall allotted energy per day per household is roughly 85

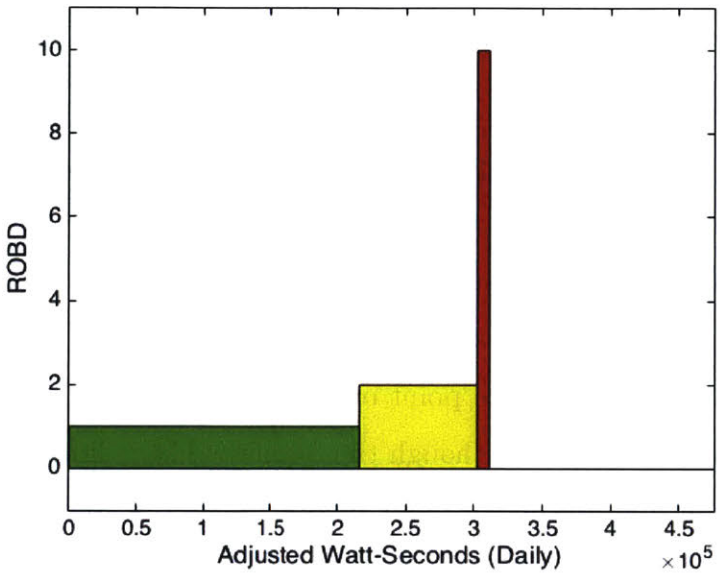


Figure 5-5: Example of ROBD-Adjusted Daily Electricity Balance Per Household Based on SOC Threshold

watt-hours — a reasonable baseline amount for the residential load scenario.

Figure 5-5 illustrates the 'supply' curve of available balance at the household level as an example, adjusted with the example ROBD values. From a regulator's perspective, the right of the red SOC threshold would be where the amount of non-served energy for a household would be; in this context, this amount can be viewed as the amount of energy an individual consumer wished to consume but that was not served. This value has an associated cost of non-served energy (CNSE, which in power systems nomenclature can also be referred to as the "value of lost load", VOLL). In centralized power systems, non-served energy is viewed as a high variable (and no fixed) cost generator that covers the amount of energy not served by all the available existing generation in a network [98]. As discussed in Chapter 1, the determination of this cost parameters is difficult, with various methods yielding different answers — but it is assumed to have the highest cost in order to mitigate relying on using it as a resource when conducting an optimization with an objective to minimize system-wide costs.

There are two ways to consider this notion of a rate of balance decrease — and how

to assign appropriate values. One way is to view it in relation to assigning a higher cost of operation for each battery threshold. In a conventional unit-commitment mindset, each battery state-of-charge threshold can be viewed as a series of three costlier generators that "bid" in and are "dispatched" as necessary. Again, only an isolated micro-grid (i.e. not grid-tied) relying solely on solar panels and batteries is considered herein, therefore removing the option to incorporate a higher cost diesel generator if necessary or to draw from the centralized grid if available. Yet because the operational cost of a battery is the same regardless of the thresholds, coming up with differences across the ROBD with costs in mind can be considered to be arbitrary. However, this is the importance of conducting a combined generation and load forecast — as with this available knowledge, albeit probabilistic, the ROBD and even the SOC threshold values can be dynamic as well. The accuracy of the forecasts can affect the operational costs of a micro-grid, as shown based on regularly receiving short-term solar generation forecasts from the Weather Research and Forecasting (WRF) Model and tested across various time horizons (i.e. 15 minutes) in [101].

The alternative approach is to consider the values for setting the ROBD dependent on the demand; demand herein is assumed to be relatively active, in that it is responding to some proxy of price (versus passive demand, that assumes a static price and is unable to respond to a dynamic price signal) [98]. This comes back to obtaining some notion of elasticity that needs to be tested and learned in a real implementation. Both the threshold and the available balance need to be conveyed to the user — and what needs to be tested is a user-response, in the form of selectively keeping loads on or turning them off, to different ROBD's. A true inelastic demand would not react to the changes in ROBD, but controlling the method (i.e. via LED's or SMS) and the choice of information to convey to user's would be necessary experiments to conduct from a social science perspective. And the learning of these ROBD values can be used to build some notion of a more granular demand curve within a particular village or locale for a micro-grid.

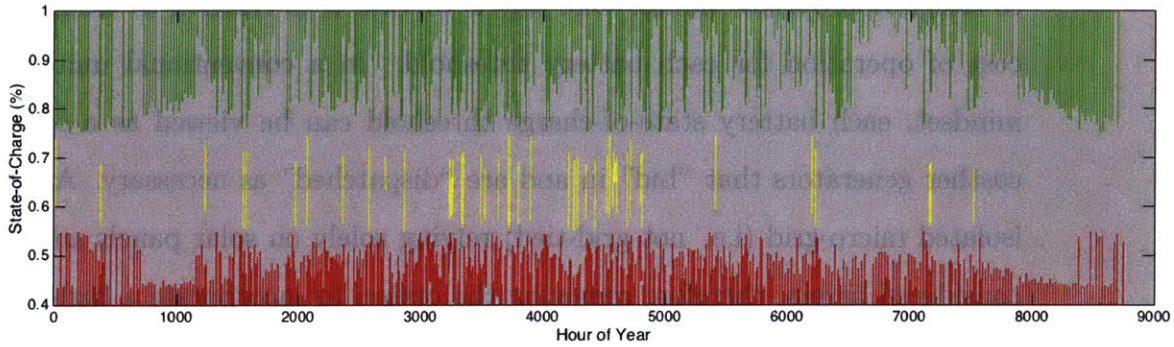


Figure 5-6: Simulated Battery State-of-Charge Over Entire Year

5.6.3 Extrapolation from Telecommunication Industry's Service Level Agreements

As discussed both in this and previous chapters, a key facet of micro-grids with demand-side management is their ability to differentiate and distinguish appliances at the household level. What this allows for is a provision of varying levels of service depending on individualized willingness-to-pay, preferences, and can even incorporate regulatory requirements. By way of example of such potential, Chapters 3 and 4 focused on simple differentiation of critical and total load profiles — determining the least cost combination of solar and battery assets required to meet predetermined reliability thresholds. These thresholds can be considered as service levels, and for reasons discussed in this chapter such as diverse and low initial willingness-to-pay and need for reasonable cost recovery, it may be of benefit to provide differentiated service levels — as the cost of a micro-grid scales with the reliability desired.

This concept has not been integrated historically in the design and operation of centralized power systems, partially due to the lack of technical abilities to regulate and curtail at high resolution (i.e. at the outlet level) — versus relying on intermittent and unreliable supply. Thus, with the advent of technologies such as the power management device described herein, next generation technologies can take root that can also open up the potential for new operating strategies and business models. Regarding the latter, key learnings can be extrapolated from the information and telecommunication industries during its onset several decades ago.

There have been a handful of theoretical approaches and practical implementations of tiered internet services, in varying bandwith in relation to customers' differentiated demand. As outlined in [74], a key aspect is determining the delineation and the number of tiered services to provide to consumers in a network, as there is a tradeoff between optimal pricing strategies and network operating complexities. The theoretical baseline for determining this strategy is based off the *p-median* problem, in assessing the optimal number of "supply points" that minimizes the total sum of distances (thought of from each consumer's expected demand).

Internet-service providers have utilized a baseline bandwith, and subsequently provide 'exponential' tiers of increasing bandwith options to consumers. The argument for considering tiered pricing is that it "is likely to spur adoption by providing a wide menu of customized services from which users may select based on needs and affordability" — relevant to the thought processes regarding tiers of service in micro-grids with demand-side management [74].

Referencing service level agreements for internet provision is analogous to a number of relevant topics in the context of advanced micro-grids with demand-side management. With tiered-services in the form of either varying reliabilities and/or amount of energy demanded (across appliances), this allows for the flexibility for user's to incorporate individual preferences which can change over time. Undoubtedly, implementing such a scheme would increase in complexity given the number of users, diversity of appliances, and number of tiers. In [76], a proposed approach to overcome this is to rely on a 'multi-class flat-rate pricing scheme', known as the Paris Metro pricing strategy. This approach is considered with the inclusion of a baseline regulation on a minimum service tier on the access rate (megabytes per second). These are useful reference points to consider in electricity access contexts, given the advent of power management technologies and strategies to enable demand-side management in micro-grids of tomorrow.

5.7 Conclusion

This chapter aimed to cover a number of key aspects related to policy, regulatory, and social issues related to next generation micro-grids. The challenges facing India's existing distribution companies and tariff structuring are well-known and well-established, and these issues must be addressed. This chapter also outlines additional policy recommendations to catalyze private sector investment in next generation micro-grids, the potential and value of an example has been described in the previous chapters of this work. Interconnection policy must be made clear and existing subsidies can be better targeted to help with investment certainty and long-term operation. Furthermore, insight is shared regarding the issue of dynamic price setting and provision of tiers of service in micro-grids with demand-side management; however, these aspects need to be further researched from a social science perspective — but encouraged from a policy perspective.

Chapter 6

Conclusions and Future Work

6.1 Introduction

As discussed in Chapter 1, distributed generation is playing a larger and more viable role in electricity access efforts in the developing world. However, even with cost reductions in solar panels, micro-grids and solar home systems can still be costly due to the over-sizing of generation assets to ensure operation autonomy and a lack of ability to actively manage demand. Next generation micro-grids can help lower costs of electricity service by integrating low-cost sensors, power electronics, and controllable switches combined with on-site computation and communication to enable some form of demand-side managemet — in disaggregating, prioritizing, and dispatching demand at the household level.

With this increased complexity and costs, the question arises: how can one assess the benefit in the design and operation of such micro-grids? This has been the key motivation, answered through modeling and simulation. The previous five chapters provided insight on technical, economic, and regulatory aspects in regards to the design and operation of decentralized micro-grids with demand-side management capabilities. To start, Chapter 1 positioned this work in context, reviewing relevant topical areas touched upon in this work: demand modeling and classification, battery modeling in simulation and real-time applications, the design and operation of micro-grids, extrapolation to system economics, and associated policy implications of

advanced micro-grids with the ability to prioritize loads and convey a real-time price to users. The remainder of this chapter walks through the key takeaways of the first four chapters, including areas of future work and improvements.

6.2 Conclusions on Data-Driven, Activity-Based Demand Profile Construction

Based on electricity data from solar home systems in rural Jharkhand, the work presented in Chapter 2 is based on a methodology for acquiring, calibrating, and analyzing load profiles. Given that the load profiles were not directly measured in this case, Chapter 2 presents heuristics for considering the separation of spillage from load — the choice of which clearly affects subsequent analysis on what may be considered as day-time usage of appliances.

In addition, Chapter 2 constructs activity-based models at the household level — and extrapolating this ability of load disaggregation to provide probability distributions of exogenous variables (i.e. time of day and ambient temperature) paired with user activities (i.e. light and fan usage). Lastly, Chapter 2 assesses the performance of using clustering algorithms for conducting load disaggregation, showing the various effects of initializing K-Means and Gaussian Mixture Models with a priori information on power consumption levels associated with appliance combinations. It is useful to understand the potential for such algorithms to be relied upon in the field — in situations where on-site computation was available and household-level electricity consumption measurements were being taken, and with a known combination of appliances.

6.2.1 Generating Household Level Demand Forecasting Models

Chapter 2 discussed that the data sets acquired were only available at three households to-date — and required periodical manual uploads of the logged data. Future

work should extend to remote monitoring — connecting such metering devices to a cloud-based infrastructure for real-time analytics; there have been examples of such an architecture presented in [10], but could also rely on low-cost, open-source hardware platforms such as Particle.io. The intent to gather quantitative data for monitoring electricity consumption must be accompanied with useful algorithms and visualization techniques to drive insight. Subject to the advent of more publicly available data sets (which, as discussed, will vary by timescale and resolution), load forecasting techniques should be tested for efficacy, replicability, and usability in relevant contexts (appliance-level, household-level, micro-grid-level, etc.). However, as has been stated before, access to data sets of user's electricity consumption is not readily available or shared in this space. Generating and sharing more of these data sets will only further inform electricity planning efforts. As Chapter 2 discussed, use-cases include assessing the performance of real-time load disaggregation algorithms in future implementation of micro-grids with demand-side management and retrospectively understanding whether and by how much existing systems are over- or under-designed to meet certain levels of demand.

As is typical of load forecasting in centralized power systems in the developed world, relevant features include time of day and ambient temperature. But given day-to-day variability across individual households in micro-grids, a tailored, probabilistic, state-based approach that can take into account such exogenous variables — such as input/output Hidden Markov Models — may be an appropriate technique to consider when conducting a demand forecast locally. Markov Models are an efficient way for storing observed values and associated probability of the (latent) state variables; each observation in a Markov chain is solely dependent on the previous observation — and as such, is independent on all previous observations (as depicted in Figure 6-1). To give context, for a set of observations of power consumption $X_1 ... X_n$, each observation can be described by a latent variable $Z_1 ... Z_n$, with the number of states, K, equal to 10 based on the combination of appliances (as described in the Table 2.2). Thus, an HMM can factor to a series of conditional distributions for each latent variable Z_n. The transition matrix (A) encodes these probabilities, and the emission matrix,

$\phi = P(X_n|Z_n)$), encodes the probabilities across the states for a particular observation X_n.

However, one potential drawback to this approach is that if there is a high proportion of user states with no appliance on (which is seen in Chapter 2 for state 1), a standard HMM will be disproportionately affected to accommodate this bias in the data set. More specifically, for a particular house, the output of the transition matrix will likely have the first column a vector of ones, and the rest of the values equal to zero. Again, this outcome will potentially be because the transition matrix was naïve, given the large number of zeros (i.e. state 1 occurrences) in the household's data set on hand in Chapter 2. In a situation where there are few appliances used only a few hours a day, the algorithm will choose state 1 more often than not, which is logical but doesn't yield interesting results. This is not to say that observations of when no appliances are on are not valid — as those are in fact observed values. The interpretation here is that running an HMM for even one particular day for one particular house will heavily weigh the results to the most commonly occurring state, which is not useful to make predictions for a future time frame such as the next day.

This underscores the fact that having the ability to conduct activity-based load disaggregation is important, as it can extrapolate consumption to critical state inputs such as time of day and temperature. The input of the time of day and temperature is a critical factor not included in an original construction of the HMM — which leads to the potential usage of an input-output Hidden Markov Model (I/O HMM). As an example, with the additional sequential and observed variables U_n corresponding to time, the graphical model for an I/O HMM for the data sets presented in Chapter 2 is shown in Figure 6-2, with the addition of the input variables U_n for the time-of-day or temperature.

Another key point in demand forecasting is the timescale of which a forecast is being conducted for. Using historical electricity consumption, say over many months of data, may not be useful or appropriate in predicting the next 50 or 100 days worth of electricity consumption. Thus, future work may also include incorporating appropriate sampling (i.e. Gibbs sampling) methods of time periods of electricity

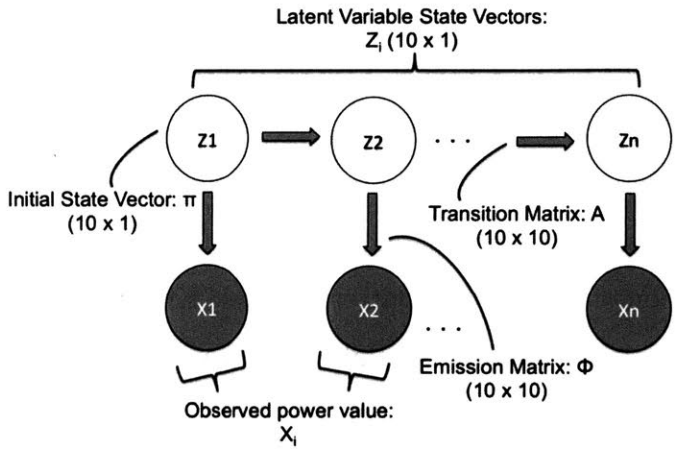


Figure 6-1: Use-Case for Hidden Markov Model [85]

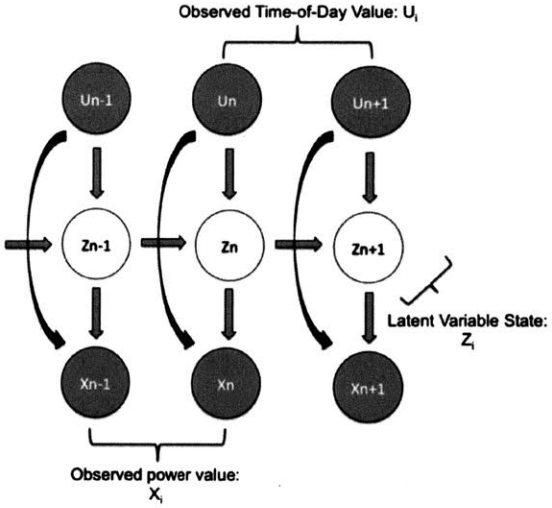


Figure 6-2: Use-Case for Input Hidden Markov Model [85]

consumption data to learn the most probable sequence of user states — and then sampling another time period of which to compare the predicted energy consumption values with the observed values.

6.3 Conclusions on Battery Modeling in Simulation & Real-Time Implementation

Chapter 3 focuses the importance and implementation of appropriate battery models for both simulation and reliance in real-time operation. Specifically, Chapter 3 includes the adaptation of the Kinetic Battery Model (KiBaM) framework — a realistic model that indicates the real-time available and bound charge due to the dynamics of diffusion processes taking place within a lead-acid battery. To represent a microgrid's ability to have an on-board battery management system, the modeling effort includes battery management constraints for times when excess solar may over-charge the battery (and vice versa for the load). The results from an example net load profile fed into the battery model to illustrate how and which constraints are reached during simulation.

The latter part of Chapter 3 focuses on extending the parameters and dynamic equations of the KiBaM for use in a real-time battery management system — a unique approach given that the KiBaM has typically been relied upon for simulation purposes in various modeling platforms. This extension relies on the initialization of the three KiBaM parameters for a Universal 100 Ah battery in the case presented. Additional parameters to accurately represent voltage effects (in the form of IR losses) expected in a lead-acid battery, specifically in conductive and dynamic diffusive resistances as a function of the real-time available charge and a modified version of the Nernst Equation. Based on a charge and discharge cycle data acquired, an optimization technique is presented to minimize the predicted voltage with the actual voltage response of the battery, based on the induced current over the duration of the cycle, yielding a RMSE of 0.11 volts.

6.3.1 Accurately Modeling Battery Degradation

In a micro-grid, the frequency and depth of discharge is dependent on the incident net profile — from the solar power generation and the demand. Integrating an MPPT charge controller and either a battery management system can help mitigate periods of over-discharge — a capability assumed in the micro-grid modeled herein based on the state-of-charge battery constraints implemented in this adapted version of KiBaM presented here. As discussed previously, the MDOD constraint is not reached the majority of the times in the particular example shared in Chapter 3, but situations that force higher power discharge — such as with more productive loads or higher power appliances, in geographical areas with poor solar resource, and/or an undersized solar panel — will effect the number of times the battery reaches that constraint.

In simulation, a key element *not* taken into account in this model is the issue of battery degradation and state-of-health in real-time. A rule of thumb with lead-acid batteries is that a battery needs replacement when it reaches 80% of its nominal rated capacity — but assessing when is the appropriate time for replacement relies on techniques to compute degradation and capacity fade. One approach for assessing lithium-ion degradation is described in [102], taking into account expected parameters such as depth of discharge, C-rate, cycle temperature, and number of cycles to predict the faded capacity (partially due to the physical formation of a solid electrolyte interface, SEI) and battery performance (in a frequency regulation application). In lead-acid batteries, the physical phenomenon taking place is that as battery cycling increases, an increase in sulphation of the electrodes takes place — essentially irreversible reactions. The result of these reactions is the reduced availability of reaction sites in the electrode's surface area [89]. Accounting for the associated incremental degradation will be an important aspect to integrate in the future.

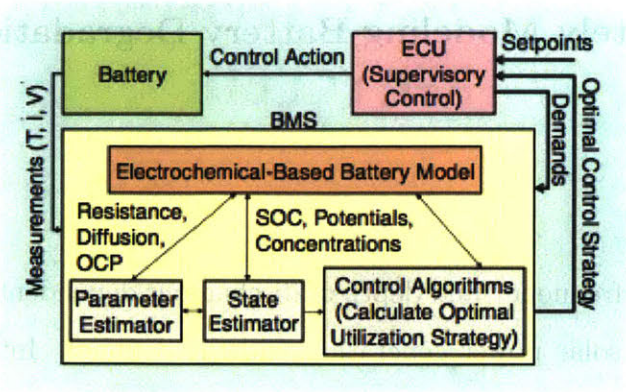


Figure 6-3: Representation of Battery Management System Architecture [103]

6.3.2 Integration of Battery Model within Control System Architecture

As presented in Chapter 3, even with a model that is parameterized for a particular battery, a battery management system (BMS) needs to be incorporated for effective management in the field. Capabilities required in any BMS include employing real-time state estimation and optimal control strategies, and the specifics of a BMS operating strategy is based on the battery model relied upon and the expected dispatch strategy to meet the load. A pictorial representation of an example of a holistic battery management system architecture, based on an electro-chemical based model outlined in [103], is shown in Figure 6-3.

6.3.3 Further Representing Micro-Grid Operational Dispatch and Demand-Side Management Algorithms

Furthermore, as has been discussed, micro-grid companies today face challenges with operating and dispatching energy in an efficient and optimal way; but without a combined hardware and software solution to manage and dispatch electricity in real-time, micro-grid companies will have to continue relying on over-sizing generation assets. In simulations described herein, it is assumed that a micro-grid with computational and demand-side management capabilities can provide different service levels subject

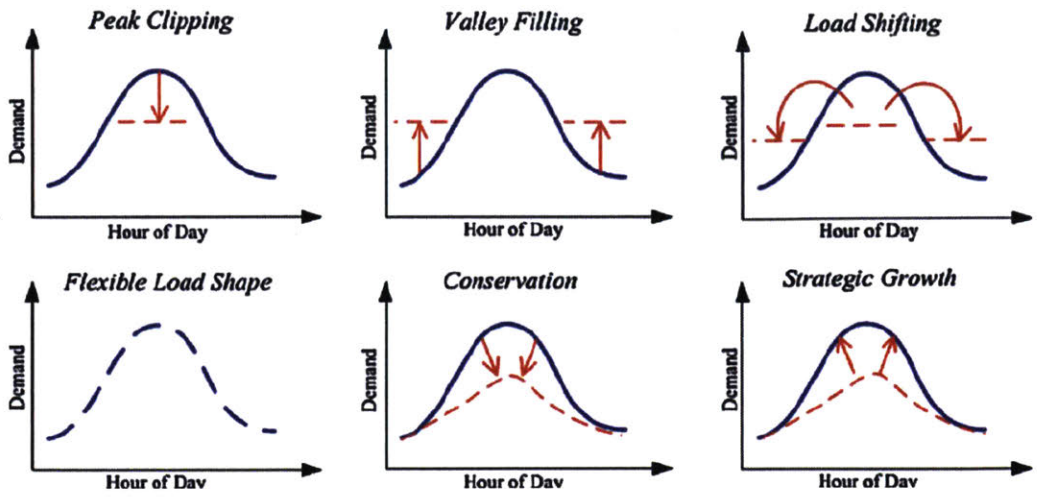


Figure 6-4: Depiction of Various Demand-Side Management Approaches [104]

to reliability thresholds.

In the current modeling approach presented in Chapter 3, the dispatch heuristic determination is made on whether load (separately for total and critical load) can be served based on energy available (i.e. directly from solar) or based on the available energy stored (subject to the KiBaM and SOC constraints for lead-acid batteries). In simulation, though both the solar and load vectors are determined beforehand, a decision is made at every time step. On the dispatch side presented in Chapter 3, the model is only taking into account curtailing energy not able to be served at the network level as a proxy for demand-side management — versus identifying/disconnecting discrete loads at the household level. However, in reality, serving a fractional amount of load may not be feasible, and so future iterations of the model should focus on including binary decision variables on whether the entirety of the appliance's energy demand was served or not. Relatedly, another area for improvement is to assign 'household identifiers' in the model when determining which household — and appliances — to discretely curtail. This could be a useful way to incorporate some notion of fairness constraints, prioritization decisions, and/or simulation of agents' response to resource scarcity signals (i.e. price thresholds based on battery state-of-charge) during micro-grid operation.

As shown in Figure 6-4, the curtailment of energy not able to be served in the

simulations presented herein can be considered as 'peak clipping', but there are various other demand-side management methods to consider, whether at the utility-scale or in isolated micro-grids [104]. Representing other demand-side management approaches, such as 'valley filling' and 'load shifting', in simulation would be a useful endeavor and would rely on a more sophisticated approach to model dynamics of users' activities in determining whether appliance usage is deferrable and/or deadline-constrained.

Advanced implementation in the field may require a probabilistic forecast on both the generation and the demand, given that the load profile will not be exactly known beforehand. The key facet of a power management device with demand-side management is to disaggregate, differentiate, and control loads. With this knowledge, the on-board micro-processor would be able to make decisions on prioritizing and serving individual household loads in real-time, in reference to the availability of solar power for day-time loads or battery charge for evening loads (or during cloudy/rainy periods); an example of a real-time dispatch approach is shown in Figure 6-5. One technique would be to rely on model predictive control, a method relied on in chemical processing facilities which incorporates desired future scenarios (such as meeting yearly reliability constraints) when making decisions in the present. Additional operational approaches, such as incorporating a rolling horizon method (as used in [11]), cycle charging or load following strategies (as simulated with multiple generators in a micro-grid network, including the cost of non-served energy (CNSE), in [105]), or assessing 'bids' from households in a market for reliability (as proposed in [106]) could be considered for real-time operation.

When multiple power generators are on the same network with topological and transmission line capacity constraints, such as is the case in centralized power systems, a process for unit commitment and real-time dispatch takes place, based on solving least-cost optimization methods. One such parameter typically included in those calculations is for the cost of non-served energy (CNSE), which penalizes the power system economically — at a high enough cost — for demand that is not served [98]. However, in isolated micro-grids with one generating source, typically powered by 100% renewables, an alternative viewpoint of such dispatch heuristics can be con-

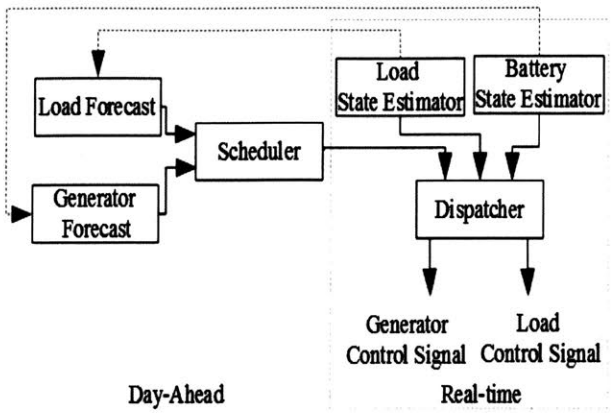


Figure 6-5: Proposed Process for Forecasts, State Estimation, and Real-Time Dispatch [91]

sidered as dispatching demand. Instead of treating demand as a fixed variable, the ability to disaggregate and prioritize loads allows for the option for demand to be served or curtailed. In a cost- and resource-constrained environment such as providing access to electricity in off-grid areas, minimizing the overall system costs is the governing constraint, subject to meeting baseline reliability thresholds as discussed in Chapter 4.

6.4 Conclusions on Techno-Economic Analysis of Micro-Grid Design and Operation

Based on the construction and aggregation of residential load profiles at the household level, Chapter 4 walks through the construction of the micro-grid simulation model designed for understanding the cost-performance tradeoffs of micro-grids with demand-side management. Specifically, the discussion highlights the technical aspects of the model, in the solar module output based on average historical irradiance along with the wiring losses and the operational efficiencies of DC/DC converters based on a low-voltage network architecture — the latter of which is included as part of the load profile required to be served. For every available combination of solar panels

and lead-acid batteries, the average yearly reliabilities are calculated and stored in matrices — separate for serving the critical and total load profiles. They key decision point of the model is to determine the least-cost combination of solar generation and battery capacity to meet the reliability thresholds, defined to be the average reliability over the entire year.

These results are then aggregated with the equipment costs of the network, and financial analysis is conducted to determine the financial viability of such an investment, and how it corresponds with a viable business model in terms of monthly payments required. These input parameters are varied to get a sense of how technical operating decisions (in the maximum depth of discharge and reliability thresholds) and financial inputs (in discount rates and connection fees) affect the financial viability. This combination of detailed technical modeling, extrapolation to system economics, and sensitivity analysis across key inputs is the main contribution of this chapter.

6.4.1 Including Topological Constraints, Larger Number of Households, & Productive Loads

One of the limitations of the modeling approach presented in Chapter 4 is that it is unable to provide a specific design configuration (i.e. physical panel/battery placement, wiring topology, etc.) for a particular locale. This would require a geospatial visualization and machine vision approach to identify households, the subject of current work undertaken by the Reference Electrification Model group for example [107]. Related to topology, the model is also not taking into account network stability issues to ensure system operation within a specified voltage range. This separate effort would require understanding state of individual switches, simulating response times, and identifying worst-case scenarios. Such an analysis would yield insights into operating situations where over-loading of the system may happen, which again is subject to the topological layout of the micro-grid.

The second drawback of this approach is that it is considered for serving 5 house-

holds per installation with basic residential appliances. Again, part of the rationale for this is because that a decentralized micro-grid (i.e. installation at the sub-village scale) can take advantage of economies of scale of drawing from the same solar panel and battery, while alleviating some of the challenges with customer acquisition costs and site location challenges seen in the design and implementation of conventional micro-grids. Furthermore, enabling small-scale micro-grids of this size can potentially catalyze individuals in off-grid areas to invest in and monetize their own electricity infrastructure.

However, in relation to the model developed, using the model at larger scales to serve more households can be done by extending the available solar / battery capacities beyond the maximum individual sizes by replicating available combinations towards kW solar power arrays and even MWh lead-acid battery banks (albeit wiring gauge and changes in voltage selection, the potential for alternating current (AC) power electronics, power flow, and series/parallel resistive losses would have to be appropriately considered). Similarly, the incorporation of small-scale productive loads profiles that could be powered by distributed solar generation would be a logical extension of the model built. These types of loads can include appliances such as refrigeration, agricultural water pumping, grain milling, etc. [108]. However, constructing realistic load profiles for each of these are use-case specific and can be seasonally dependent.

6.5 Final Concluding Remarks

Overall, the work presented herein aimed to cover a wide array of technical and economic aspects associated with the potential and opportunity for next generation micro-grids with demand-side management. Chapters 2, 3, and 4 provided a framework for both the optimization of generation asset sizes and insight for real-time operation of decentralized micro-grids with demand-management capabilities, and Chapter 5 laid out and analyzed relevant regulatory and social issues that need to be addressed. It is the hope that this work will be found useful by both researchers, prac-

titioners, and policy-makers to make next generation micro-grids viable on the ground in providing electricity access — and improving quality of life — in the developing world.

Bibliography

[1] P. Alstone et al. "Decentralized energy systems for clean electricity access." *Nature Climate Change: Perspective* (Mar. 2015).

[2] S.J. Ahn and D. Graczyk. *Understanding Energy Challenges in INdia: Policies, Players, and Issues.* International Energy Agency (IEA). 2012.

[3] Ministry of New and Government of India Renewable Energy. *Operational Guidelines for Implementation of Off-Grid and Decentralised Solar Applications During 12th.* `http://mnre.gov.in/file-manager/UserFiles/operational-guidelines-off-grid-and-decentralized-solar-application-2014-15.pdf`. May 2014.

[4] Dan Schnitzer et al. *Microgrids for Rural Electrification: A critical review of best practices based on seven case studies.* United Nations Foundation. Feb. 2014.

[5] Government of India: Ministry of New and Renewable Energy. *Remote Village Electrification.* `http://mnre.gov.in/schemes/offgrid/remote-village-electrification/`.

[6] *The Business Case for Off-Grid Energy in India.* The Climate Group. 2014.

[7] *Achieving Universal Electrification in India.* Institute for Transformative Technologies (ITT). Apr. 2016.

[8] *Network Optimized Distributed Energy Systems (NODES): Funding Opportunity Announcement.* Advanced Research Projects Agency - Energy (ARPA-E). Feb. 2015.

[9] M. Harper. *Review of Strategies and Technologies for Demand-Side Management on Isolated Mini-Grids.* Schatz Energy Research Center, Humboldt State University. Mar. 2013.

[10] M. Buevich et al. *Fine-Grained Remote Monitoring, Control and Pre-Paid Electrical Service in Rural Microgrids.* EarthSpark International.

[11] R. Palma-Behnke et al. "A Microgrid Energy Management System Based on the Rolling Horizon Strategy". *IEEE Transactions on Smart Grid* 4.2 (June 2013), pp. 996–1006.

[12] T.G. Quetchenbach et al. "The GridShare solution: A smart grid approach to improve service provision on a renewable energy mini-grid in Bhutan". *Environment Resource Letters* 8 (2013), pp. 1–11.

[13] L. Parshall. "National electricity planning in settings with low pre-existing grid coverage: Development of a spatial model and case study of Kenya". *Energy Policy* 47 (June 2009), pp. 2395–2410.

[14] B.J. Ruijven. "Model projections for household energy use in India". *Energy Policy* 39 (2011), pp. 7747–7761.

[15] MIT Building Technology Program. *Design Advisor Model.* `http://designadvisor.mit.edu/design/`.

[16] D. Ellman. "The Reference Electrification Model: A Computer Model for Planning Rural Electricity Access". Master's project. Engineering Systems Division: Massachusetts Institute of Technology, May 2015.

[17] K.C. Armel et al. "Is disaggregation the holy grail of energy efficiency? The case of electricity". *Energy Policy* 52 (Jan. 2013), pp. 213–234.

[18] G. Hart. "Nonintrusive Appliance Load Monitoring". *Proceedings of the IEEE.* 1992, pp. 1870–1891.

[19] S. Patel et .al. "ElectriSense: single-point sensing using EMI for electrical event detection and classification in the home". *Proceedings of the 12th ACM International Conference on Ubiquitous Computing*, pp. 139–148.

[20] H. Kim et al. "Unsupervised Disaggregation of Low Frequency Power Measurements". *Society for Industrial and Applied Mathematics (SIAM).*

[21] J.Z. Colter and M.J. Johnson. "REDD: A Public Data Set for Energy Disaggregation Research". *SustKDD 2012.*

[22] F. Jazizadeh et al. "An unsupervised hierarchical clustering based heuristic algorithm for facilitated training of electricity consumption disaggregation systems". *Advanced Engineering Informatics* 28.4 (Oct. 2014), pp. 311–326.

[23] R. Granell et al. "Clustering disaggregated load profiles using a Dirichelet process mixture model". *Energy Conversion and Management* 92 (Aug. 2014), pp. 507–516.

[24] S. Piller et al. "Methods for state-of-charge determination and their applications". *Journal of Power Sources* 96 (2001), pp. 113–120.

[25] Claudio Ricardo Vergara Ramirez. "Representing Battery Energy Storage in Electric Power System Studies". PhD Dissertation. Faculdade de Engenharia: Universidade do Porto, Mar. 2015.

[26] S.M. Mousavi and M. Nikdel. "Various battery models for various simulation studies and applications". *Renewable and Sustainable Energy Reviews* 32 (2014), pp. 477–485.

[27] X. Hu et al. "A comparative study of equivalent circuit models for Li-ion batteries". *Journal of Power Sources* 198 (2012), pp. 359–367.

[28] C.G. Zoski. "Handbook of Electrochemistry". Elsevier, 2007.

[29] M. Park et al. "A review of conduction phenomena in Li-ion batteries". *Journal of Power Sources* (2010).

[30] R. Painter et al. *A Single Particle Thermal Model for Lithium Ion Batteries.* `https://www.comsol.com/paper/download/194481/painter_paper.pdf`.

[31] O. Tremblay and L. Dessaint. "Experimental Validation of a Battery Dynamic Model for EV Applications". *World Electric Vehicle Journal* 3 (2009).

[32] R.E. Ciez and J.F. Whitacre. "Comparative techno-economic analysis of hybrid micro-grid systems utilizing different battery types". *Energy Conversion and Management* 112 (Mar. 2016), pp. 435–444.

[33] M.R. Jongerden and B.R. Haverkort. *Battery Modeling.* University of Twente.

[34] N. Omar et al. "Peukert Revisited—Critical Appraisal and Need for Modification for Lithium-Ion Batteries". *Energies* 6.11 (2013), pp. 5625–5641.

[35] J.F. Manwell and J.G. McGowan. "Lead Acid Battery Storage Model for Hybrid Energy Systems". *Solar Energy* 50.5 (1993), pp. 399–405.

[36] N. DiOrio et al. *Technoeconomic Modeling of Battery Energy Storage in SAM.* National Renewable Energy Laboratory.

[37] T. Lambert et al. "Micropower System Modeling with HOMER". *IEEE: Integration of Alternative Sources of Energy* (2006).

[38] I. Kaj and V. Konané. "Modeling battery cells under discharge using kinetic and stochastic battery models". *Applied Mathematical Modelling* 40 (Sept. 2016), pp. 7901–7915.

[39] S.D. Downing and D.F. Socie. "Simple rainflow counting algorithms". *International Journal of Fatigue* 4 (1982), pp. 31–40.

[40] A. Nielsony. "A Determination of fragments of multiaxial service loading strongly influencing the fatigue of machine components". *Mechanical Systems and Signal Processing* 23 (2009), pp. 2172–2721.

[41] E. Krieger. "A comparison of lead-acid and lithium-based battery behavior and capacity fade in off-grid renewable charging applications". *Energy* 60 (2013), pp. 492–500.

[42] Energy Sector Management Assistance Programme (ESMAP). *Mini-Grid Design Manual.* The World Bank. Sept. 2000.

[43] *Off Grid PV Power Systems: System Design Guidelines.* Sustainable Energy Industry Association of the Pacific Islands. Sept. 2012.

[44] A. Campanella. "An Analysis of the Viability and Competitiveness of DC Microgrids in Northern India". Master's of Science Thesis. Engineering Systems Division: Massachusetts Institute of Technology, Aug. 2013.

[45] M. Lee. "Cost versus reliability sizing strategy for isolated photovoltaic microgrids in the developing world". *Renewable Energy* 69 (Sept. 2014), pp. 16–24.

[46] Kurtis Unger. *Organically Grown Microgrids: the Development and Simulation of a Solar Home System-based Microgrid.* Master's Thesis. Department of Electrical and Computer Engineering: University of Waterloo, 2012.

[47] Dimitrios Thomas et al. "Methodology for optimal sizing of stand-alone photovoltaic/wind-generator systems using genetic algorithms". *Solar Energy* 80.9 (Sept. 2006), pp. 1072–1088.

[48] T. Markvart. "Sizing of hybrid photovoltaic-wind energy systems". *Solar Energy* 4 (1996), pp. 277–281.

[49] B.S. Borowy and Z.M. Salameh. "Methodology for optimally sizing the combination of a battery bank and PV array in a wind/PV hybrid system". *IEEE Transactions on Energy Conversion* 11.2 (1996), pp. 367–373.

[50] R. Chedid and S. Rahman. "Unit sizing and control of hybrid wind-solar power systems". *IEEE Transactions on Energy Conversion* 12.1 (1997), pp. 79–85.

[51] Jose Daniel Lara. *Robust Energy Management Systems for Isolated Microgrids Under Uncertainty.* Master's project. Department of Electrical and Computer Engineering: University of Waterloo, 2014.

[52] J.P. Torreglosa et al. "Control strategies for DC networks: A systematic literature review."" *Renewable and Sustainable Energy Reviews* 58 (2016), pp. 319–330.

[53] Bharat Menon Radhakrishnan and Dpti Srinivasan. "A multi-agent based distributed energy management scheme for smart grid applications". *Energy* 103 (May 2016), pp. 192–204.

[54] B. Nordman and M. Bugossi. "Optimizing Device Operation with a Local Electricity Price". *Micro-Energy International.* Berkeley, CA, Apr. 2014.

[55] H. Fernandez. "Selection and configuration of inverters and modules for a photovoltaic system to minimize costs". *Renewable and Sustainable Energy Reviews* 58 (May 2016), pp. 16–22.

[56] A. Chaurey and T.C. Kandpal. "A techno-economic comparison of rural electrification based on solar home systems and PV microgrids". *Energy Policy* 38 (2010), pp. 3118–3129.

[57] X. Han et al. "Economic evaluation of grid-connected micro-grid system with photovoltaic and energy storage under different investment and financing models". *Applied Energy* 184 (Dec. 2016), pp. 103–118.

[58] Daniel O. Akinyele and Ramesh K. Rayudu. "Techno-economic and life cycle environmental performance analyses of a solar photovoltaic microgrid system for developing countries". *Energy* 109 (Aug. 2016), pp. 160–179.

[59] Dimitrios Thomas et al. "Optimal design and techno-economic analysis of an autonomous small isolated microgrid aiming at high RES penetration". *Energy* 116 (Dec. 2016), pp. 364–379.

[60] A. Bhatt et al. "Feasibility and sensitivity analysis of an off-grid micro hydro–photovoltaic–biomass and biogas–diesel–battery hybrid energy system for a remote area in Uttarakhand state, India". *Renewable and Sustainable Energy Reviews* 61 (Aug. 2016), pp. 53–69.

[61] H. M. Alireza et al. "Techno-economic feasibility of photovoltaic, wind, diesel and hybrid electrification systems for off-grid rural electrification in Colombia". *Renewable Energy* 97 (Nov. 2016), pp. 293–305.

[62] Varun Mehra. *GitHub Repositories.* `https://github.com/vmehra813?tab=repositories`. 2017.

[63] S. Pargal and S.G. Banerjee. *More Power to India: The Challenge of Electricity Distribution.* Directions in Development. World Bank. 2014.

[64] *Current Status of Rural Electrification and Electricity Service Delivery in Rural Areas of India.* Vasudha Foundation. Aug. 2013.

[65] M. Filippini et al. "Elasticities of electricity demand in urban Indian households". *Energy Policy* 32 (2004), pp. 429–436.

[66] H. Gundimeda. "Fuel demand elasticities for energy and environmental policies: Indian sample survey evidence". *Energy Economics* 30 (2008), pp. 517–546.

[67] TERI. *Cost of unserved energy.* World Bank and Department for International Development. 2001.

[68] H. Gunatilake et al. "Willingness to Pay for Electricity Supply Improvements in Rural India". *Journal of Resources, Energy, and Development* 10.2 (Sept. 2013), pp. 55–77.

[69] M. Aklin et al. *Consumer Demand and Experience with Mera Gao Power in Barabanki, Uttar Pradesh.* Columbia University. Dec. 2014.

[70] Oracha Chotimongkol Peter Bailey and Shinji Isono. *Demand Analysis and Optimization of Renewable Energy: Sustainable Rural Electrification of Mbanayili, Ghana.* Master's Thesis. Center for Sustainable Systems: University of Michigan, 2015.

[71] Nikhilesh Dharmala. *A decentralized energy option for rural electrification–Using polygeneration in India.* Master's Thesis. Division of Energy, Climate Studies: KTH School of Industrial Engineering, and Management, 2015.

[72] T. Kobayakawa and T.C. Kandpal. "Analysis of electricity consumption under a photovoltaic micro-grid system in India". *Solar Energy* 116 (June 2015), pp. 177–183.

[73] H. Camblong et al. "Micro-grids project, Part 1: Analysis of rural electrification with high content of renewable energy sources in Senegal". *Renewable Energy* 34.10 (Oct. 2009), pp. 2141–2150.

[74] G.N. Rouskas. "Internet Tiered Services: Theory, Economics, and Quality of Service". Springer, 2009.

[75] C. Verhoel et al. "Optimal resource allocation in synchronized multi-tier Internet services". *Performance Evaluation* 68.11 (2011), pp. 1072–1084.

[76] S.H. Lee et al. "Optimal pricing and capacity partitioning for tiered access service in virtual networks". *Computer Networks* 57.18 (2013), pp. 3941–3956.

[77] D. Soto and V. Modi. "Simulations of Efficiency Improvements using Measured Microgrid Data". *IEEE Global Humanitarian Technology Conference*. 2012.

[78] Varun Mehra. *Solar Home System Data Log*. GitHub Repository. Aug. 2016. DOI: https://zenodo.org/record/60424.

[79] *Open Energy Information (OpenEI) Data Set*. Aug. 2016. DOI: http://en.openei.org/datasets/dataset/solar-home-system-jharkhand-india.

[80] CAS Data Loggers. *VersaLog DCV-2 Voltage Data Logger*. http://www.dataloggerinc.com/products/VersaLog_DCV2_Voltage_Data_Logger/293/.

[81] Wardah Inam. "Adaptable Power Conversion for Grid and Microgrid Applications". PhD Dissertation. Department of Electrical Engineering and Computer Science: Massachusetts Institute of Technology, May 2016.

[82] Linear Technology Corporation. *High-Voltage, High-Current Buck-Boost Battery Charge Controller with Maximum Power Point Tracking*. http://cds.linear.com/docs/en/datasheet/8490fa.pdf.

[83] National Renewable Energy Laboratory (NREL). *PV Watts Calculator*. http://pvwatts.nrel.gov/.

[84] MathWorks. *Kernel Distribution*. https://www.mathworks.com/help/stats/kernel-distribution.html.

[85] Christopher Bishop. "Pattern Recognition and Machine Learning". Springer, 2006.

[86] MathWorks. *Cluster Analysis.* https://www.mathworks.com/help/stats/cluster-analysis.html.

[87] Texas Instruments. *Battery Fuel (Gas) Gauge Overview.* http://www.ti.com/lsds/ti/power-management/battery-fuel-gauge-overview.page.

[88] Linear Technology Corporation. *Precision Zero Drift Current Sense Amplifier.* http://cds.linear.com/docs/en/demo-board-manual/dc1113A.pdf.

[89] J. Newman and K.E. Thomas-Alyea. "Electrochemical Systems". Wiley, 2004.

[90] A. Sakti et al. "Enhanced representations of lithium-ion batteries in power systems models and their effect on the valuation of energy arbitrage applications". *Journal of Power Sources* 342 (2017), pp. 279–291.

[91] W. Inam. "Architecture and System Analysis of Microgrids with Peer-to-Peer Electricity Sharing to Create a Marketplace which Enables Energy Access". *9th International Conference on Power Electronics* (June 2015).

[92] Microchip Technology Inc. *16-Bit Digital Signal Controllers with High-Speed PWM ADC and Comparators.* http://ww1.microchip.com/downloads/en/DeviceDoc/70000591f.pdf.

[93] P. Meier et al. *The Design and Sustainability of Renewable Energy Incentives: An Economic Analysis.* Directions in Development. World Bank. 2015.

[94] T. Baskaran et al. "Election cycles and electricity provision: Evidence from a quasi-experiment with Indian special elections". *Journal of Public Economics* (2015).

[95] Ministry of Law Government of India and Justice. *The Electricity Act.* May 2003.

[96] Ministry of New and Government of India Renewable Energy. *National Renewable Energy Act 2015 (Draft).* http://mnre.gov.in/file-manager/UserFiles/draft-rea-2015.pdf. 2015.

[97] B. Tenebaum et al. *From the Bottom Up: How Small Producers and Mini-Grids Can Deliver Electrification and Renewable Energy in Africa.* Directions in Development. World Bank. 2014.

[98] I.J. Perez-Arriaga. "Regulation of the Power Sector". Springer, 2013.

[99] Jharkhand State Electricity Regulatory Commission. *Terms and Conditions for Determination of Distribution Tariff.* Nov. 2010.

[100] Government of India Ministry of Power. *Tariff Policy Resolution.* `http://thecleannetwork.org/downloads/87-Tariff_Policy-Resolution_Dated_28012016.pdf`. Jan. 2016.

[101] S. Mazzola et al. "Assessing the value of forecast-based dispatch in the operation of off-grid rural microgrids". *Applied Energy* (Oct. 2016).

[102] Bolun Xu. *Degradation-limiting Optimization of Battery Energy Storage Systems Operation.* Master's Thesis. Power Systems Laboratory: ETH Zurich, Sept. 2013.

[103] N.A. Chaturvedi et al. *Algorithms for Advanced Battery-Management Systems: Modeling, Estimation, and Control Challenges for Lithium-Ion Batteries.* IEEE Control Systems Magazine. June 2010.

[104] C.W. Gellings. "The concept of demand-side management for electric utilities". *Proceedings of the IEEE* 73.10 (Nov. 1985), pp. 1468–1470.

[105] Vivian Li. *The Local Reference Electrification Model: comprehensive decision-making tool for the design of rural microgrids.* Master's Thesis. Engineering Systems Division: Massachusetts Institute of Technology, June 2016.

[106] D. Strawser et al. "A Market for Reliability for Electricity Scheduling in Developing World Microgrids". *Proceedings of the 2015 International Conference on Autonomous Agents and Multiagent Systems* (May 2015), pp. 1833–1834.

[107] Universal Energy Access Research Group. *The Reference Electrification Model.* `http://universalaccess.mit.edu`.

[108] GIZ. *Photovoltaics for Productive Use Applications: A Catalogue of DC-Appliances.* http://thecleannetwork.org/downloads/97-GIZ_(2016)_Catalogue_PV_Appliances_for_Micro_Enterprises.pdf. Jan. 2016.